Copyright Warning & Restrictions

The copyright law of the United States (Title 17, United States Code) governs the making of photocopies or other reproductions of copyrighted material.

Under certain conditions specified in the law, libraries and archives are authorized to furnish a photocopy or other reproduction. One of these specified conditions is that the photocopy or reproduction is not to be "used for any purpose other than private study, scholarship, or research." If a, user makes a request for, or later uses, a photocopy or reproduction for purposes in excess of "fair use" that user may be liable for copyright infringement,

This institution reserves the right to refuse to accept a copying order if, in its judgment, fulfillment of the order would involve violation of copyright law.

Please Note: The author retains the copyright while the New Jersey Institute of Technology reserves the right to distribute this thesis or dissertation

Printing note: If you do not wish to print this page, then select "Pages from: first page # to: last page #" on the print dialog screen

INFORMATION TO USERS

This material was produced from a microfilm copy of the original document. While the most advanced technological means to photograph and reproduce this document have been used, the quality is heavily dependent upon the quality of the original submitted.

The following explanation of techniques is provided to help you understand markings or patterns which may appear on this reproduction.

1. The sign or "target" for pages apparently lacking from the document photographed is "Missing Page(s)". If it was possible to obtain the missing page(s) or section, they are spliced into the film along with adjacent pages. This may have necessitated cutting thru an image and duplicating adjacent pages to insure you complete continuity.

2. When an image on the film is obliterated with a large round black mark, it is an indication that the photographer suspected that the copy may have moved during exposure and thus cause a blurred image. You will find a good image of the page in the adjacent frame.

3. When a map, drawing or chart, etc., was part of the material being photographed the photographer followed a definite method in "sectioning" the material. It is customary to begin photoing at the upper left hand corner of a large sheet and to continue photoing from left to right in equal sections with a small overlap. If necessary, sectioning is continued again — beginning below the first row and continuing on until complete.

4. The majority of users indicate that the textual content is of greatest value, however, a somewhat higher quality reproduction could be made from "photographs" if essential to the understanding of the dissertation. Silver prints of "photographs" may be ordered at additional charge by writing the Order Department, giving the catalog number, title, author and specific pages you wish reproduced.

5. PLEASE NOTE: Some pages may have indistinct print. Filmed as received.

University Microfilms International
300 North Zeeb Road
Ann Arbor, Michigan 48106 USA
St. John's Road, Tyler's Green
High Wycombe, Bucks, England HP10 8HR

FLOW OF POLYMER MELT BLENDS THROUGH POROUS MEDIA

BY

JAMES ATWOOD PARKER, JR

A DISSERTATION

PRESENTED IN PARTIAL FULFILLMENT OF

THE REQUIREMENTS FOR THE DEGREE

OF

DOCTOR OF ENGINEERING SCIENCE

IN

CHEMICAL ENGINEERING

AT

THE NEW JERSEY INSTITUTE OF TECHNOLOGY

Newark, New Jersey
1977

ABSTRACT

The flow of molten polystyrene, poly(methyl methacrylate) and three blends of these polymers has been studied in a rheogoniometer and in packed beds of unconsolidated spherical glass beads. One primary purpose of the study was to determine the behavior of polymer melt blends in porous media flow. The second major purpose of the work was to develop and test a new and powerful model for packed bed flow based upon the Huang generalized rheological constitutive equations.

Rheological characterization of the pure polymers and blends was obtained using a Roberts-Weissenberg rheogoniometer. Shear and normal stresses were measured at shear rates from .002 to 20 sec^{-1} and temperatures from 180 to 220 °C. Both the four parameter Huang and three parameter Ellis equations of state provided excellent representations of the viscometric data.

The Huang rheological equation was combined with an hydraulic radius capillary model for a porous medium leading to a generalized Darcy's law. This expression defined an effective non-Newtonian viscosity applicable to packed bed fluid flow. A packed bed friction factor

and Reynolds number were developed to correlate experimental data.

Pressure drop of the pure polymers and blends was measured over a range of flow rates through packed beds of various bead sizes and packing depths. Temperature was maintained at 204°C.

Data for each pure polymer and blend was successfully correlated using a friction factor-Reynolds number relationship, which specifies that the product of these dimensionless quantities is constant. The value of this constant for pure poly(methyl methacrylate) was approximately one half the value for pure polystyrene and the three blends.

No significant differences in the behavior of the pure polymers and blends was observed. The Huang equation of state provided excellent representation of molten polymer viscometric data and successfully correlated packed bed flow data. The difference in packed bed flow behavior of poly(methyl methacrylate) and the other materials was tentatively ascribed to unidentified surface interaction effects between the fluids and the packed beds. Using the defined expressions, pressure drop for packed bed flow can be estimated from the rheological properties of the fluid and the physical properties of the packed bed.

APPROVAL OF DISSERTATION

FLOW OF POLYMER MELT BLENDS

THROUGH POROUS MEDIA

BY

JAMES ATWOOD PARKER, JR.

FOR

DEPARTMENT OF CHEMICAL ENGINEERING

AND CHEMISTRY

THE NEW JERSEY INSTITUTE OF TECHNOLOGY

BY

FACULTY COMMITTEE

APPROVED: _____ Chairman

_____

_____

_____

_____

NEWARK, NEW JERSEY

MAY, 1977

PREFACE

This dissertation is the culmination of research first proposed by Professor R.G. Griskey six years ago. Under his direction, the basic goal of studying the porous media flow of melt blend polymers jelled.

Design and fabrication of the equipment was directed by Dr. Nandor Siskovic, and accomplished through the skill of Mr. Walter Schmeideskamp and his able shop personnel.

Shortly after experimental work began, Professor Griskey left NCE and Professor C.R. Huang assumed the task of research advisor for the study. Under his direction, a second important aspect of the effort materialized. The opportunity was to develop and test a new theoretical model for a packed bed. The basis for the new model was a statistical thermodynamic constitutive equation proposed by Professor Huang. With his considerable expertise and patience, the goal was accomplished.

Actual conduct of the packed bed experiments required two to three people. In addition to Dr. Siskovic, fellow students Minh Ho Choi and Yon-Li Shanghuan par-

ticipated extensively in the work.

The large quantities of polymer required for the packed bed experiments were supplied free of charge by the Dow Chemical Company and at discount by Rohm and Haas Company.

Financial support for the 1971 school year in which full time research was conducted was through Graduate Assistanceships made available by the Graduate Division.

Time, financial support, materials and encouragement were liberally bestowed throughout these years by my employer, Celanese Corporation.

Those needs, problems and motivations to which no one else could respond were cheerfully shared by my wife, Sandee. She also contributed significantly to this final manuscript.

To each person and organization I have named and to others whose influence has touched this work, my hearty and lasting thanks!

TABLE OF CONTENTS

LIST OF FIGURES

LIST OF TABLES

CHAPTER I. INTRODUCTION

Statement of the Problem

The occurrence of porous media is universal. Living organisms are porous, soil is porous, graphite, ceramics, wood, textiles and molecular sieves are all porous materials. The importance of an understanding of the processes which occur in porous materials has long been recognized. Investigators have used a variety of approaches to characterize porous structures. Because of the diversity, complexity and universality of porous media, no rigorous comprehensive mathematical descriptions have been formulated - nor does such a model seem possible for some time to come. Meanwhile, significant extensions of existing theory can be made through the practical solution of specific problems.

Significance of the Problem

Applications of the theory and technology of porous media flow abound. One of the most important applications is in secondary oil recovery. The problem of how to extract oil which remains in pores underground after primary recovery is extremely complex. Present widespread recognition of the importance of conserving our not unlimited natural resources further highlights this application. Studies of the flow of non-Newtonian fluids

through various types of porous media contribute to a phenomenological understanding of this task.

Chemical engineering applications of porous media flow include catalytic fixed bed reactors, packed towers to perform separations, filtration operations and packed bed polymer melt processing - particularly as applied to filament extrusion.

In the mid 1960's and early 1970's, many investigators focused on the flow of non-Newtonian fluids through porous media. Even so, the bulk of our present knowledge of the subject relates to Newtonian flow. The behavior of Newtonian fluids flowing in porous media provides satisfactory design criteria for many gas and simple liquid systems. In addition, the techniques of Newtonian fluid analysis form the basis for the successfully applied non-Newtonian treatments.

The majority of the experimental studies of non-Newtonian systems are for dilute polymer solutions. Investigators have thus been able to readily control and vary the degree of non-Newtonian behavior exhibited. As discussed later, only a few published studies deal with the flow of molten polymers. These studies are of great practical importance to the present work since they address some of the same equipment design, exper-

imental, and data analysis challenges.

What is sought in this investigation is to extend the work of previous studies in several ways. Great attention is devoted to the design of the experimental apparatus, that it relate in practical terms to commercially important extrusion equipment and that it provide accurate measurement of the experimental variables. Polymers of commercial importance are chosen for study - namely, polystyrene and poly(methyl methacrylate). Perhaps of greatest significance, the study is not limited to pure component single phase systems, but is extended to melt blends of the subject polymers as well.

Increasing attention is being focused on polyblends as a result of attempts to extend the applications of polymeric materials by combining them. Enhanced strength, toughness, durability and other features are sought. Systems of commercial importance include impact rubber modified polystyrene, rigid polyvinyl chloride blended with poly(butadiene-co-acrylonitrile), and acrylonitrile-butadiene-styrene plastics. Industry continues to research bicomponent fibers which exhibit self bulking characteristics for use in fashion design. Other studies of blend systems have been made, but no

previous study of melt blend porous media flow is known.

Methodology

The study is divided into two parts, each requiring theoretical and experimental development. Rheological melt behavior of the pure components and blends is characterized over a broad range of temperatures and shear rates in a Weissenberg type cone and plate instrument. A satisfactory rheological model to describe the data is sought. In the second phase, isothermal flow data through packed beds of unconsolidated particles of regular geometry is generated. These results are analyzed by coupling a generalized Darcy's law and the rheological equation of state with an hydraulic radius capillary model for the porous media. A test of a new thermodynamically based generalized equation of state is made. Further, an analytic solution of the hydraulic radius packed bed model is developed using this phenomenological equation.

Behavior of the pure component and blend systems is assessed relative to studies of the same or similar systems in other flow geometries.

CHAPTER II. THEORY

General

The several components of fluid flow theory required to analyze porous media flow are outlined below. A derivation of the fundamental rheological relationships for generalized Newtonian fluids is given. Several equations of state based on this development are reviewed. An alternate statistical thermodynamic approach leading to a generalized rheological expression for pseudoplastic fluids is given.

The approaches to porous media flow analysis are outlined and the Darcy law development for Newtonian fluids is detailed. Extension of the Darcy law concept to non-Newtonian fluids is made for several models of interest. Finally, the behavior of polymer melt blends in other geometries is presented as a guide to the type of results which might be observed in porous media flow.

Rheological Models for Non-Newtonian Fluids

A generally accepted development of the basic laws governing the isothermal flow of incompressible fluids is given by Bird, Stewart and Lightfoot (7). The equation of continuity describing the rate of change of density within a volume element fixed in space as a function of net mass efflux from the element is

given as

$$\frac{\partial \rho}{\partial t} = -\left[\underline{\nabla} \cdot \rho \underline{v}\right] \tag{II.1}$$

The equivalent expression as a substantial derivative of density is

$$\frac{D\rho}{Dt} = -\rho\left[\underline{\nabla} \cdot \underline{v}\right] \tag{II.2}$$

For the special case of incompressible fluids, (II.2) reduces to

$$\left[\underline{\nabla} \cdot \underline{v}\right] = 0 \tag{II.3}$$

The momentum balance carried out on a volume element gives expressions analogous to (II.1) and (II.2) above, i.e.

$$\frac{\partial}{\partial t}(\rho \underline{v}) = -\left[\underline{\nabla} \cdot \rho \underline{v}\,\underline{v}\right] - \underline{\nabla} P - \left[\underline{\nabla} \cdot \underline{\underline{\tau}}\right] + \rho \underline{g} \tag{II.4}$$

for an observer at a fixed point, and

$$\rho \frac{D\underline{v}}{Dt} = -\underline{\nabla} P - \left[\underline{\nabla} \cdot \underline{\underline{\tau}}\right] + \rho \underline{g} \tag{II.5}$$

for an observer traveling at the local velocity of the volume element. These equations are completely general and apply to all continuous media.

To be able to use these expressions, one must define the various stresses in terms of fluid charac-

teristics. For the Newtonian fluid, the simplified relationship between the stress tensor and the velocity gradient or rate of deformation tensor is

$$\underline{\underline{\tau}} = -\mu \underline{\underline{\Delta}} \qquad \text{(II.6)}$$

In this case, the coefficient of viscosity, μ, depends on pressure and temperature, but not on the stress and velocity gradient tensors.

For the non-Newtonian fluid, a constitutive model of similar type is proposed

$$\underline{\underline{\tau}} = -\eta \underline{\underline{\Delta}} \qquad \text{(II.7)}$$

where the coefficient, η , is a scalar quantity and is a function of either the stress or velocity gradient tensors. This generalized Newtonian fluid model is the basis for all of the specific constitutive equations presented in the following section (6).

The functionality of η on either $\underline{\underline{\tau}}$ or $\underline{\underline{\Delta}}$ is now required. Arguments as to the relative importance of the three scalar invariants of $\underline{\underline{\Delta}}$ on which η may depend are given by Bird (7) and by Sadowski (91) and need not be recast here. The practical result of the assumptions which are made is that η is a function of the second invariant

$$I_2 = [\underline{\underline{\Delta}} : \underline{\underline{\Delta}}] = \Sigma_i \Sigma_j \Delta_{ij}\Delta_{ji} \qquad \text{(II.8)}$$

Thus

$$\eta = \eta[\underline{\underline{\Delta}} : \underline{\underline{\Delta}}] \quad \text{or} \quad \eta = \eta\,[\underline{\underline{\tau}} : \underline{\underline{\tau}}] \qquad \text{(II.9)}$$

The development is thereby restricted to incompressible, inelastic fluids and to systems in which the fluid behaves as though the flow geometry were simple. The only justification for ignoring the effects of complex geometry (as in a packed bed) is the success of various investigators in correlating flow data without admitting a geometrical dependence.

Generalized Newtonian fluid equations of state.

Many rheological models have been formulated which conform to equations (II.7) and (II.9). No one model has been proposed which is universally applicable to all non-Newtonian fluids. In general, the flexibility of such functions increases for a greater number of adjustable parameters, but the utility correspondingly decreases with the added complexity. The models considered here are those of demonstrated utility and relative simplicity. References to more detailed development and discussions of the equations which follow may be found in Bird (6), Ferry (30), McKelvey

(66), and Rheology (86).

Undoubtedly the most widely used generalized Newtonian model is the Ostwald-de-Waele or power law expression

$$\tau_{ij} = -\left[m \left| \tfrac{1}{2} (\underline{\underline{\Delta}} : \underline{\underline{\Delta}}) \right|^{\frac{n-1}{2}} \right] \Delta_{ij} \qquad \text{(II.10)}$$

This simple two constant model has been found applicable to many fluids over intermediate shear rate ranges. It reduces to Newton's law of viscosity for $n = 0$ and $m = \mu$. For pseudoplastic fluids ($n < 1$), the model incorrectly predicts infinite viscosity in the limit of zero shear stress (6). Further, Reiner (85) has objected that no physical significance can be attached to the coefficient m since the dimension of m depends upon the value of n. In spite of these deficiencies and objections, the model has been successfully applied to many flow systems. References include application to axial tube flow and to annular tube flow by Fredrickson and Bird (31, 32, 33), to the analysis of capillary rheometer data by Han, Yu and Kim (40), to flow around a sphere by Slattery (106), and to porous media flow by Kozicki (59), Gregory, Griskey and Siskovic (37, 38, 105), Christopher and Middleman (18, 19), Marshall and Metzner (64),

and Harvey (49). Additional discussion and examples of the power law are given by Bird (7).

A simple superposition of the power law and Newton's Law of viscosity leads to the widely applied three parameter Ellis model, viz.,

$$\Delta_{ij} = -\left[\phi_0 + \phi_1 \left| \tfrac{1}{2} (\underline{\underline{\tau}} : \underline{\underline{\tau}}) \right|^{\frac{\alpha-1}{2}}\right] \tau_{ij} \qquad \text{(II.11)}$$

The model correctly predicts a constant and finite zero shear viscosity. Ellis model solutions to problems including circular tube flow, falling film, coating a moving strip, radial annular flow and tangential annular flow have been given by Matsuhisa and Bird (65). It has also been used to describe axial annular flow (2), circular tube heat transfer (65) and packed bed flow by Sadowski and Bird (91, 92).

The Sisko model is closely related to the Ellis model and represents another possible superposition of the power law and Newton's law of viscosity.

$$\tau_{ij} = -\left[\eta_0 - \beta \left| \tfrac{1}{2} (\underline{\underline{\Delta}} : \underline{\underline{\Delta}}) \right|^{\frac{\alpha-1}{2}}\right] \Delta_{ij} \qquad \text{(II.12)}$$

Sisko applied the model to a tube flow problem (104).

Neither the Ellis nor the Sisko model correctly predicts an upper limiting viscosity observed at high shear rates. The more complex Eyring model (36) was

developed based on considerations of the molecular structure of matter. It has been simplified to forms including the Powell-Eyring model (83) which correctly describes the lower and upper limiting viscosities.

$$\tau_{ij} = -\left[\eta_N + \left(\frac{\chi\beta}{\alpha}\right) \frac{\sinh^{-1}\left[\beta\left|\frac{1}{2}\left(\underline{\underline{\Delta}}:\underline{\underline{\Delta}}\right)\right|^{\frac{1}{2}}\right]}{\beta\left|\frac{1}{2}\left(\underline{\underline{\Delta}}:\underline{\underline{\Delta}}\right)\right|^{\frac{1}{2}}}\right]\Delta_{ij} \quad \text{(II.13)}$$

Another simplification of the Eyring model results in the Sutterby model (113):

$$\tau_{ij} = -\left[\eta_o\left(\frac{\sinh^{-1}\left[\beta\left|\frac{1}{2}\left(\underline{\underline{\Delta}}:\underline{\underline{\Delta}}\right)\right|\right]}{\beta\left|\frac{1}{2}\left(\underline{\underline{\Delta}}:\underline{\underline{\Delta}}\right)\right|}\right)^{\frac{\alpha-1}{2}}\right]\Delta_{ij} \quad \text{(II.14)}$$

This model has given better representation of data for some fluids than the Ellis model. It has been applied to tube flow and to converging section flow (113).

The Huang generalized equation of state. One exception to the generalized Newtonian fluid approach to rheological modeling is that developed by C.R. Huang (53). The approach is based on application of the general principles of statistical mechanics and irreversible thermodynamics through the entropy. Changes in the entropy as a result of the stress/strain behavior of the fluid are mapped by a molecular arrangement parameter. The resulting rheological equations of state describe time-dependent and time-independent non-Newtonian fluids.

The equation

$$S = k \ln \Omega \tag{II.15}$$

is a basis of statistical mechanics relating the entropy, S, to the number of micromolecular states of an assembly, Ω, through the Boltzmann constant, k. For a simple idealized assembly, Ω can be expressed as a function of thermodynamic state variables of the assembly. For non-Newtonian fluids, however, additional molecular arrangement parameters are required to describe the order-disorder transitions which occur when the fluid is subjected to shear stress. The equation for the overall specific entropy change due to heat transfer, viscous dissipation and change in molecular arrangement is proposed to be

$$\rho \frac{d\hat{S}}{dt} = - \frac{1}{T}\left[q^i_{,i} + \tau^{ij} \frac{d\gamma_{ij}}{dt} + \tau^{ij} \frac{d\beta_{ij}}{dt}\right] \tag{II.16}$$

where β_{ij} is the molecular arrangement parameter of the fluid. The rate of entropy generation, σ, is then

$$\sigma = - \frac{1}{T}\left[\frac{1}{T} q^i T_{,i} + \tau^{ij} \frac{d\gamma_{ij}}{dt} + \tau^{ij} \frac{d\beta_{ij}}{dt}\right] \tag{II.17}$$

where q^i is the heat flux vector and $T_{,i}$, the temperature gradient vector.

The forms of the phenomenological equations for

heat flux, strain rate and molecular arrangement are assumed to be

$$q^i = -\lambda\, g^{ik} T_{,k} \tag{II.18}$$

$$\tau^{ij} = -\eta\, \frac{d\gamma^{ij}}{dt} \tag{II.19}$$

$$\tau^{ij} = -\xi\, \frac{d\beta^{ij}}{dt} \tag{II.20}$$

Equations (II.18), (II.19) and (II.20) may be substituted into (II.17) to give

$$\sigma = \frac{1}{T}\left[\frac{\lambda}{T} g^{ik} T_{,k} T_{,i} + \eta\, \frac{d\gamma^{ij}}{dt}\frac{d\gamma_{ij}}{dt} + \xi\, \frac{d\beta^{ij}}{dt}\frac{d\beta_{ij}}{dt}\right] \tag{II.21}$$

The two final terms in equation (II.21) are shear stress related and may be combined to express the rheological behavior of the fluid:

$$\tau^{ij} = -\eta\, \frac{d\gamma^{ij}}{dt} - \xi\, \frac{d\beta^{ij}}{dt} = -\eta_t\, \frac{d\gamma^{ij}}{dt} \tag{II.22}$$

where the overall apparent viscosity is

$$\eta_t = \eta + \xi\, \frac{\dot{\beta}^{ij}}{\dot{\gamma}_{ij}} \tag{II.23}$$

For pseudoplastic fluids such as those considered in this study, it is assumed that the molecular arrangement parameter changes very rapidly from its equilibrium value β_e^{ij} to a new value β_0^{ij} when a shear stress is applied. The kinetics of the change are given as:

$$\frac{d\beta^{ij}}{dt} = -c_5 \beta^{ij} \left|\dot{\gamma}^{ij}\right|^n \qquad 0 \leq t \leq t_0 \qquad \text{(II.24)}$$

$$\frac{d\beta^{ij}}{dt} = -c_6 \beta_0^{ij} \left|\dot{\gamma}^{ij}\right|^n \qquad t_0 \leq t \qquad \text{(II.25)}$$

Integrating equation (II.24) gives:

$$\beta_0^{ij} = \beta_e^{ij} \exp\left(-c_5 \left|\dot{\gamma}^{ij}\right|^n t_0\right) \qquad \text{(II.26)}$$

Combining equations (II.25) and (II.26); noting $c_5 = c_6$:

$$\frac{d\beta^{ij}}{dt} = -c_5 \beta_e^{ij} \left|\dot{\gamma}^{ij}\right|^n \exp\left(-c_5 \left|\dot{\gamma}^{ij}\right|^n t_0\right) \qquad \text{(II.27)}$$

Introducing (II.27) into (II.23), the overall apparent viscosity becomes

$$\eta_t = \eta - c_5 \xi \beta_e^{ij} \frac{\left|\dot{\gamma}^{ij}\right|^n}{\dot{\gamma}^{ij}} \exp\left(-c_5 \left|\dot{\gamma}^{ij}\right|^n t_0\right) \qquad \text{(II.28)}$$

Assuming $\eta \equiv \mu$ = constant, the generalized equation for pseudoplastics from (II.22) becomes

$$\tau^{ij} = -\left[\mu - c_5 \xi \beta_e^{ij} \frac{\left|\dot{\gamma}^{ij}\right|^n}{\dot{\gamma}^{ij}} \exp\left(-c_5 \left|\dot{\gamma}^{ij}\right|^n t_0\right)\right] \dot{\gamma}^{ij} \qquad \text{(II.29)}$$

Until the present study, tests of this fluid model were limited to computer simulation of pseudoplastic rheograms with arbitrary constants. With such data, qualitatively correct agreement with experimental flow curves was found.

Recently, other studies not related to polymer melts and blends have successfully used variations of the Huang model to represent experimental data. The fluids studied included whole human blood (53a, 53b), latex paint (53c) and silicone grease (53d). Thus, the behavior of many different and rheologically complex fluids can be represented by this powerful model.

Limitations and extensions of the rheological equations. Several points must be emphasized about the rheological equations discussed above. Each involves a degree of empiricism in its formulation and so is not rigorous. The adjustable parameters of each must be determined from experimental data, thereby limiting utility to regions near the data base. None of the models describes normal stress or time dependent effects.

Reviews of some models which describe nonlinear viscoelastic effects have been given by Bogue and Doughty (12), Metzner, White and Denn (69, 70), and Spriggs, Huppler and Bird (111, 112). Alternate forms of the Huang model (53), and functions such as the Oldroyd model as simplified by Williams (124), the Spriggs and Bird model (111), the models of Rivlin and Ericksen (90), and the Coleman and Noll expression (20) address time dependent effects. Application of these complex equations to even simple flow geometries results in formidable mathematical difficulties. The usefulness of this group of models is restricted in practical, experimental studies. Further development of the theories and functional relationships is required before they can be applied to problems of the complexity of

porous media flow.

Porous Media Flow - Newtonian Fluids

The basic physical relationship governing the flow of a viscous fluid through an isotropic, homogenous porous medium was deduced experimentally by Henry Darcy in 1856 (23). Generalizations and extensions of that work constitute the field of porous media flow. Excellent general discussions of relevant background are provided by Bear (3), Carman (16), Collins (21), Dallavalle (22), Muscat (75, 76) and Scheidegger (94, 97, 98) among others. In the brief review which follows, Darcy's law is presented and generalized to its possible differential forms. The several types of models proposed to functionally define the proportionality constant in the law are described. The discussion follows primarily the authorative presentations of Bear and Scheidegger referenced above.

Darcy's law. The original experiment upon which present day porous media theory rests was performed by H.P.G. Darcy in 1856. His apparatus consisted of a filter bed through which water percolated. Pressure drop across a known depth of the homogenous packing was measured as a function of flow rate. Darcy deduced

the following relationship among the variables:

$$Q = K A_r \frac{\Delta P}{L} \qquad \text{(II.30)}$$

The flow was found to be directly proportional to the bed cross sectional area A_r and pressure gradient. The proportionality constant depended upon the nature of the packed bed and the properties of the fluid. Many experimental studies of the flow of isothermal, incompressible fluids through beds of unconsolidated particles of regular geometry have substantiated this type of relationship.

The form of Darcy's law in (II.30) is of limited utility. First, some statement of the significance of the constant K is required. Then, a differential form of the law must be developed to allow variations in boundary conditions.

For Newtonian fluids, separation of the effects due to the porous medium and to the fluid's properties can be achieved by redefining the constant K as

$$K = \frac{k}{\mu} \qquad \text{(II.31)}$$

where k is the permeability of the medium and μ is the fluid viscosity. The permeability has fundamental

units of L^2 . The permeability concept has been found to adequately characterize many types of porous media.

Using equation (II.31), Darcy's law for flow through a horizontal bed becomes

$$V_0 = \frac{Q}{A_r} = - \frac{k}{\mu} \left(\frac{P_2 - P_1 + \rho g h}{h} \right) \tag{II.32}$$

where the usual expanded representation of the pressure gradient is shown. Two differential forms have been suggested which lead to (II.32):

$$V_0 = - \frac{k}{\mu} \left(\underline{\nabla} P - \rho \underline{g} \right) \tag{II.33}$$

and

$$V_0 = - \underline{\nabla} \frac{k P}{\mu} + \frac{k \rho \underline{g}}{\mu} \tag{II.34}$$

Equation (II.33) introduces a force potential

$$\phi = g z + \int_{P_0}^{P} \frac{d P}{\rho} \tag{II.35}$$

such that

$$V_0 = - \frac{k \rho}{\mu} \underline{\nabla} \phi \tag{II.36}$$

with z as a vertical coordinate. Equation (II.34) is a velocity potential of the form

$$\Psi = \frac{k \rho}{\mu} + \int_{z_0}^{z} \frac{k \rho g \, dz}{\mu} \tag{II.37}$$

and

$$V_0 = - \underline{\nabla} \Psi \qquad \text{(II.38)}$$

While it has not been possible to justify either of these forms as fundamentally valid, the force potential form, equation (II.36), has come to be generally accepted. Derivations by Collins (21), Hall (39), Hubbert (54), Irmay (56) and Mokadam (72) led to this form.

Modeling porous structures. In general, the approaches which have been taken to modeling porous media may be divided into three types: viz., geometric theories including the capillary and particle models, statistical theories and theories in which averaged forms of the governing differential equations are developed. Each approach is reviewed below with reference to specific studies. Emphasis is placed on the hydraulic radius capillary models used to characterize the flow system of the present study.

Although not directly relevant to the development of particular models, studies directed to the determination of the structure of porous media by theoretical and analytical methods also contribute to an understanding of flow phenomena in them. A good general review with an extensive bibliography has been given by Dullien and Batra (25).

Geometric theories of porous media. As pointed out in the discussion of Darcy's law, the porous structure is characterized by the permeability factor, k. The drag theory of permeability treats the walls of the media pores as resistances to fluid flow (96). The drag of each obstacle in the field of flow is estimated from the Navier-Stokes equations and the total resistance is the sum of the individual contributions. The drag theory is the basis of work by Brinkman (14), Iberall (55), Mott (73) and more recently by Brenner (13), Dullien (26, 27) and LeClair (61, 62).

Brinkman perceived a packed bed as an assemblage of particles held in place by external forces and exerting a damping force on the flowing fluid. The total force acting on a volume element of fluid was given by the sum of the shearing and normal stresses through the Navier-Stokes equation and a damping force related to the fluid velocity amd viscosity. A permeability expression was developed as

$$k = \frac{D_p^2}{72}\left[3 + \frac{4}{1-\epsilon} - 3\sqrt{\frac{8}{1-\epsilon} - 3}\right] \qquad \text{(II.39)}$$

Iberall dealt with a random distribution of circular cylinder fibers, approximating the total drag force as the sum of individual element contributions.

Interactions among the flow streamlines of adjacent fibers were ignored. Creeping flow Reynolds number was assumed. An expression for pressure gradient was developed which, when compared to Darcy's law, gave for permeability:

$$k = \frac{3}{16} \frac{D_p^2 \epsilon}{1-\epsilon} \left[\frac{2 - \ln\left(\frac{D_p V_0 \rho}{\mu \epsilon} \right)}{4 - \ln\left(\frac{D_p V_0 \rho}{\mu \epsilon} \right)} \right] \qquad \text{(II.40)}$$

Brenner assumed a spacially periodic porous medium consisting of an array of unit cells, each containing one or more particles of arbitrary shape. He analyzed the model in terms of both the drag forces parallel to the stream velocity and the lateral forces at right angles to a settling particle. The extension of this analysis to creeping flow in porous media led to a symmetric permeability tensor with non-zero diagonal components of the form:

$$K_{ij} = k \delta_{ij} \qquad \text{(II.41)}$$

for an isotropic medium.

These approaches are representative of drag theory geometric modeling.

Capillary models of porous media have been more extensively investigated than any other representation. The success of numerous investigators in correlating

experimental data accounts for the attention given these models. Again, the 1960 review by Scheidegger (97) serves as an authorative guide to early basic developments.

The simplest capillary picture of a packed bed is that of a bundle of straight, parallel tubes. Comparison of the Hagan-Poiseuille and Darcy expressions for flow leads to a permeability of

$$k = \frac{\epsilon \bar{D}^2}{32} \tag{II.42}$$

where $\bar{D}$ is the single capillary average diameter. Replacement of the numerical factor "32" by a tortuosity term T and the capillary diameter by a specific surface area S gives a modified permeability

$$k = \frac{\epsilon^3}{T^2 S^2} \tag{II.43}$$

Such expressions are poor representations of what is observed experimentally.

Arranging the capillaries in each of the three principle directions (thereby lowering the permeability by a factor of three) results in an expression not significantly better than (II.42).

Inherent in all variations of the capillary tube

models is the assumption that each capillary is a direct path through the porous medium. Obviously, this is not a realistic picture. At the other extreme, it is assumed that all the capillaries are in series, forming a tortuous channel the entire length of which is traversed by each fluid element. The permeability expression under this assumption is

$$k = \frac{1}{96} \frac{\epsilon \bar{D}^2}{T^2} \qquad \text{(II.44)}$$

Scheidegger suggested that the capillary tubes could be better described in terms of a distribution $\alpha(D)$ of variable diameter (95). The resulting expression for permeability was

$$k = \frac{\epsilon}{96\, T^2} \frac{1}{\int_0^\infty [D^2 \alpha(D)\, dD]^2 \int_0^\infty \frac{\alpha(D)}{D^6}\, dD} \qquad \text{(II.45)}$$

This differs from the other values of k discussed in that average pore diameter has a specific meaning:

$$\bar{D}^2 = \frac{1}{\int_0^\infty [D^2 \alpha(D)\, dD]^2 \int_0^\infty \frac{\alpha(D)}{D^6}\, dD} \qquad \text{(II.46)}$$

In summary, the simpler of the capillary models are inadequate to describe real systems. The more complex models containing a tortuosity factor can be forced to fit any porous structure, but do not contribute to a satisfactory understanding of the phenomena involved.

Extension of capillaric modeling to a more realistic description of pore geometry is possible through the concept of hydraulic radius. From the theory of flow through non-circular channels, hydraulic radius is defined as the ratio of conduit volume to wetted surface area, having the units of length. For porous media, it may be regarded as a length characteristic of the complex passages of the matrix. Since permeability has units of length squared, it is taken as proportional to the square of hydraulic radius. In general, permeability is also related to a shape factor $f(s)$ and to a porosity factor $f(\epsilon)$:

$$k = f(s)\, f(\epsilon)\, R^2 \qquad \text{(II.47)}$$

Investigators have sought to give meaning to the shape and porosity factors (4). One of the most widely accepted developments is that traced to work conducted between 1922 and 1957 by Blake (11), Kozeny (58), Carman (15, 16), Ergun (28), Fair and Hatch (29), Leva (63) and Wyllie (126). By solving the Navier-Stokes equation for all channels passing through a cross section normal to the flow direction, Kozeny obtained a Darcy law form

$$Q = - \frac{c_0 \epsilon^3}{\mu S^2} \underline{\nabla} \phi \qquad \text{(II.48)}$$

Thus

$$k = \frac{c_0 \epsilon^3}{S^2} \tag{II.49}$$

The Kozeny constant, c_0 , is a function of channel cross section shape. Further, the specific surface may be expressed per unit volume of solid, S_0, rather than per unit volume of porous medium, S , through the porosity :

$$S = S_0 \left(1-\epsilon\right) \tag{II.50}$$

Then

$$k = \frac{c_0}{S_0^2} \frac{\epsilon^3}{\left(1-\epsilon\right)^2} \tag{II.51}$$

For spheres

$$D_p = \frac{6}{S_0} \tag{II.52}$$

Thus

$$k = \frac{c_0 D_p^2}{36} \frac{\epsilon^3}{\left(1-\epsilon\right)^2} \tag{II.53}$$

Various values assigned to c_0 lead to numerically different permeabilities of the form:

$$k = \frac{D_p^2}{c} \frac{\epsilon^3}{\left(1-\epsilon\right)^2} \tag{II.54}$$

It is further possible to incorporate a tortuosity factor into the constant c , but the form of (II.54) is

not changed. This expression for the permeability is the well known Blake-Kozeny-Carman equation.

A great many investigators using various media and fluids have tested this form of permeability expression. Scheidegger discusses a number of these studies. For non-spherical systems, still further improvements in the model are required (89). In general, the shape and tortuosity factors are ill defined and cannot be tested independently. Thus, the overall constant, c, in equation (II.54) is treated as an adjustable parameter, lacking any unambiguous physical significance. The justification for such an approach is the success which has been achieved in correlating flow data from many systems.

Statistical theories of porous media. The appeal of a statistical mechanical treatment of porous media flow is that the random disordered nature of such systems need not be compromised to apply the techniques. In the geometric theories, simplified ordered models were constructed to keep the resulting mathematical expressions simple enough to be solved analytically. Adjustable parameters were added to achieve agreement with experiment.

Reviews of statistical treatments for porous media are given by Bear (5) and Scheidegger (97). Specific reference may be made to the theories advanced by Aranow (1), De Jong (24), Haring and Greenkorn (48), Pakula (78) and Scheidegger (99, 100) as representative of this approach.

Fundamental to the statistical theories is a third factor, the dispersivity, in addition to the shape and porosity factors discussed previously. Dispersivity may be regarded as a measure of the sideways dispersion which a stream of fluid undergoes in flowing through a packed bed. In Scheidegger's treatment, the differential equations of flow are formulated in terms of the probability distribution of an elementary fluid displacement vector. The permeability expression

$$k = b \cos^2 \theta \qquad \text{(II.55)}$$

results, where b is a factor related to the reciprocal of the flow resistance of a pore and θ is the angle between the displacement vector and pressure gradient. The exercise leads to a modified Darcy's law.

Alternatively, the randomness may be attributed to the medium and models such as that proposed by

Haring and Greenkorn may be formulated. Their model of the medium is of ramdomly ordered cylindrical pores of variable length and radius distributed according to the beta function. The permeability expression developed is

$$\frac{k}{\epsilon} = \frac{R^2}{24} \frac{(a+2)\ (a+b+2)}{(a+b+3)\ (a+1)} \qquad \text{(II.56)}$$

where a and b are parameters of the radius distribution, R is the largest pore radius and ϵ is the porosity. Dispersivity coefficients in the longitudinal and transverse directions are also developed.

These and other statistical approaches, while quite successful in describing general flow characteristics, have not been effectively applied to practical data analysis. As with some geometrical theories, the complexity of the mathematics developed in statistical analyses presently limits the utility of this approach.

Averaged equation theories of porous media. The most rigorous, if least studied, approach to modeling porous media is the development of correct averaged forms of the governing differential equations. Since this technique leads to generalized equations, results should be in accord with any geometric or statistical development.

References to this averaged differential equation technique include work by Payatakes (80), Slattery (108, 109, 110) and Whitaker (121, 17). In his study, Whitaker proposed a skewed capillary model and developed a permeability tensor of the form

$$K_{ij} = B(1)\delta_{ij} + B(2)\lambda_i\lambda_j \qquad \text{(II.57)}$$

where the $\underline{\underline{B}}$ tensor is a polynomial function defining the magnitude of a general orientation vector and λ is the unit orientation vector. Description of orthotropic materials requires a symmetric second order tensor.

The complexity of the averaged equation theories is immediately evident. Correlative forms of these equations have not been developed. Thus, data analysis is not possible with this powerful, but mathematically limiting method.

Porous Media Flow - Non-Newtonian Fluids

As late as 1960 there were no published reports of the flow of non-Newtonian fluids in porous media. Extensive work on non-Newtonian flow in other systems was in the literature, but packed bed flow studies were limited to Newtonian fluids. Then, beginning with the

work of Sadowski and Bird in 1963 (91, 92), interest in the theoretical and experimental aspects of non-Newtonian porous media flow quickened.

Several approaches to describing such flow have been forwarded. An excellent review of these given by Savins in 1969 is abstracted here to provide a basis for the present theoretical development (93).

Scheidegger was apparently the first to suggest that a capillary model and a generalized Newtonian rheological equation could be combined to describe non-Newtonian flow in a porous medium (97). The hydraulic radius approach was illustrated for one dimensional flow of a power law fluid in a packed bed by Bird (10). Subsequently, modifications of this development were utilized by Christopher and Middleman (18, 19), Giatonde and Middleman (35), Marshall and Metzner (64), Payne and Parker (81), Wampler and Gregory (119), Wissler (125) and Siskovic, et al (105).

The work of Sadowski extended Scheidegger's concept to the more complex Ellis equation of state (91, 92). Gregory provided the first study of melt flow (poly-ethylene) and used the Mooney-Rabinowitsch rheological model to describe the melt behavior. Recently, Park,

et al successfully described packed bed flow of aqueous poly(methyl cellulose) using a Hershel-Bulkley fluid model (79).

Details of the application of the hydraulic radius approach to the description of packed bed flow will be covered as part of the present theoretical development. In principle, the method is similar to those referenced above.

Another way of describing porous media flow involves direct adaptation of Darcy's law to non-Newtonian flow without using a particular rheological model. The rheological description must then be derived from viscometric and packed bed data. McKinley, et al (68) and Kozicki, et al (59) have used this technique. McKinley, studying flow in underground reservoirs, replaced the porous medium with a capillary of equivalent radius proportional to the square root of the ratio of permeability to porosity. The proportionality constant was determined from a capillary rheogram and porous media flow data for a specific bed. In principle, this single determination should allow prediction of non-Newtonian flow in the same type of medium regardless of porosity or permeability. The study by Kozicki

furthered this approach to include anomalous effects attributed to an anisotropic layer of fluid particles on the medium surface.

Dimensional analysis has been applied by Slattery to the flow of an arbitrary viscoelastic fluid in porous media (107, 108). This treatment involved a tensorial description of an incompressible, simple fluid having a characteristic time and viscosity. Marshall and Metzner observed anomalous behavior in the flow of several polymer solutions through a sintered bronze disk (64). They attributed departure of the Deborah number from expected behavior to viscoelastic effects. Wissler proposed a correction factor for these effects which successfully explained the Marshall and Metzner results (125).

Still other correlation methods and systems have been used such as that by Hassell and Bondi who estimated shear rate in rubber cements, then entered corresponding capillary stress and shear rate data directly into a friction factor - Reynolds number expression (50). White applied the power law form of Darcy's law to the equation of continuity giving differential equations linking pressure distribution and the stream function (122). Additional insight into

the variety of related problems may be gained by consulting Herzig, et al (51), Payne and Parker (81), and Volssoughi and Seyer (118).

Generalized Darcy's law. Of the approaches briefly reviewed above, the coupling of a suitable rheological equation of state with a capillary form of porous medium model to give a generalized Darcy's law is the most successful technique for representing experimental data. In most cases, a packed bed friction factor is calculated and plotted against an effective Reynolds number in accordance with the usual practice of correlating flow data in other geometries. Using this approach, a new friction factor - Reynolds number relationship is developed for the Huang generalized equation of state.

The shear stress distribution and volumetric flow rate of a fluid in a tube of regular cross section are given by Bird as (8):

$$\tau_{rz} = \left| \frac{\Delta P}{2 L} \right| r \qquad \text{(II.58)}$$

and

$$Q = \int_0^{2\pi} \int_0^R v_z \, r \, dr \, d\theta \qquad \text{(II.59)}$$

From (II.58):

$$\tau_R = \left| \frac{\Delta P}{2 L} \right| R \quad @ \; r = R \qquad \text{(II.60)}$$

Thus

$$\tau_{rz} = \tau_R \left(\frac{r}{R}\right) \tag{II.61}$$

The Huang generalized equation of state for pseudo-plastics was given previously as

$$\tau^{ij} = -\left[\mu - c_5 \xi \beta_e^{ij} \frac{|\dot{\gamma}^{ij}|^n}{\dot{\gamma}^{ij}} \exp\left(-c_5 |\dot{\gamma}^{ij}|^n t_0\right)\right] \dot{\gamma}^{ij} \tag{II.29}$$

For isothermal, incompressible flow in a tube, this equation has the form below with $\dot{\gamma}_{rz} = \left(-\frac{dV_z}{dr}\right)$

$$\tau_{rz} = A\dot{\gamma}_{rz} + B\dot{\gamma}_{rz}^n \exp\left(-C\dot{\gamma}_{rz}^n\right) \tag{II.62}$$

where the constants A , B , C , and n have been substituted for the original parameters in (II.29). Equating (II.61) and (II.62) gives

$$r = \frac{R}{\tau_R}\left[A\dot{\gamma}_{rz} + B\dot{\gamma}_{rz}^n \exp\left(-C\dot{\gamma}_{rz}^n\right)\right] \tag{II.63}$$

From (II.59)

$$Q = 2\pi \int_0^{R} \frac{V_z}{2} \, d(r^2) \tag{II.64}$$

Integration by parts follows:

$$Q = \pi \left[V_z r^2 \right]_0^R - \pi \int_0^R r^2 \, dV_z$$

$$= -\pi \int_0^R r^2 \, \frac{dV_z}{dr} \, dr$$

$$= -\pi \int_0^R \frac{1}{3} \frac{dV_z}{dr} \, d(r^3)$$

$$Q = \frac{\pi}{3}\int_0^R \dot{\gamma}_{rz}\, d(r^3) \tag{II.65}$$

A second application of integration by parts gives:

$$Q = \frac{\pi}{3}\left[\left(-\frac{dV_z}{dr}\right)r^3\Big|_0^R - \int_0^R r^3\, d\dot{\gamma}_{rz}\right]$$

$$= \frac{\pi}{3}\left[\dot{\gamma}_R R^3 - \int_0^R r^3\, d\dot{\gamma}_{rz}\right] \tag{II.66}$$

Combining (II.63) and (II.66) and inserting proper limits of integration:

$$Q = \frac{\pi}{3}\left\{\dot{\gamma}_R R^3 - \frac{R^3}{\tau_R^3}\int_0^{\dot{\gamma}_R}\left[A^3\dot{\gamma}_{rz}^3 + 3A^2B\dot{\gamma}_{rz}^{n+2}\exp\left(-C\dot{\gamma}_{rz}^n\right)\right.\right.$$

$$\left.\left. + 3AB^2\dot{\gamma}_{rz}^{2n+1}\exp\left(-2C\dot{\gamma}_{rz}^n\right) + B^3\dot{\gamma}_{rz}^{3n}\exp\left(-3C\dot{\gamma}_{rz}^n\right)\right]d\dot{\gamma}_{rz}\right\} \tag{II.67}$$

The first of the four terms in brackets in (II.67) may readily be integrated:

$$A^3\int_0^{\dot{\gamma}_R}\dot{\gamma}_{rz}^3\, d\dot{\gamma}_{rz} = \frac{A^3}{4}\dot{\gamma}_R^4 \tag{II.68}$$

A transformation of variable is performed on each of the three remaining terms to be integrated of the form

$$C_1\, x^{C_2} = y \tag{II.69}$$

Correspondence between this form and the terms to be integrated is as follows:

second term: $C_1 x^{C_2} \Rightarrow C \dot{\gamma}_{rz}^{n}$ (II.70)

third term: $C_1 x^{C_2} \Rightarrow 2C \dot{\gamma}_{rz}^{n}$ (II.71)

fourth term: $C_1 x^{C_2} \Rightarrow 3C \dot{\gamma}_{rz}^{n}$ (II.72)

After substituting and rearranging variables, the following transformed integrals are obtained:

$$\frac{3A^2B}{n}\left(\frac{1}{C}\right)^{\frac{(n+3)}{n}}\int_0^{C\dot{\gamma}_R} \exp(-y)\; y^{\left(\frac{3}{n}\right)}\, dy \qquad \text{(II.73)}$$

$$\frac{3AB^2}{n}\left(\frac{1}{2C}\right)^{\frac{2n+2}{n}}\int_0^{2C\dot{\gamma}_R} \exp(-y)\; y^{\left(\frac{n+2}{n}\right)}\, dy \qquad \text{(II.74)}$$

$$\frac{B^3}{n}\left(\frac{1}{3C}\right)^{\frac{3n+1}{n}}\int_0^{3C\dot{\gamma}_R} \exp(-y)\; y^{\left(\frac{3n+1}{n}\right)}\, dy \qquad \text{(II.75)}$$

From Abramowitz and Stegun (46), the gamma function is defined to be of the form

$$\Gamma(a,z) = \int_0^z \exp(-t)\; t^{a-1}\, dt \qquad \text{(II.76)}$$

Each of the transformed integrals (II.73), (II.74) and (II.75) is the same form as the gamma function. The same reference (47) defines the probability function

$$\frac{\Gamma(a,z)}{\Gamma(a)} = P\left(\frac{\chi^2}{\nu}\right) = 1 - Q\left(\frac{\chi^2}{\nu}\right) \qquad \text{(II.77)}$$

$$\nu = 2a$$
$$\chi^2 = 2z$$

If (II.73), (II.74) and (II.75) are each compared in

turn with (II.76) and (II.77), a further set of corresponding terms is developed, viz,

second term:

$$a = \frac{n+3}{n}; \quad z = y@\left(\dot{\gamma}_{rz} = \dot{\gamma}_R\right) = C\dot{\gamma}_R^n$$

$$t = y; \quad \nu = 2\left(\frac{n+3}{n}\right); \quad \chi^2 = 2C\dot{\gamma}_R^n \qquad \text{(II.78)}$$

third term:

$$a = \frac{2n+2}{n}; \quad z = y@\left(\dot{\gamma}_{rz} = \dot{\gamma}_R\right) = 2C\dot{\gamma}_R^n$$

$$t = y; \quad \nu = 2\left(\frac{2n+2}{n}\right); \quad \chi^2 = 4C\dot{\gamma}_R^n \qquad \text{(II.79)}$$

fourth term:

$$a = \frac{3n+1}{n}; \quad z = y@\left(\dot{\gamma}_{rz} = \dot{\gamma}_R\right) \; 3C\dot{\gamma}_R^n$$

$$t = y; \quad \nu = 2\left(\frac{3n+1}{n}\right); \quad \chi^2 = 6C\dot{\gamma}_R^n \qquad \text{(II.80)}$$

With appropriate substitutions of (II.78) into (II.73), (II.79) into (II.74) and (II.80) into (II.75), the final form of the integrated expressions is obtained in terms of real parameters as:

$$\frac{3A^2B}{n}\left(\frac{1}{C}\right)^{\frac{n+3}{n}}\Gamma\left(\frac{n+3}{n}\right)\left[1 - Q\left(\frac{2C\dot{\gamma}_R^n}{2\left(\frac{n+3}{n}\right)}\right)\right] \qquad \text{(II.81)}$$

$$\frac{3AB^2}{n}\left(\frac{1}{2C}\right)^{\frac{2n+2}{n}}\Gamma\left(\frac{2n+2}{n}\right)\left[1 - Q\left(\frac{4C\dot{\gamma}_R^n}{2\left(\frac{2n+2}{n}\right)}\right)\right] \qquad \text{(II.82)}$$

$$\frac{B^3}{n}\left(\frac{1}{3C}\right)^{\frac{3n+1}{n}}\Gamma\left(\frac{3n+1}{n}\right)\left[1 - Q\left(\frac{6C\dot{\gamma}_R^n}{2\left(\frac{3n+1}{n}\right)}\right)\right] \qquad \text{(II.83)}$$

Equation (II.68) for volumetric flow becomes:

$$Q = \frac{\pi R^3}{3}\left\{\dot{\gamma}_R - \frac{1}{\tau_R^3}\left[\frac{A^3}{4}\dot{\gamma}_R^4 + \frac{3A^2B}{n}\left(\frac{1}{C}\right)^{\frac{n+3}{n}}\Gamma\left(\frac{n+3}{n}\right)\right.\right.$$

$$\left(1-Q\left(\frac{2C\dot{\gamma}_R^n}{2\left(\frac{n+3}{n}\right)}\right)\right)+\frac{3AB^2}{n}\left(\frac{1}{2C}\right)^{\frac{2n+2}{n}}\Gamma\left(\frac{2n+2}{n}\right)$$

$$\left(1-Q\left(\frac{4C\dot{\gamma}_R^n}{2\left(\frac{2n+2}{n}\right)}\right)\right)+\frac{B^3}{n}\left(\frac{1}{3C}\right)^{\frac{3n+1}{n}}\Gamma\left(\frac{3n+1}{n}\right)$$

$$\left(1-Q\left(\frac{6C\dot{\gamma}_R^n}{2\left(\frac{3n+1}{n}\right)}\right)\right)\Bigg]\Bigg\} \qquad \text{(II.84)}$$

The average velocity for tube flow is (8):

$$\langle V\rangle = \frac{\int_0^{2\pi}\int_0^R V_z\, dr\, d\theta}{\int_0^{2\pi}\int_0^R r\, dr\, d\theta} = \frac{Q}{\pi R^2} \qquad \text{(II.85)}$$

For packed bed flow the commonly accepted Dupuit-Forscheimer assumption is (94):

$$V_0 = \langle V\rangle \epsilon \qquad \text{(II.86)}$$

relating superficial and average pore velocities. Following Bird (10), capillary and packed bed parameters may be related through the hydraulic radius:

$$R = 2R_h \qquad \text{(II.87)}$$

$$R_h = \frac{\epsilon}{S} \qquad \text{(II.88)}$$

Then

$$S = S_0(1-\epsilon) \qquad \text{(II.89)}$$

defines a specific surface area S_0, and

$$D_p = \frac{6}{S_0} \qquad \text{(II.90)}$$

defines a mean particle diameter D_p, (exact for spheres). Combining equations (II.84) through (II.90), the expression for superficial velocity through the packed bed becomes:

$$V_0 = \frac{D_p}{9}\left(\frac{\epsilon^2}{1-\epsilon}\right)\left\{\dot{\gamma}_{Rh} - \frac{1}{\tau_{Rh}^3}\left[\frac{A^3}{4}\dot{\gamma}_{Rh}^4 + \frac{3A^2B}{n}\left(\frac{1}{C}\right)^{\frac{n+3}{n}}\Gamma\left(\frac{n+3}{n}\right)\left(1-Q\left(\frac{2C\dot{\gamma}_{Rh}^n}{2\left(\frac{n+3}{n}\right)}\right)\right) + \frac{3AB^2}{n}\left(\frac{1}{2C}\right)^{\frac{2n+2}{n}}\Gamma\left(\frac{2n+2}{n}\right)\left(1-Q\left(\frac{4C\dot{\gamma}_{Rh}^n}{2\left(\frac{2n+2}{n}\right)}\right)\right) + \frac{B^3}{n}\left(\frac{1}{3C}\right)^{\frac{3n+1}{n}}\Gamma\left(\frac{3n+1}{n}\right)\left(1-Q\left(\frac{6C\dot{\gamma}_{Rh}^n}{2\left(\frac{3n+1}{n}\right)}\right)\right)\right]\right\} \quad \text{(II.91)}$$

Use of τ_{Rh} and $\dot{\gamma}_{Rh}$ acknowledges substitution of the hydraulic radius as an effective radius of the pores in the packed bed. Further, from (II.60),

$$\tau_{Rh} = \frac{\Delta P}{L} R_h = \frac{\Delta P}{L}\,\frac{D_p}{6}\left(\frac{\epsilon}{1-\epsilon}\right) \quad \text{(II.92)}$$

Equations (II.91) and (II.92) can be combined to give a form corresponding to a generalized Darcy's law, i.e.,

$$V_0 = \frac{k}{\eta_{eff}}\,\frac{\Delta P}{L} \quad \text{(II.93)}$$

which is analogous to (II.32) with the Newtonian viscosity replaced by an effective viscosity. The complete expression is

$$V_0 = \frac{D_p^2 \epsilon^3}{54(1-\epsilon)^2} \frac{1}{\tau_{Rh}} \left\{ \dot{\gamma}_{Rh} - \frac{1}{\tau_{Rh}^3} \left[\frac{A^3}{4} \dot{\gamma}_{Rh}^4 + \frac{3A^2B}{n} \left(\frac{1}{C}\right)^{\frac{n+3}{n}} \Gamma\left(\frac{n+3}{n}\right) \left(1 - Q\left(\frac{2C\dot{\gamma}_{Rh}^n}{2\left(\frac{n+3}{n}\right)}\right)\right) + \frac{3AB^2}{n} \left(\frac{1}{2C}\right)^{\frac{2n+2}{n}} \Gamma\left(\frac{2n+2}{n}\right) \left(1 - Q\left(\frac{4C\dot{\gamma}_{Rh}^n}{2\left(\frac{2n+2}{n}\right)}\right)\right) + \frac{B^3}{n} \left(\frac{1}{3C}\right)^{\frac{3n+1}{n}} \Gamma\left(\frac{3n+1}{n}\right) \left(1 - Q\left(\frac{6C\dot{\gamma}_{Rh}^n}{2\left(\frac{3n+1}{n}\right)}\right)\right) \right] \right\} \quad \text{(II.94)}$$

The term

$$\frac{D_p^2 \epsilon^3}{54(1-\epsilon)^2}$$

is the same form as the Blake-Kozeny-Carman permeability relationship presented earlier as (II.54). In practice, the factor **c** or 54 is adjusted to give agreement with experimental data.

The classical method of correlating tube flow data is through the dimensionless groupings friction factor and Reynolds number. As shown by Bird (9), the friction factor for tube flow is

$$f = \frac{1}{4} \left(\frac{D}{L}\right) \frac{\Delta P}{\frac{1}{2}\rho \langle V \rangle^2} \quad \text{(II.95)}$$

Again applying equations (II.86) through (II.90), the analogous packed bed friction factor is

$$f^* = \frac{1}{3} \frac{D_p}{L} \frac{\Delta P}{\rho V_0^2} \frac{\epsilon^3}{1-\epsilon} \qquad \text{(II.96)}$$

Combining equations (II.54), (II.93) and (II.96) and rearranging leads to an expression proposed by Ergun (28) in 1952, based upon the dimensionless groupings obtained by Blake in 1922 (11):

$$f^* = \frac{D_p}{L} \frac{\Delta P}{\rho V_0^2} \frac{\epsilon^3}{1-\epsilon} = c\left[\frac{(1-\epsilon)\,\eta_{eff}}{D_p\, V_0\, \rho}\right] \qquad \text{(II.97)}$$

The right side of (II.97) is of the form of a modified Reynolds number, differing from (II.96) only in that the numerical factor $\frac{1}{3}$ has been lumped with the empirical constant c. Thus

$$f^* = \frac{c}{N_{re,eff}} \qquad \text{(II.98)}$$

where by comparing (II.93) and (II.94) it is evident that η_{eff} in $N_{re,eff}$ is given by

$$\frac{1}{\eta_{eff}} = \frac{1}{\tau_{Rh}}\left\{\dot\gamma_{Rh} - \frac{1}{\tau_{Rh}^3}\left[\frac{A^3}{4}\dot\gamma_{Rh}^4 + \frac{3A^2B}{n}\left(\frac{1}{C}\right)^{\frac{n+3}{n}}\Gamma\left(\frac{n+3}{n}\right)\left(1-Q\left(\frac{2C\dot\gamma_{Rh}^n}{2\left(\frac{n+3}{n}\right)}\right)\right) + \frac{3AB^2}{n}\left(\frac{1}{2C}\right)^{\frac{2n+2}{n}}\Gamma\left(\frac{2n+2}{n}\right)\left(1-Q\left(\frac{4C\dot\gamma_{Rh}^n}{2\left(\frac{2n+2}{n}\right)}\right)\right) + \frac{B^3}{n}\left(\frac{1}{3C}\right)^{\frac{3n+1}{n}}\Gamma\left(\frac{3n+1}{n}\right)\left(1-Q\left(\frac{6C\dot\gamma_{Rh}^n}{2\left(\frac{3n+1}{n}\right)}\right)\right)\right]\right\} \qquad \text{(II.99)}$$

As will be outlined in the chapter on experimental results, the equations developed above may be used to analyze packed bed flow data for any system of known rheological behavior. Deviations from predicted packed bed flow behavior (excluding experimental error) may be attributed to various effects related to the complex geometry of the porous medium and to unaccounted viscoelastic fluid properties.

Rheological Behavior of Melt Blends

One of the principle differences between this and and previous porous media flow studies is the inclusion of three blends of the two polymers being investigated into the experimental plan. No other comparable study is known. An opportunity is thus afforded to learn whether polymer blends exhibit unusual behavior in both pure shear fields (the rheometer) and in the complex flow geometry of the packed bed. Further, the dependent variables (shear stress and pressure drop) may be determined as a function of composition for the system studied.

The literature on polyblends is extensive and was not exhaustively reviewed for this study. Only those papers of direct relevance by virtue of involving related systems or using pertinent analysis techniques

are considered.

Helpful general discussions of the whole field of polyblends have been provided by Platzer (82) and by Yu (74). With a simple yet convincing argument, Yu reviewed the basic requirements of compatibility in a thermodynamic sense and concluded that all polymer blends must be inhomogenous at some scale of examination greater than the moleculer level. He further highlighted the problem of defining the degree of compatibility of a polyblend since in some systems it may behave as a single phase when in fact heterogeneity exists at some micro scale.

Studies of specific blend systems have been made by Han (40 through 45), Noel and Carley (77), Hill and Maxwell (52), Seymour (101), Sieglaff (102, 103) and VanOene (116). Sieglaff studied the viscous and elastic behavior of poly(vinyl chloride) modified by various low molecular weight plasticizers. Viscosity reduction was observed in capillary rheometer data for some additives, but no evidence of two phase phenomena was noted.

A study more directly relevant to the present work was that by Hill and Maxwell at Princeton University.

They determined the dynamic mechanical response of two component blends of polyethylene, polystyrene and poly(methyl methacrylate) using an orthogonal rheometer. Measurements of the out-of-phase modulus (simply related to the shear viscosity at low frequency and shear rate) and the in-phase modulus (related to elastic behavior) for PMMA/PS blends were reported. The out-of-phase modulus varied smoothly as a function of composition, showing no evidence of phase separation or inversion. The in-phase modulus showed a maximum at about 50/50 PMMA/PS, and the relaxation spectrum was shifted with respect to a theoretical spectrum. This effect was attributed to slight solubility of one polymer in the other.

Han has used a sophisticated capillary rheometer (40) coupled with photomicroscopy to examine blend systems including high/low density polyethylenes, polystyrene/polypropylene, polystyrene/polyethylene and the same polystyrene/poly(methyl methacrylate) polymers used in this work. In a much higher shear rate range than that explored by Hill and Maxwell, Han found broad, distinct minima in the viscosity of PS/PE and PS/PP blends as a function of composition. Capillary exit pressure (a measure of elastic behavior) showed a single maximum and minimum for PS/PE and a double

maximum, single minimum for PS/PP. Micrographs showed the distinct phases of the two components in each case, but no evidence of phase inversion (continuous to dispersed or vice-versa) at any composition.

As an extension of the Weissenberg cone and plate data generated for this study, Han characterized the same PS/PMMA blends in the capillary rheometer. Shear and normal stress results over a total four decade range of shear rate are in excellent agreement (45).

VanOene (116) has shown that for PS/PMMA blends, polystyrene is the continuous phase.

To summarize, viscometric studies of various polymer blend systems generally confirm the incompatibility of polymers. Some examples of unexpected behavior have been observed, but no consistent pattern of deviation from normal single phase behavior has been ascertained. It is evident that studies of polyblends in a variety of flow geometries will be necessary to fill the gaps in the existing information base.

CHAPTER III. RHEOLOGICAL EXPERIMENTS

As reviewed above, the method of analysis of this study required coupling a rheological model for the fluids with a model for the porous medium. In order to test the theoretical development made by this approach, both reliable viscometric data and packed bed flow data were required. The testing instrument used in the study was a modified Roberts-Weissenberg Model 18 rheogoniometer. In the following sections, the polymers and blends are described, sample preparation is discussed, the experimental procedure is reviewed and the rheological data are fitted to several equations of state including the power law, Ellis and Huang models.

Description of the Polymers

Several factors affected the choice of materials for study. Chief among these was the desire to use polymers of commercial significance which would normally be processed in full scale extrusion equipment of the type to be described. Polymers of general interest, the rheology of which had been characterized in other systems, were sought. Discussions of polymers and polymer processing by McKelvey (66), Middleman (71), Bernhardt (84), Eirich (86, 88), Kwei (60), Tobolsky (114, 115) and VanOene (116) among others were consulted. Certain

similarities of the polymers seemed desirable such as crystallinity, melt viscosity, solubility and melt processing conditions, to assure the feasibility of blending. Comparable melt temperatures and flow indices would minimize the possibility of channeling in the packed bed tests. Finally, since the experimental program required several thousand pounds of each polymer, cost and availability was a factor.

These requirements narrowed the materials of choice to five; i.e., polyethylene, polypropylene, poly-(ethylene terephthalate), polystyrene and poly(methyl methacrylate). PET was eliminated based upon its sensitivity to moisture in melt processing which requires sophisticated screws and vacuum degassing (123). Sample quantities of various grades of the other candidates were procured, blended either as pellets or ground, and pressed into sheets in a laboratory press. Ease of fabrication and visual uniformity were noted.

Ultimately, specific commercial grades of polystyrene and poly(methyl methacrylate) were selected for study. These gave the most uniform pressed sheets, were least sensitive to melt temperature conditions, were both amorphous polymers, and were available at comparable melt indices.

Polystyrene. Polystyrene (PS) is a linear, amorphous, thermoplastic polymer formed by the peroxide-catalyzed free radical polymerization of styrene monomer. The structure of the polymer may be represented as

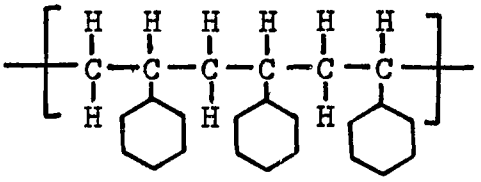

Polystyrene is clear, transparent and reasonably thermally stable. Commercial polymer grades are atactic.

Typically, pure styrene monomer is prepolymerized in a stirred vessel with a peroxide initiator to a solution containing about 30% polymer. The viscous syrup is transferred to the top of a cylindrical tower where polymerization is completed through an increasing temperature gradient to the bottom of the tower where molten polymer is fed to the extrusion, cooling and chopping operations. In addition to pure styrene polymer, many derivatives including acrylonitrile-butadiene-styrene (ABS) and styrene-butadiene-rubber (SBR) resins are prepared. Uses include packaging, appliances, toys, lighting fixtures and others.

General properties of polystyrene are summarized in Table I. The commercial polymer used in this study

was manufactured by The Dow Chemical Company and designated as Styron® 678. This material is referred to hereafter as PS-678. Resin properties of commercial significance are summarized in Table II. This molding compound was supplied as one eighth inch pellets.

Poly(methyl methacrylate). Poly(methyl methacrylate) (PMMA) is likewise a linear, amorphous, thermoplastic polymer noted for its optical clarity and resistance to weathering and ultraviolet degradation. The polymer structure may be represented as

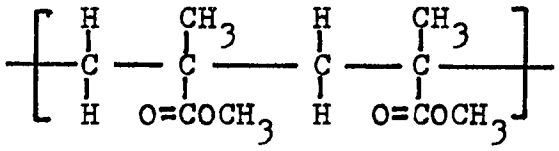

Commercial preparation is by bulk or suspension polymerization of methyl methacrylate monomer. Suspension polymerization is often preferred when possible (as for molding powders) since the reaction is highly exothermic and difficult to control in bulk. Typical commercial polymer is 70 to 75% syndiotactic. PMMA is clear, transparent and offers better impact strength than polystyrene. Sheets, rods, tubes and molded parts are usual product forms. Applications include automotive lenses and signs where outdoor exposure is required, as well as jewelry and decorative objects.

Table I

Physical Properties of PS and PMMA

Property	Polystyrene	Poly(methyl-methacrylate)
Structure (4)	$-[-CH_2-CH(C_6H_6)-]-$	$-[-CH_2-C(CH_3)(\overset{O}{\overset{\|}{C}}OCH_3)-]-$
Specific Gravity (1, 2)	1.04-1.09	1.17-1.20
Clarity (2)	Transparent	Transparent
Tacticity (1)	Atactic	70-75% Syndiotactic
Melt Transition, °K (2, 3)	378	433
Glass Transition, °K (2, 3)	354, 373	408
Solubility Parameter $(cal/cm^3)^{\frac{1}{2}}$ (1)	8.6	9.1
Heat Deflection Temperature, °F @ 264 psi (1)	220	155-210

Sources:

1. Billmeyer, F.W., Textbook of Polymer Science, New York: John Wiley and Sons, Inc., 2nd ed., 1971, pp. 25, 230, 404-414, 504,506.

2. Polymer Handbook, J. Brandrup and E.H. Immergut (eds.) New York: John Wiley and Sons, Inc., 1966.

3. Rheology - Theory and Applications - Volume 1, F.R. Eirich (ed.), New York: Academic Press, 1969, p. 453.

4. Ibid., Volume 2, pp. 172-174.

Table II

Commercial Specifications of PS-678 and PMMA-VM

Property	PS-678	PMMA-VM
Lot Nos.	FK 01105 FF 10912	7-11103 7-11112 7-15196
Specific Gravity	1.04	1.18
Deflection Temperature @ 264 psi, °F	177	182
Vicat Softening Point °F	194	190
Melt Viscosity, poise	800	--
Melt Index, g/10min	18.0	15.0
Flow Temperature, °F	--	284
Processing	Injection	Injection
Form	$\frac{1}{8}$"pellets	$\frac{1}{8}$"pellets

Data from respective product specification brochures for Styron®678, The Dow Chemical Company and Plexiglas® VM, Rohm and Haas Company.

The properties of PMMA are given in Table I. A Rohm and Haas Company acrylic molding powder designated Plexiglas® VM was used in this study. This material is referred to as PMMA-VM. Significant commercial processing properties are given in Table II. As with the PS-678, the molding powder was supplied as one eighth inch pellets.

The similarities of the two polymers are readily apparent in Tables I and II. Thermal transitions, solubility parameters, non-crystalline structure, carbon backbone, product form and recommended uses are all similar for the two materials. While no quantitative measure of compatibility was attempted, the uniform, homogenous visual appearance of the melt blends qualitatively confirmed that the polymers were of a common type.

Before use in either the rheogoniometer or packed bed tests, the polymers were blended (if required) and dried for a minimum of two hours at 85 °C under 45 mm of mercury vacuum in a Patterson-Kelly "V" type blender. Approximately 150 pounds of the molding powder could be dried in a batch. The dried and blended materials were stored in plastic bags in sealed cans prior to use. No evidence of bubbles or other moisture-related

problems was observed in the melts. The further preparation of samples for use in the rheometer tests is described below.

Equipment and Procedures

Preparation of thin sheets of the polymers in a laboratory hydraulic press as samples for the rheological testing is described below. The modified Model R-18 instrument and the experimental procedure are briefly reviewed.

Small quantities of the previously dried pure polymers were separately ground in a Wiley mill with dry ice to prevent softening due to the heat generated. Several sieve fractions of each polymer were collected. The finest fraction passed through a No. 30 sieve using a Tyler Ro-Tap shaker. Maximum particle size for this fraction was 595 microns. This fraction was vacuum dried and blended as appropriate to press into sheets.

The Carver press plate apparatus used to prepare the samples is shown in Appendix Figure B-1. Briefly, the resin powder was placed between two polished nickel-plated press plates separated by a copper shim. This sandwich was heated to 190 to 200°C and pressed up to 10,000 psig between the platens of the Carver

press. After cooling under pressure, a uniform, bubble-free sheet five inches square and 0.030 inches thick was obtained. One inch diameter disks were punched from the sheets and stored in a desiccator prior to testing.

The theory and practice of rheological characterization using the Roberts-Weissenberg cone and plate rheogoniometer are well documented. References include work by Fredrickson (34), Jobling (57), McKennell (67), Eirich (87), Van Wazer (117) and Weissenberg (120). The particular instrument used for this study was equipped with a heated, inert gas-purged chamber surrounding the cone and plate to allow testing in the melt. The upper cone was heated and thermostated. Temperature could be maintained within $\pm 1\,^{\circ}C$ of a target value during a test.

A glass port was provided so that the sample was observable throughout testing. Breakup at high shear rates ($\sim 20\ sec^{-1}$) was thus visually indicated by a distorted edge appearance as well as by erratic deflection readings. In general, shear rates from about 0.002 to 20 sec^{-1} were scanned in geometric doubling steps. Stepwise changes in shear rate were set by a gearbox driven by a constant speed DC motor. Complete

specifications for the rheogoniometer are given in Appendix Table B-I.

Results and Analysis

The experimental plan for the rheogoniometer tests is presented in Table III. The two pure polymers plus 3:1 and 1:1 blends of each with the other were tested over a four decade range of shear rate at 180 to 220°C in 10 degree increments. Three separate tests of each blend/temperature combination were conducted. Both shear and normal stress measurements were taken. The normal force results are included in the complete data summary in Appendix D, but do not otherwise appear in the text or analysis. Due to the large volume of data, only the average of the three replicates of each blend/temperature is tabulated. The relationships for calculating shear rate and shear and normal stresses from the rheogoniometer readings are given in Appendix Table B-I.

Figures 1, 2, and 3 show typical τ versus $\dot{\gamma}$ curves for pure PMMA-VM, 50/50 PMMA/PS and pure PS-678, respectively. The non-Newtonian behavior of each material is evident. Further, the blend follows the same pattern as the pure polymers. Dashed extensions are based on Huang model fit of the data.

Table III

Rheological Experiments

Materials:	100% PMMA-VM 100% PS-678 75/25 PMMA/PS 50/50 PMMA/PS 25/75 PMMA/PS
Temperature, °C :	180 190 200 210 220
Shear Rate, sec^{-1} :	0.002 to 20
Reproducibility:	Three replicates per experimental condition
Responses:	Load cell deflections corresponding to shear and normal stresses

Figure 1

Rheogoniometer Results for 100% PMMA-VM

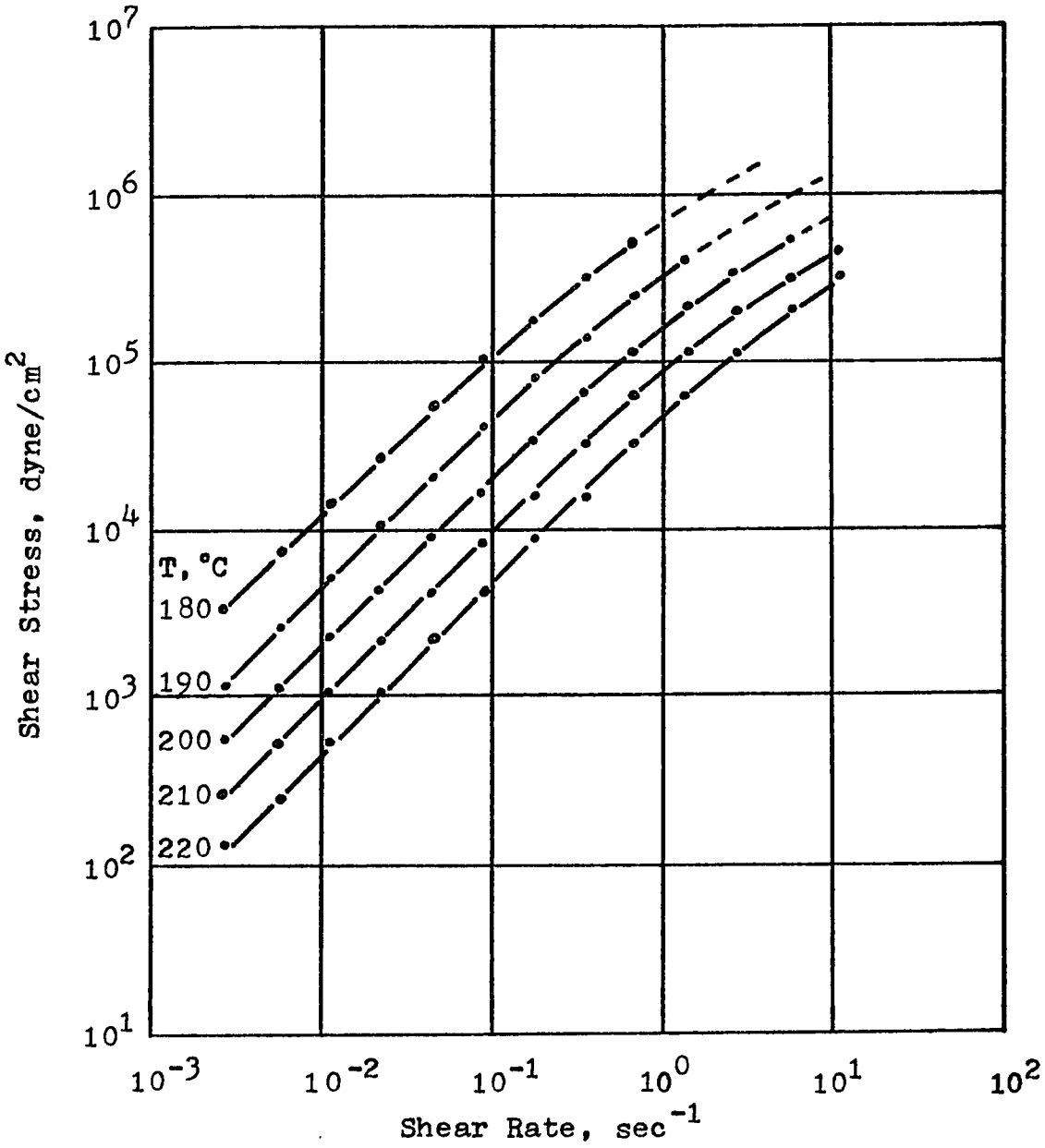

Figure 2

Rheogoniometer Results for 50/50 PMMA/PS

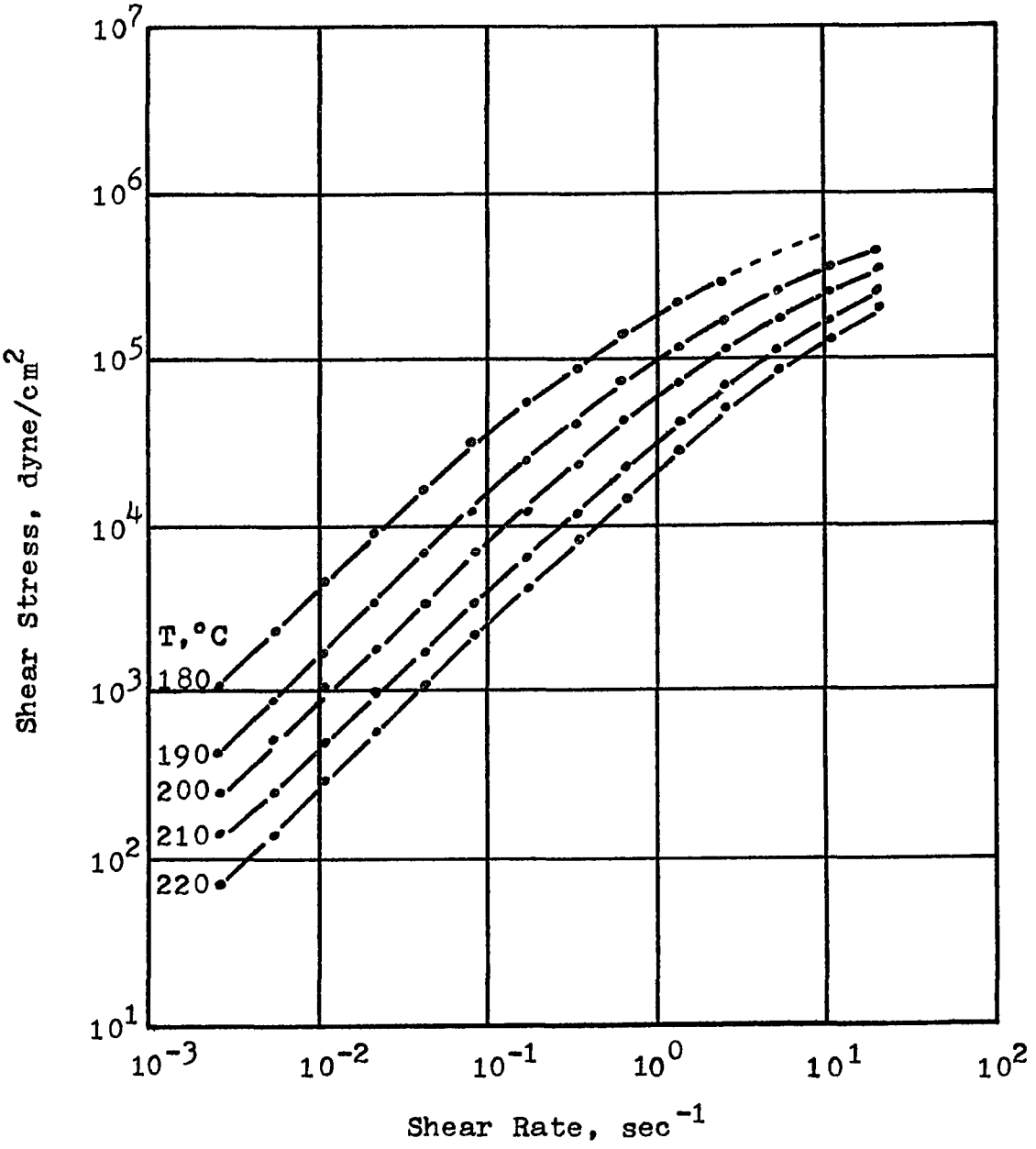

Figure 3

Rheogoniometer Results for 100% PS-678

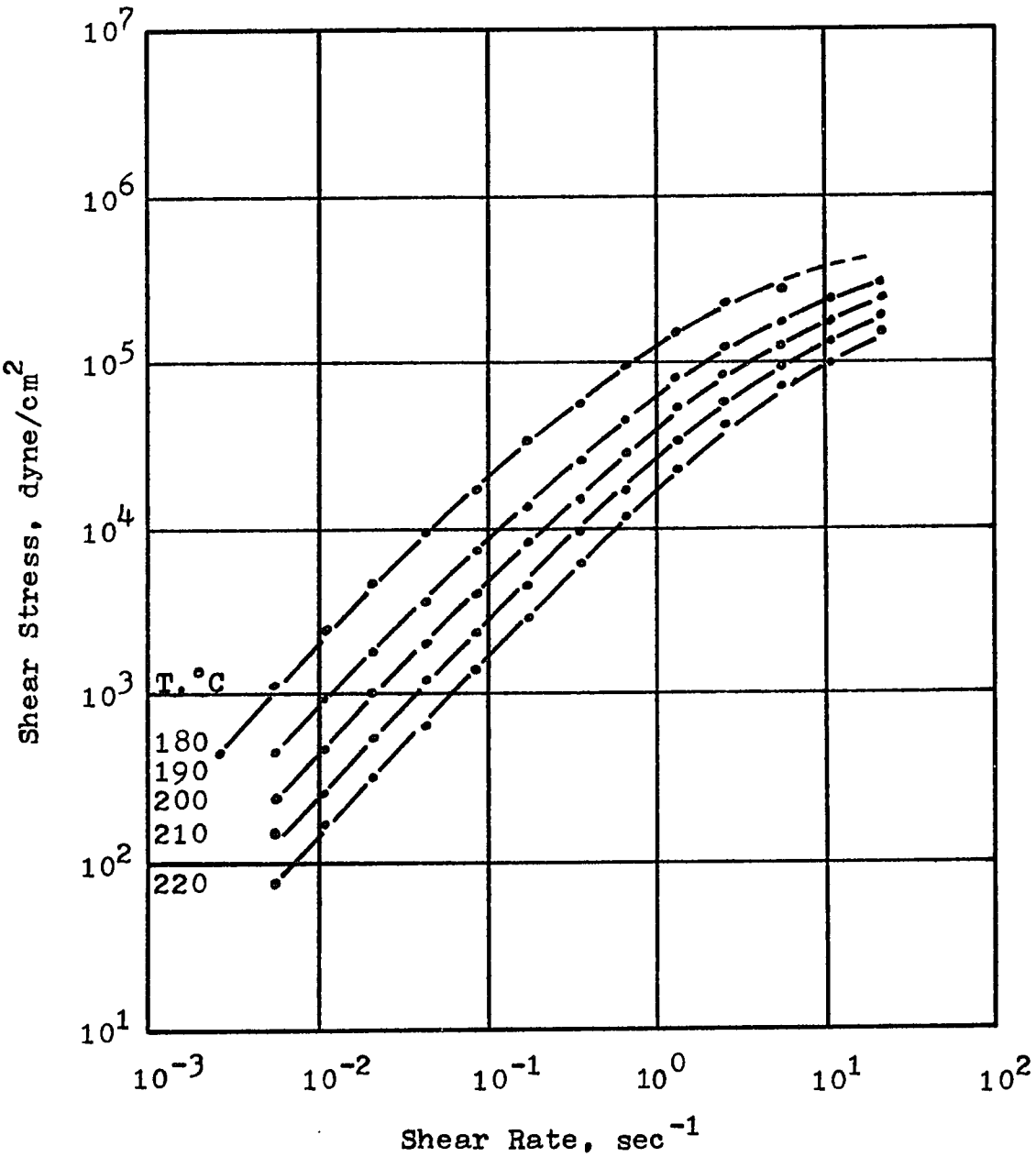

Figure 4 is a cross plot of τ on temperature at several values of $\dot{\gamma}$ for 50/50 PMMA/PS. As shear rate increased, the effect of temperature on shear stress was proportionately less.

Figure 5 is yet another type of plot in which the effect of blend composition on shear stress is shown at a constant temperature (200°C) for several shear rates. In spite of the attempt to match the rheological behavior of the two polymers, the PMMA-VM exhibited significantly higher stress at a given temperature and shear rate than the PS-678. Further, the blends did not fall linearly between the two pure components. The PS-678 had a disproportionate effect in stress reduction for a given concentration. Related behavior in the packed bed will be highlighted in Chapter IV.

The data were fitted to several of the rheological models including the power law, Ellis and Huang equations. Parameters for the Ellis and Huang models are summarized in Tables IV and V, respectively. For the Ellis equation the parameters correspond to an alternate form of (II.11); i.e.,

$$\Delta_{ij} = -\frac{1}{\eta_0}\left[1 + \left(\frac{\tau_{ij}}{\tau_{\frac{1}{2}}}\right)^{\alpha-1}\right]\tau_{ij} \qquad \text{(III.1)}$$

Figure 4

Effect of Temperature on Shear Stress

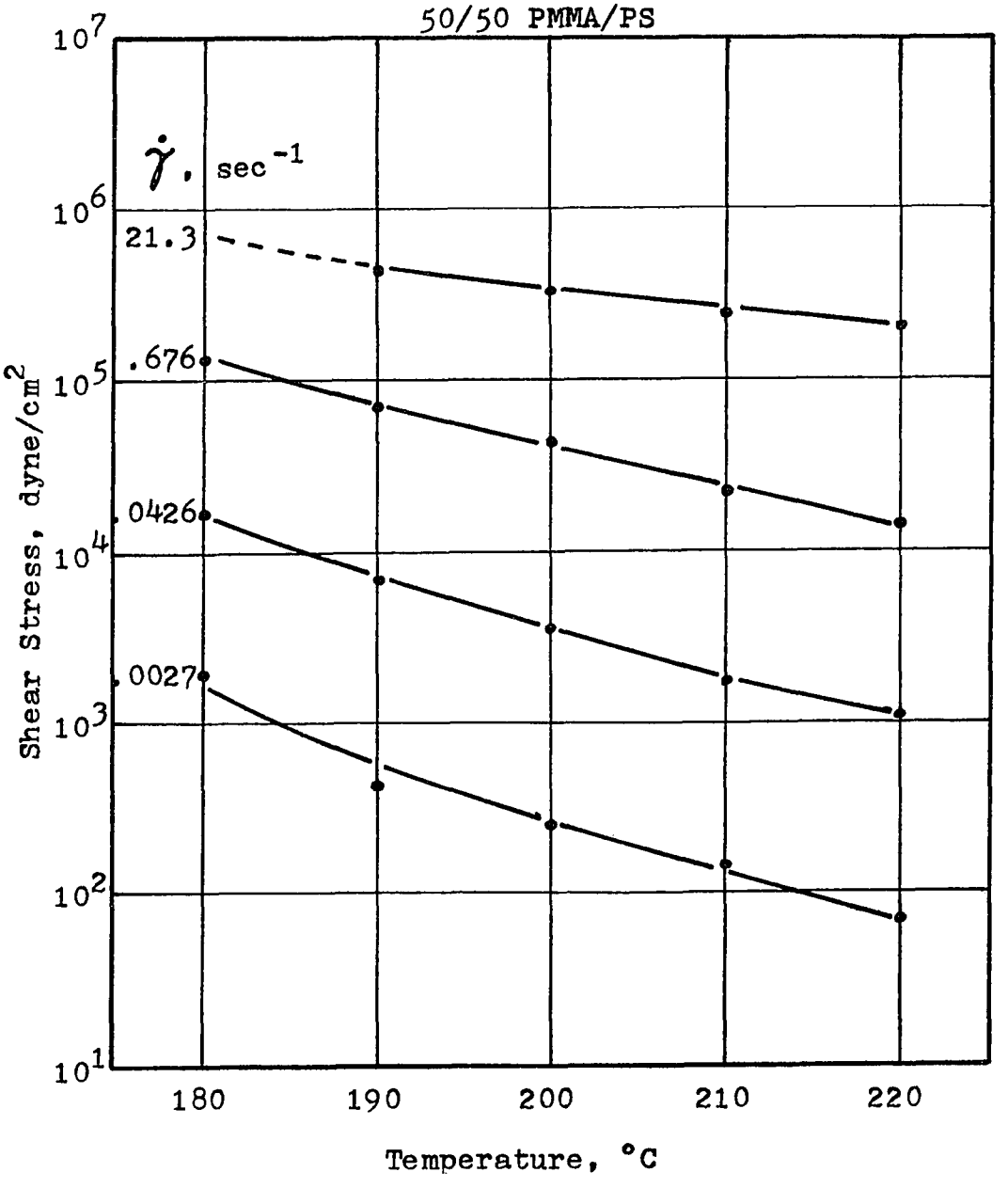

Figure 5

Effect of Material Composition on Shear Stress

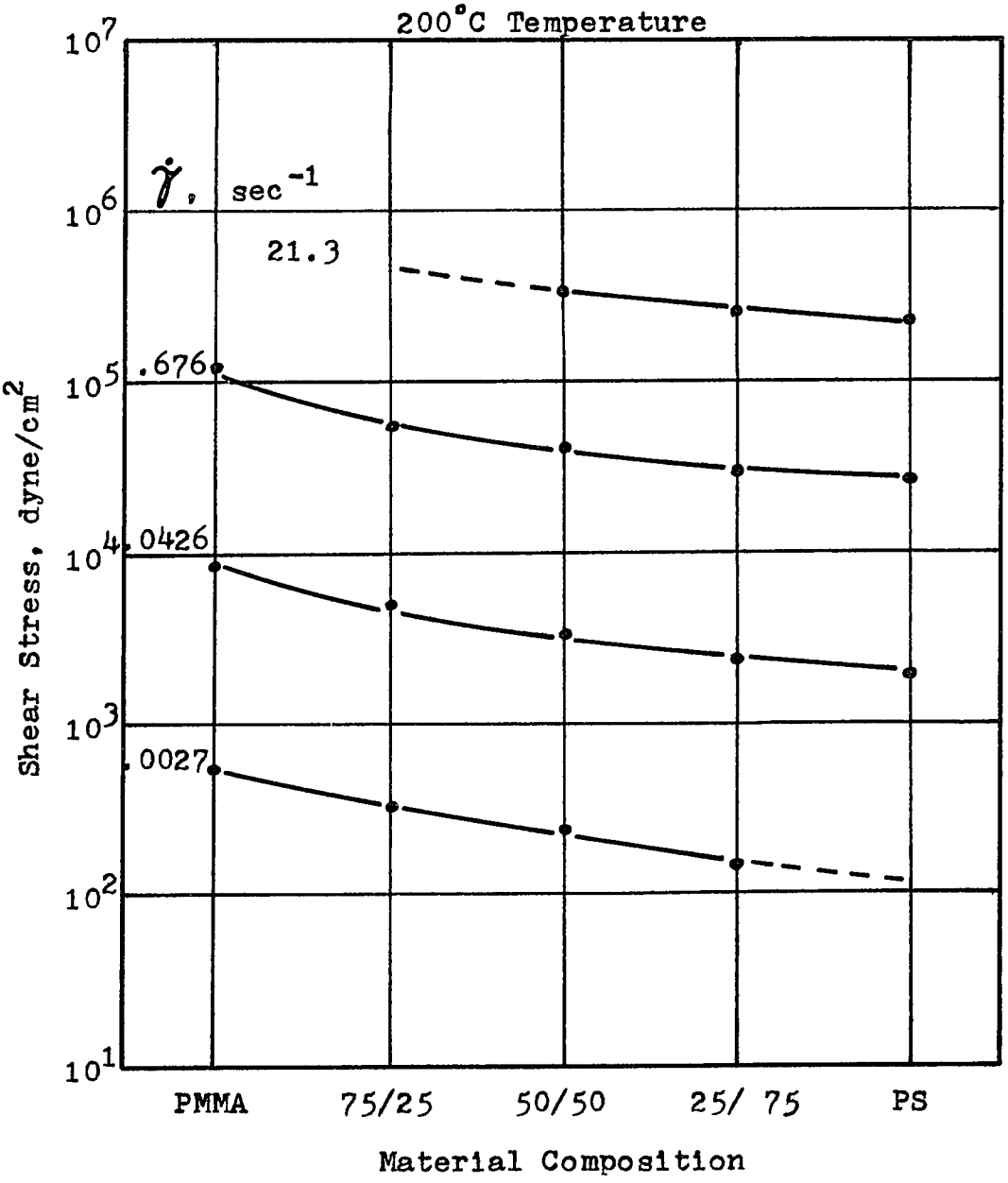

Table IV

Ellis Rheological Equation Parameters

Test Material	Parameter	Temperature, °C 180	190	200	210	220
100% PMMA-VM	η_0	1,401,000	498,900	209,000	99,700	49,800
	$\tau_{\frac{1}{2}}$	704,000	580,200	486,500	432,300	416,000
	α	2.31	2.25	2.34	2.39	2.46
75/25 PMMA/PS	η_0	613,400	311,600	134,400	67,700	40,800
	$\tau_{\frac{1}{2}}$	138,400	147,400	142,600	148,600	108,900
	α	2.71	2.63	2.48	2.43	2.23
50/50 PMMA/PS	η_0	457,300	171,900	98,200	54,300	27,300
	$\tau_{\frac{1}{2}}$	117,400	128,600	107,600	72,900	129,300
	α	2.52	2.73	2.49	2.11	2.30
25/75 PMMA/PS	η_0	232,000	107,700	57,300	34,800	21,500
	$\tau_{\frac{1}{2}}$	136,900	108,200	123,300	106,200	104,100
	α	2.67	2.44	2.47	2.26	2.16
100% PS-678	η_0	224,200	90,100	47,900	27,800	16,900
	$\tau_{\frac{1}{2}}$	152,900	129,700	135,500	134,400	124,000
	α	3.17	2.99	2.86	2.81	2.70

Table V

Huang Rheological Equation Parameters

Test Material	Parameter	Temperature, °C 180	190	200	210	220
100% PMMA-VM	A	72,800	47,200	26,900	17,400	11,300
	B	693,000	310,000	149,000	74,000	37,400
	n	.827	.883	.932	.963	.982
	C	.126	.114	.0934	.0767	.0553
75/25 PMMA/PS	A	13,100	11,500	8,220	6,960	4,500
	B	240,000	157,000	75,600	43,400	25,000
	n	.764	.815	.860	.910	.903
	C	.170	.136	.0891	.0750	.0569
50/50 PMMA/PS	A	11,100	7,630	6,130	4,900	4,400
	B	187,000	95,700	56,300	29,000	18,700
	n	.761	.842	.881	.900	.930
	C	.142	.115	.0884	.0695	.0565
25/75 PMMA/PS	A	10,500	8,290	6,320	4,780	3,980
	B	127,000	64,900	38,900	22,600	14,200
	n	.828	.865	.919	.914	.940
	C	.142	.123	.0900	.0693	.0607
100% PS-678	A	8,290	6,170	5,390	4,160	3,480
	B	129,000	61,200	36,500	21,700	13,900
	n	.833	.896	.946	.972	1.01
	C	.145	.112	.0882	.0667	.0607

as given by Bird (6) and Sadowski (91, 92) in which

$$\frac{1}{\eta_0} = \phi_0 \qquad \text{(III.2)}$$

$$\tau_{\frac{1}{2}} = \left| \phi_1 \eta_0 \right|^{\frac{1}{-\alpha+1}} \qquad \text{(III.3)}$$

$$\alpha \equiv \alpha \qquad \text{(III.4)}$$

Using this form, the lower limiting viscosity was estimated from the data as

$$\lim_{\tau \to 0} \eta = \eta_0 \qquad \text{(III.5)}$$

which was assumed to correspond to the straight line portion of the rheological data at low shear rate. Further, $\tau_{\frac{1}{2}}$ was estimated as

$$\tau_{\frac{1}{2}} = \left| \tau \right| \quad @ \quad \eta = \tfrac{1}{2} \eta_0 \qquad \text{(III.6)}$$

The third parameter, α, was estimated by computer simulation. Allowing the computer to estimate all three parameters did not significantly improve the fit of the data and was rejected in preference to the technique described above.

All four parameters in the Huang model were computer-estimated. The computer routine was based on an iterative least squares estimation of the non-linear equation

parameters. The subroutine written to enter data into the main program is included in Appendix C.

The standard error of fit for the Ellis and Huang models is summarized in Table VI. The power law proved markedly inferior to the more powerful three and four constant models and is not included in the comparison. The standard error results show equally good representation of the data with either equation. A representative comparison of the actual results and the predicted curves for both models is provided by Figure 6. The 50/50 PMMA/PS blend at 200°C is shown. Evidently, these models are excellent representations of the experimental results.

These results were used to estimate the appropriate values of the fluid parameters at the temperature of the packed bed flow experiments. In the case of the Huang model, each parameter was plotted as a function of temperature and composition as shown for A in Figure 7. Values of A, B, C, and n estimated for the packed bed analysis are presented in Table VII.

Of the Ellis model constants, only η_0 varied in a consistent manner with temperature. A similar result was reported by Sadowski for the polymer solutions he

Table VI

Standard Error of the Huang and Ellis Equations of State

Equation	Temperature °C	Blend Composition, PMMA/PS 100/0	75/25	50/50	25/75	0/100
Huang	180	.0945	.114	.112	.144	.129
	190	.110	.117	.093	.130	.116
	200	.081	.061	.066	.098	.096
	210	.067	.069	.041	.037	.090
	220	.037	.049	.040	.039	.076
Ellis	180	.094	.197	.185	.076	.148
	190	.056	.143	.141	.073	.076
	200	.061	.134	.149	.059	.046
	210	.021	.089	.157	.067	.046
	220	.023	.117	.050	.052	.076

$$\text{Standard Error} = \left[\frac{\sum_{i=1}^{n} \left(y_{actual} - a - by_{estm} \right)^2}{n-2} \right]^{\frac{1}{2}}$$

Figure 6

Comparison of Huang and Ellis Model Constitutive Equations

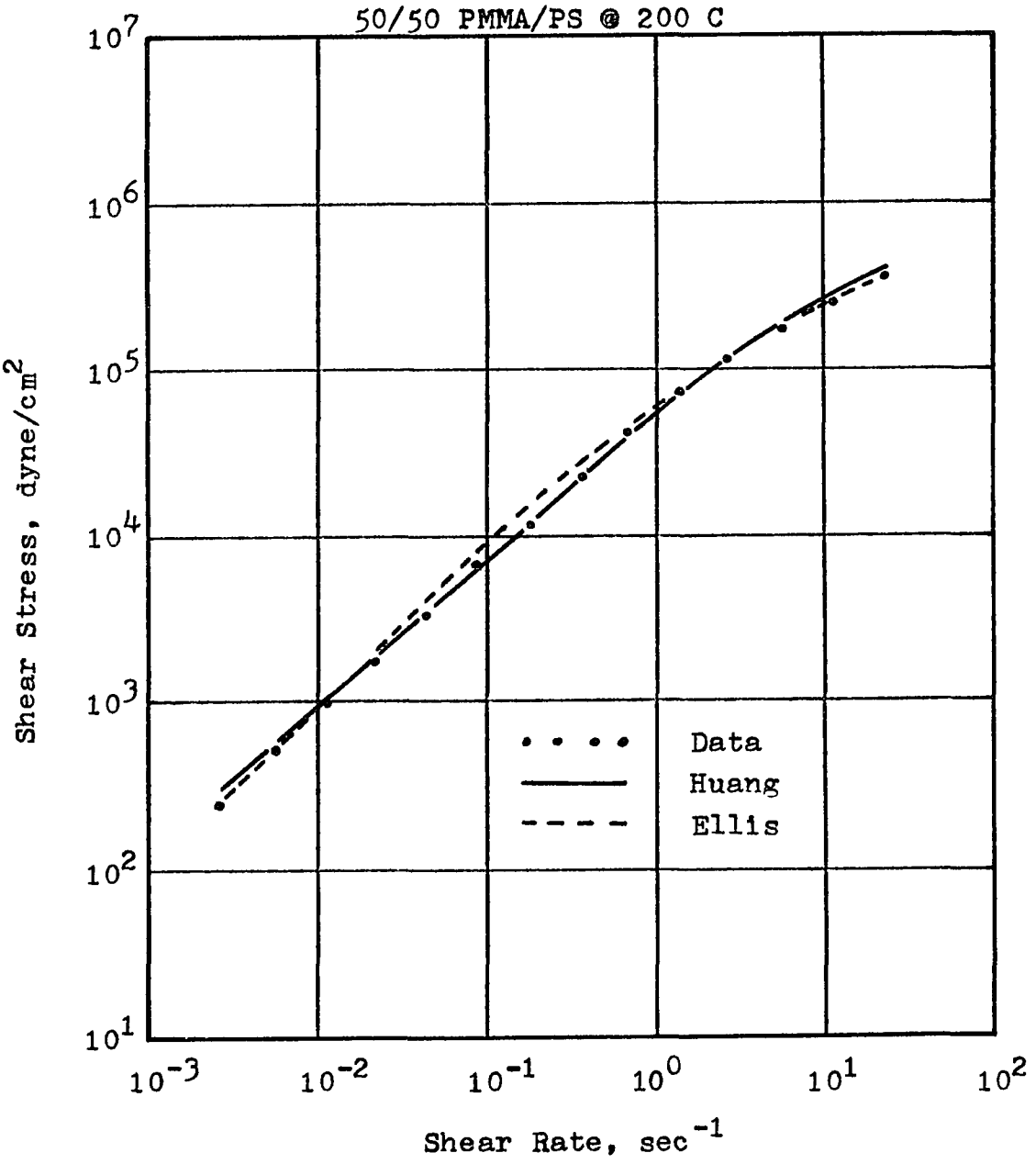

Figure 7

Temperature Dependence of Huang
Model Parameter A

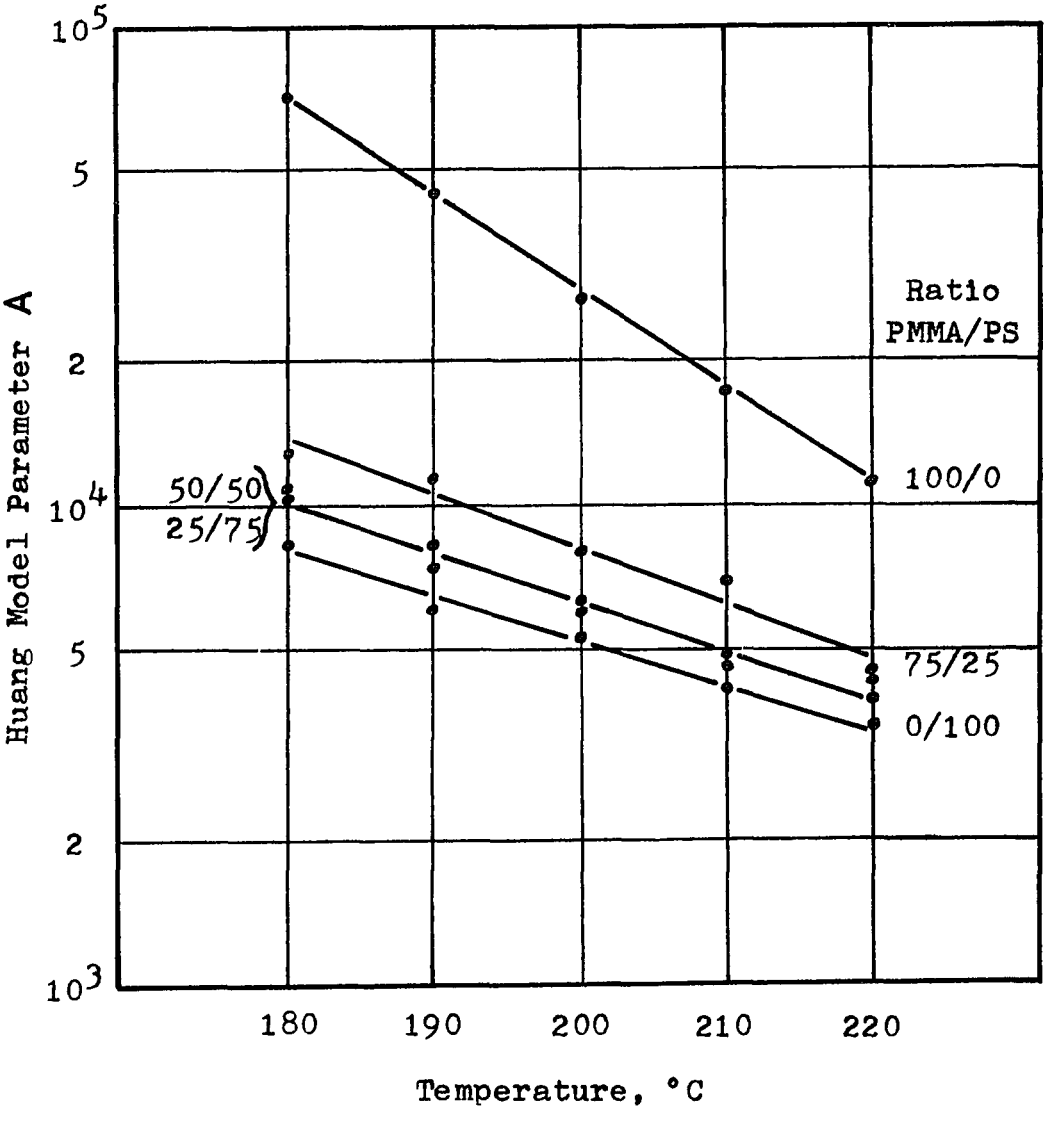

Table VII

Huang Equation Parameters for Packed Beds

Test Material	Temperature Range, °F	Temperature Average, °C	A	B	n	C
100% PMMA-VM	397-400	203.5	24,000	122,000	.945	.088
75/25 PMMA/PS	398-401	204.0	7,400	62,000	.870	.085
50/50 PMMA/PS	397-400	203.5	5,800	46,500	.885	.084
25/75 PMMA/PS	397-400	203.5	5,800	33,000	.910	.082
100% PS-678	397-400	203.5	4,800	32,000	.957	.080

studied at room temperature (91, 92). Thus, the estimates of η_0 in Table VIII were made in an analogous manner to the Huang constants, but $\tau_{\frac{1}{2}}$ and α values are arithmetic averages of the five separate rheological test results over the temperature range. A single exception is the value of $\tau_{\frac{1}{2}}$ for PMMA which was graphically estimated.

An independent check of these results has been provided by Han, et al (45) who combined them with capillary rheometer data for the same polymers and blends. The combined data covered the shear rate range from 10^{-2} to 10^{3} sec^{-1} and demonstrated excellent agreement of the two sets of results.

Table VIII

Ellis Equation Parameters for Packed Beds

Test Material	Temperature Range, °F	Temperature Average, °C	η_0	$\tau_{\frac{1}{2}}$	α
100% PMMA-VM	397-400	203.5	1.65×10^5	4.60×10^5	2.35
75/25 PMMA/PS	398-401	204.0	1.05×10^5	1.37×10^5	2.50
50/50 PMMA/PS	397-400	203.5	$.76 \times 10^5$	1.11×10^5	2.43
25/75 PMMA/PS	397-400	203.5	$.48 \times 10^5$	1.16×10^5	2.40
100% PS-678	397-400	203.5	$.39 \times 10^5$	1.35×10^5	2.85

CHAPTER IV. PACKED BED EXPERIMENTS

The packed bed test equipment for this study was designed, fabricated and instrumented to provide a complete and accurate characterization of the polymers in a commercial scale flow regime. A description of the major system components and the test procedures is given below. Results of the tests are reviewed and analyzed. The theoretical porous media flow model developed for the Huang rheological equation of state is tested using these data.

Materials

The five polymer systems characterized rheologically were also examined in the packed bed experiments. All tests were conducted at about 204°C. Reasonable flow rates and pressures were achieved at this temperature. Initial testing at temperatures up to 225°C resulted in polymer degradation due to the retention time-at-temperature of about 1.5 hours, average.

The pressure and temperature dependence for each polymer and blend was required in the analysis of the packed bed data. This information is summarized in Table B-II and Figure B-2, Appendix B. A blend density was assumed proportional to the weight fraction of each component, since the polymers are basically viewed as

incompatible. Thus, no volume change on mixing would be expected.

A description of the glass beads used for the bed packings is given in Table IX. The beads were high quality blast beads selected to provide a tenfold range of particle size. Maximum particle-to-bed diameter ratio was about 0.1. A complete description of the beads including the manufacturer's specifications is given in Appendix Table B-III.

Equipment and Procedures

A simple schematic of the major components of the melt extrusion system is shown in Figure 8. The associated hot oil circulation system is represented in Figure 9. Polymer was melted and extruded at constant pressure from the Prodex extruder to the Zenith metering pump. The molten polymer was metered by the pump through a long lead pipe section to the inlet pressure transducer, through the packed bed to the outlet pressure transducer and through the trailing pipe section to an exit nozzle. Flow rate was conveniently measured by direct weighing of timed samples caught at this nozzle. Temperature was potentiometrically measured at several points both in the oil circulation system and in the melt to assure uniformity. The pressure trans-

Table IX

Description of Glass Bead Packings

Designation	Nominal Size, cm	Average Diameter, cm	Average Density g/cm^3	Diameter Ratio to Test Section D/D_p
V-390	0.96-1.05	0.979	2.533	10.52
V-280	0.66-0.75	0.679	2.922	15.16
V-1607	0.34-0.40	0.375	2.947	27.45
V-080	0.14-0.20	0.198	2.942	51.99
P-047	0.07-0.12	0.117	2.468	87.99

Glass beads manufactured by Potters Bros. Inc., Carlstadt, NJ.

Test section diameter 4.053 in. or 10.295 cm.

Figure 8

Packed Bed Experimental Apparatus

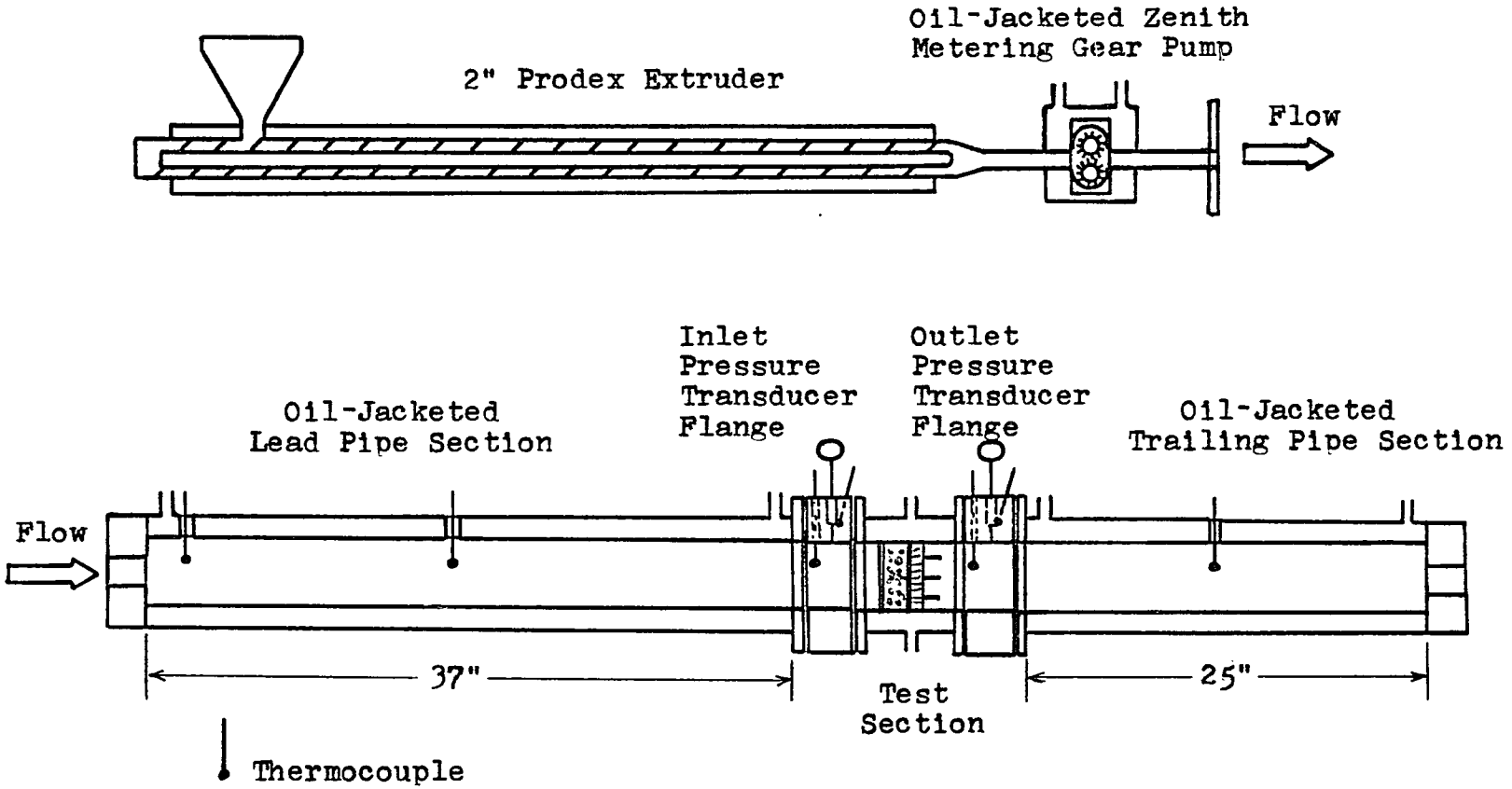

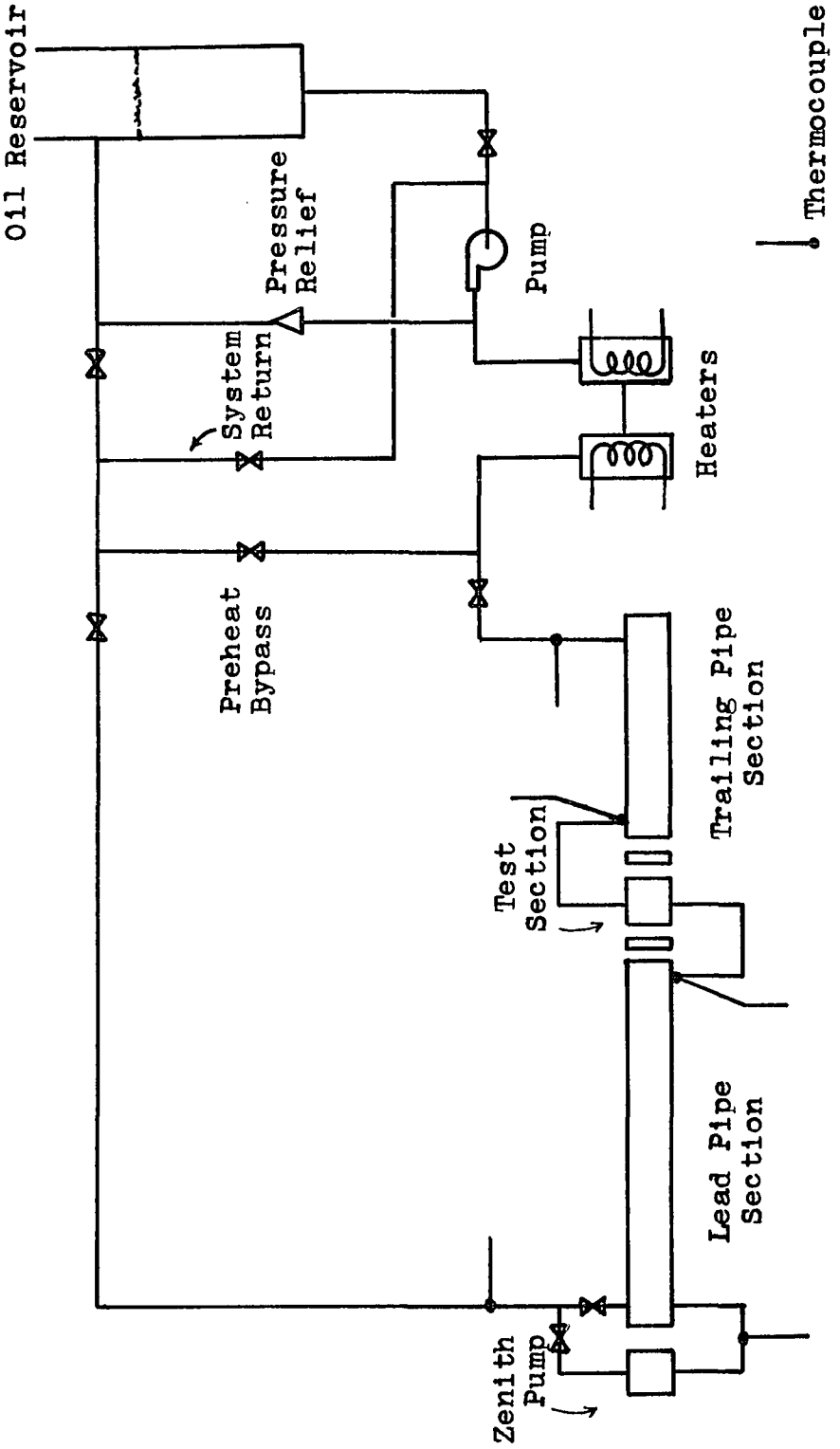

Figure 9

Hot Oil Circulation System

ducers were connected to transmitters which read out on mercury manometers. Both inlet and outlet gauge pressures and the differential between them were measured.

The extruder was a two inch Prodex equipped with a metering type screw and a 24/1 length/diameter ratio barrel. Dried polymer was hand fed to the hopper which was continuously heated by two lamps to minimize moisture regain. Melt temperature was controlled in three resistance heated zones to closely match the test piping temperature. Small diameter piping to the Zenith pump was also resistance heated and insulated.

The Zenith pump was a two gear Type HLB-4729 staple fiber hot pump with a nominal 20 cc/rev delivery. The pump was enclosed in a hot oil-fed, insulated aluminum block to maintain constant temperature.

Exiting the Zenith pump, the melt entered the main piping system. Leading and trailing section flow channel size was 3.83 inches diameter corresponding to the actual ID of nominal 4 inch, schedule 80 pipe. Both sections were fully oil-jacketed and were approximately 37 and 25 inches long, respectively. Thermocouple ports were provided in each, both in the annular oil chamber and communicating with the flow channel. Maximum

Reynolds numbers of the order of 10^{-4} are estimated for these pipe sections which were intended primarily to promote fully developed laminar flow entering and exiting the test section.

The pressure transducers were mounted in specially designed solid steel flanges, one on either side of the test section. Temperature at the transducer sensor and in the melt flow was measured in each flange. The flanges were not oil-jacketed, but were heavily insulated. Temperature difference between the transducers was generally about 1°C and did not exceed 2°C. The flow temperatures measured in these flanges (one inch radially into the melt) characterized the packed bed temperature. In general, bed inlet temperature was about 1°C lower than outlet temperature. In no case was data taken when this difference exceeded 3.5°C, since significant viscous heating was indicated by such a condition.

The elements of the packed bed are shown schematically in Figure 10. The section was oil-jacketed and was overbored to allow insertion of the sleeves and supports which defined the packed bed. The machined bed diameter was 4.053 inches. Moving in the direction of flow, the section contained a spacer sleeve, outer

Figure 10

Packed Bed Test Section

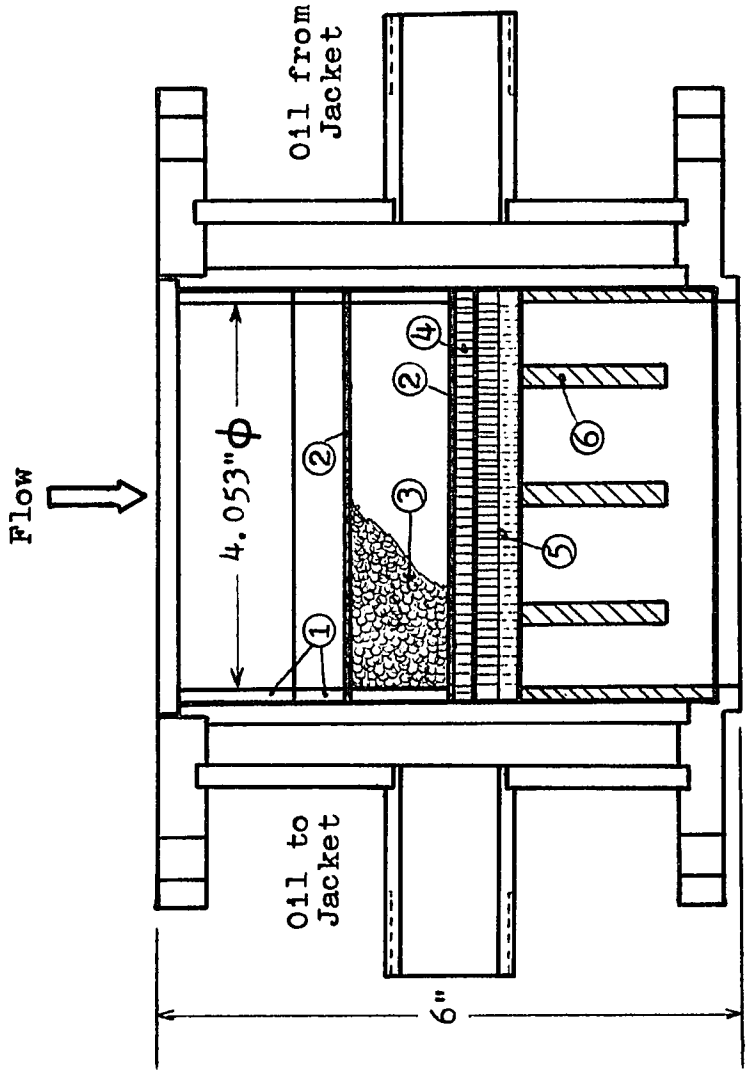

Key: 1. Spacer Sleeves
2. Screens
3. Packing
4. Screen Support
5. Breaker Plate
6. Breaker Plate Support

bead support screen, beads packed in a sleeve, inner bead support screen, perforated metal screen support plate, breaker plate and breaker plate support sleeve. The several support members were found necessary to prevent buckling of the screens which defined the packing space. The contribution of these members to overall pressure drop was accounted in the data analysis by subtracting out their contribution to the pressure difference. Data for this purpose was obtained in blank flow experiments conducted with the supports in place, but without packing. Various combinations of sleeves allowed beds of 1.75, 4.29 and 6.10 cm depth to be tested.

Pressure range of the transducers was 0 to 3000 psig. Each was initially calibrated at temperatures of 27, 160, 200 and 240°C. A special jig to hold both transducer bulbs and connect to an hydraulic dead weight tester was immersed in a constant temperature oil bath for this calibration. Small but real differences in readings between temperatures were recorded for both transducers. The data is given in Appendix Table C-III and Figure C-1. The individual transducer calibration curves at 200°C were used in the packed bed tests to convert manometer readings to psig pressure units.

Average absolute error in the net pressure difference values was calculated to be ±7 psig.

Before experimental work was begun, a method was devised to assure that identical packed beds could be repeatedly prepared. For each bed depth and bead size combination, the test section was packed by tapping and shaking until it appeared uniformly full. The beads were then poured out and weighed. This procedure was repeated several times and an average weight determined. A plot of depth versus weight for each bead was thus developed. The exact weight of beads for each bed was taken from the best line through the data points, including the origin. For all packed bed tests, the same weight of beads was used. For the largest beads (.979 cm diameter), a count was used rather than weight. This data is summarized in Table C-IV, Appendix C.

Specification of bed porosity was necessary to calculate the bed friction factor. The porosity, ϵ ,is the void space in the packed bed expressed as a fraction of the total volume of the bed. Since the packed beds were prepared with known weights (or count) of beads, an accurate bead density allowed calculation of bead volume, and void volume by difference with the total volume. The density of each bead size was determined

by displacement of water in a volumetric flask using a modified pycnometer technique. Values of ϵ are reported in Table X. Data for the determination of these values of ϵ are given in Appendix Table C-V.

The experimental procedure required preparation of an appropriate packed bed section, installation of the test section into the piping system, then preheating the system to operating temperature. Flow was begun at a low rate and continued until all temperatures and the pressures equilibrated. Flow was set and verified several times as pressure and temperature readings were recorded. Two or three consecutive sets of readings spanning at least ten minutes and showing no significant variations were accepted as equilibrium data.

Detailed descriptions and specifications for each major piece of equipment discussed above are given in Appendix B. The procedures including calibration of the pressure transducers, packed bed loading and the actual test conduct are detailed in Appendix C.

Results and Analysis

The experimental plan for the packed bed experiments is summarized in Table XI. A total of 59 separate tests were conducted including several complete repli-

Table X

Packed Bed Porosity

Bead Diameter, cm	Bead Weight g/ cm bed depth	Bead Density g/cm^3	Bead Volume cm^3/ cm bed depth	Porosity ϵ
0.979	97.9 (1)	0.492 (2)	48.17	0.421
0.679	147.48	2.922	50.47	0.394
0.375	150.35	2.947	51.02	0.387
0.198	153.94	2.942	52.32	0.371
0.117	130.43	2.468	52.85	0.365

Volume of bed is 83.236 cm^3/cm depth.

1. Number of beads per cm depth.

2. Volume of single bead, based on average diameter.

Table XI. Design of Packed Bed Experiments

Variable	Levels
Test Material	
PMMA, %	100, 75, 50, 25, 0
PS, %	0, 25, 50, 75, 100
Flow Rate, g/min	140, 210, 300, 400, 520
Bead Diameter, cm	.117, .198, .375, .679, .979
Bed Depth, cm	0, 1.75, 4.29, 6.10
Temperature, °F	398

Notes:

1. Total 59 tests (different beds) conducted.
2. PMMA and PS selected for similarities, availability and flowability.
3. Minimum flow rates limited by extruder speed; maximum flow rates limited by pressure developed.
4. Smallest particles limited by estimated pressures; largest particles conformed to guideline of 10/1 bed/bead diameter ratio to avoid wall effects.
5. Bed depth limited by pressure developed.
6. For 0.979 cm diameter beads, bed depths were 1.83 and 4.37 cm.

cations and selected tests at the greatest bed depth. Combinations of conditions in which pressure exceeded 3000 psig or significant viscous heating precluded isothermal equilibrium operation were discarded from the data analysis.

The data summary for the packed bed experiments is given in Appendix E, Tables E-I through E-V. Many readings in addition to those summarized were taken as control points in monitoring the system. A summary of a complete set of test readings is given in Appendix Table C-VI.

Many possibilities for examining such an array of data exist. Checks of trends and consistency are possible by simple graphical representations. Figures 11, 12 and 13 illustrate the basic results in which flow rate through the packed bed is related to pressure drop. Development of high pressures with the PMMA-VM even for large particles (0.679 cm diameter) is indicated in Figure 11. Further, viscous heating effects were particularly restrictive and limited the data obtained for PMMA-VM. Progressively smaller bead sizes are illustrated for 50/50 PMMA/PS in Figure 12 (0.375 cm diameter) and for pure PS-678 in Figure 13 (0.198 cm diameter). Reproducibility of the data is illustrated in Figure 14

Figure 11

Packed Bed Flow Curves for 100% PMMA-VM

V-280 Beads, 0.679 cm Diameter

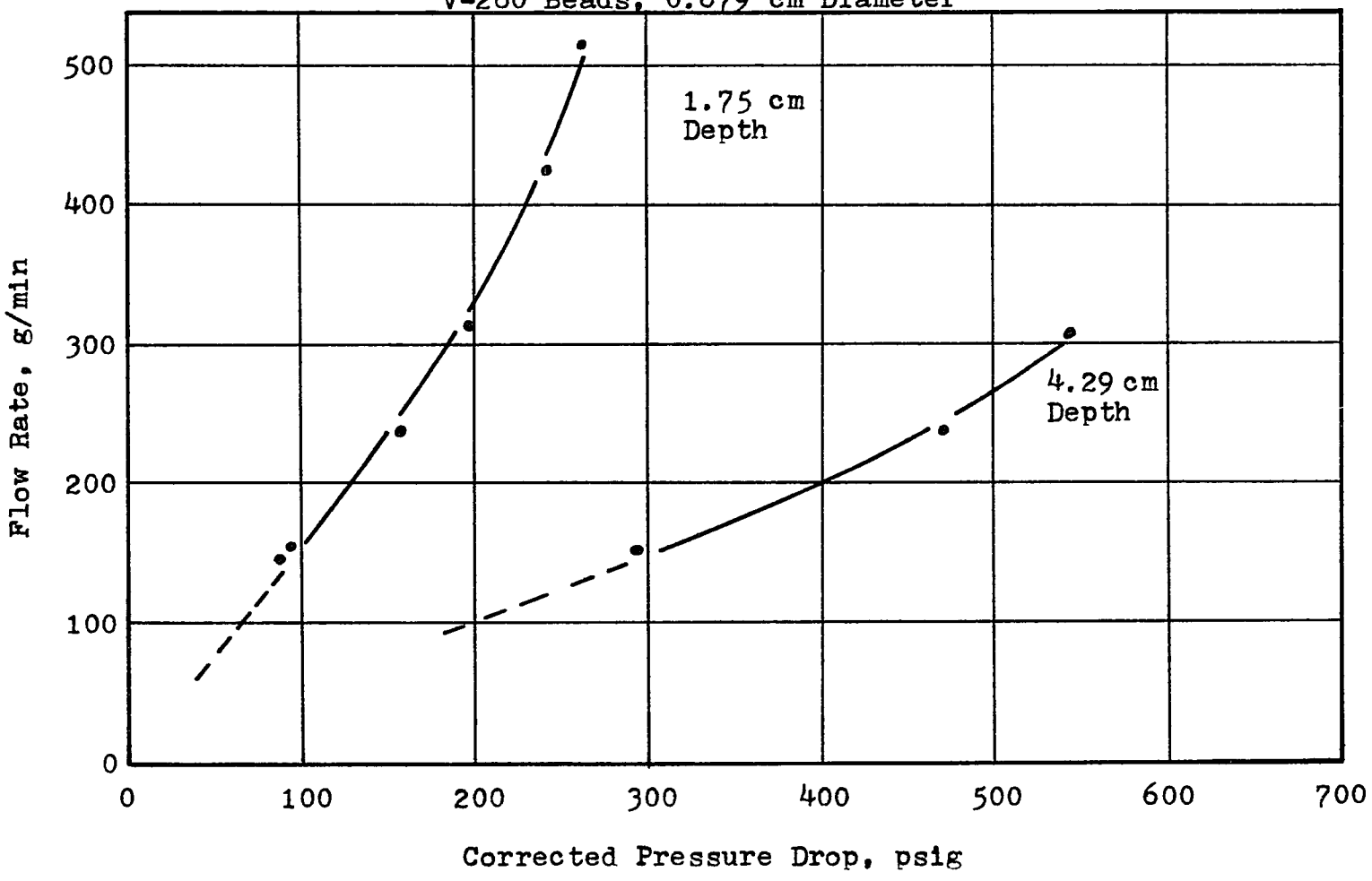

Figure 12

Packed Bed Flow Curves for 50/50 PMMA/PS

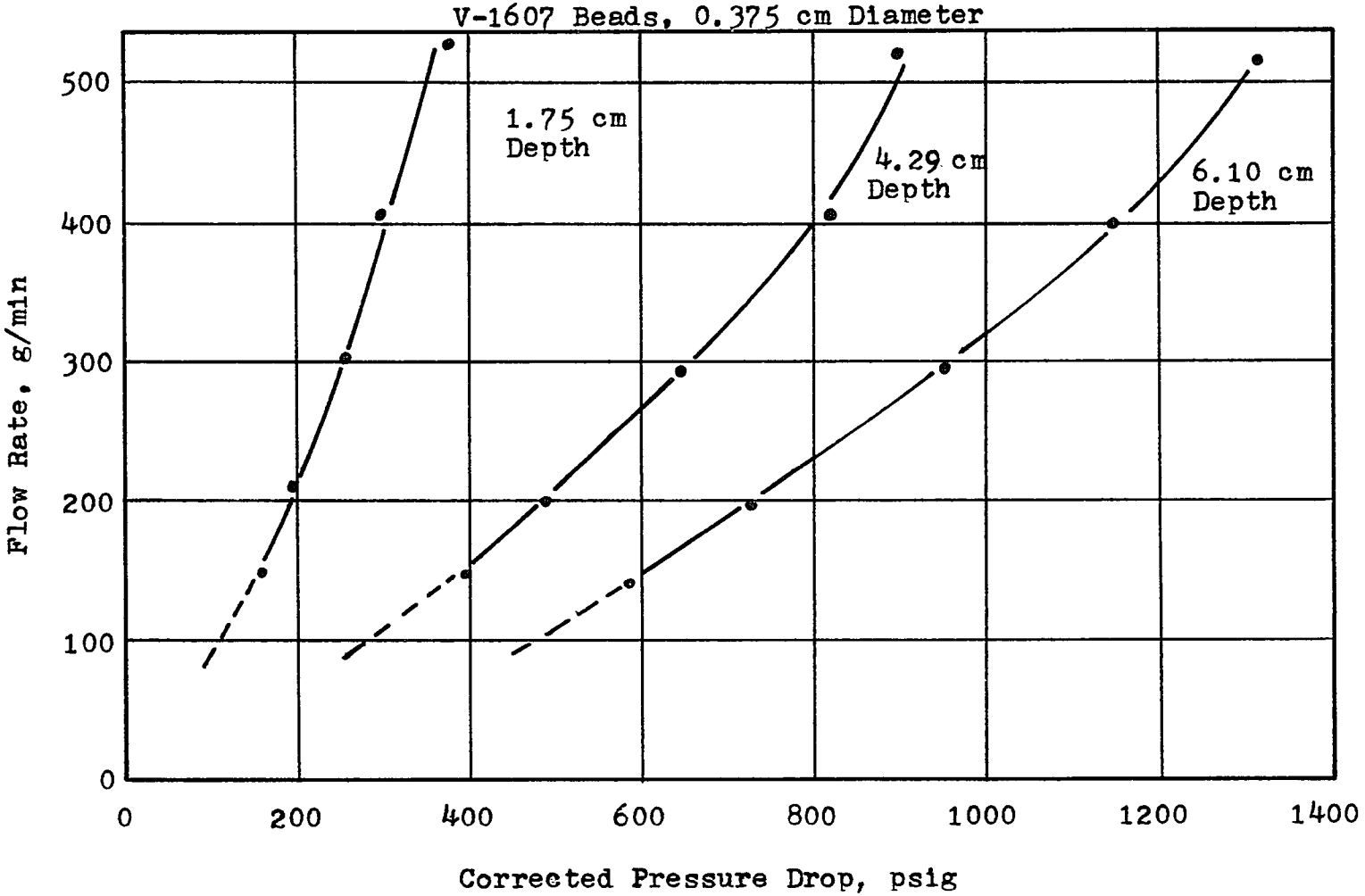

Figure 13

Packed Bed Flow Curves for 100% PS-678

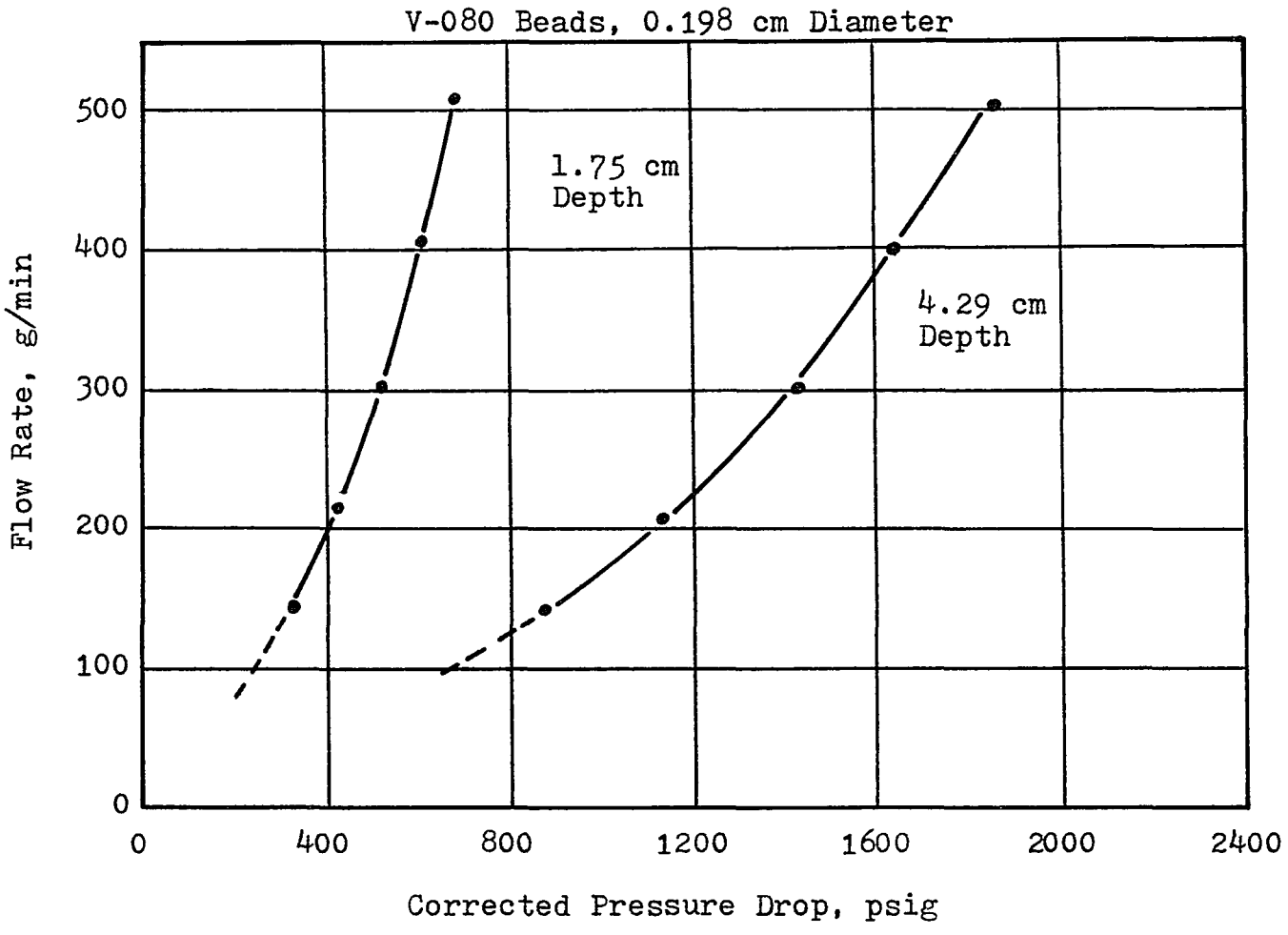

Figure 14

Packed Bed Flow Curves for 50/50 PMMA/PS

V-080 Beads, 0.198 cm Diameter

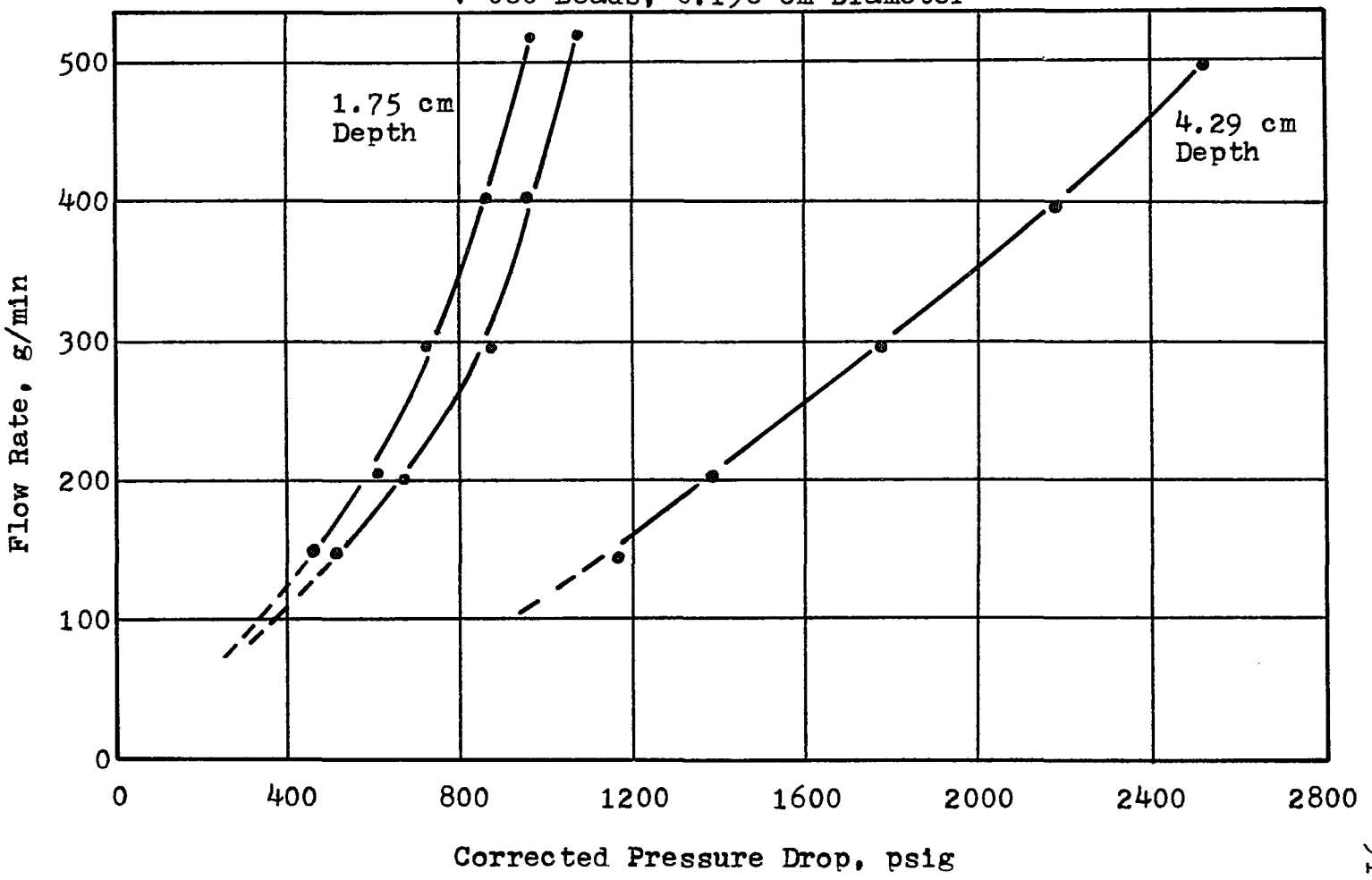

for 50/50 PMMA/PS where the data from two tests (numbers 39 and 46) conducted a week apart are plotted. Average difference in the pressure drop at a given flow rate is 5.5%.

The effect of bead size on pressure drop is illustrated for several flow rates and two packing depths for 50/50 PMMA/PS in Figure 15. For tube flow, pressure drop is directly proportional to tube length and inversely proportional to the square of tube diameter. Thus, at a given pressure drop, the ratio D^2/L is constant, for the same flow. Very nearly the same dependence is calculated for the sets of curves in Figure 15. Similar results were reported for polyethylene by Gregory (37, 38).

The composition dependence for pressure drop is presented in Figure 16. The three largest particle sizes at two intermediate flow rates are shown for a bed depth of 4.29 cm. Addition of relatively small amounts of PS-678 to the blend gives large pressure reductions. This effect is analogous to the stress reduction in the rheological experiments noted in Chapter III, Figure 5. Greater proportional effect is evident at smaller particle size.

Figure 15

Particle Size Dependence of Pressure Drop

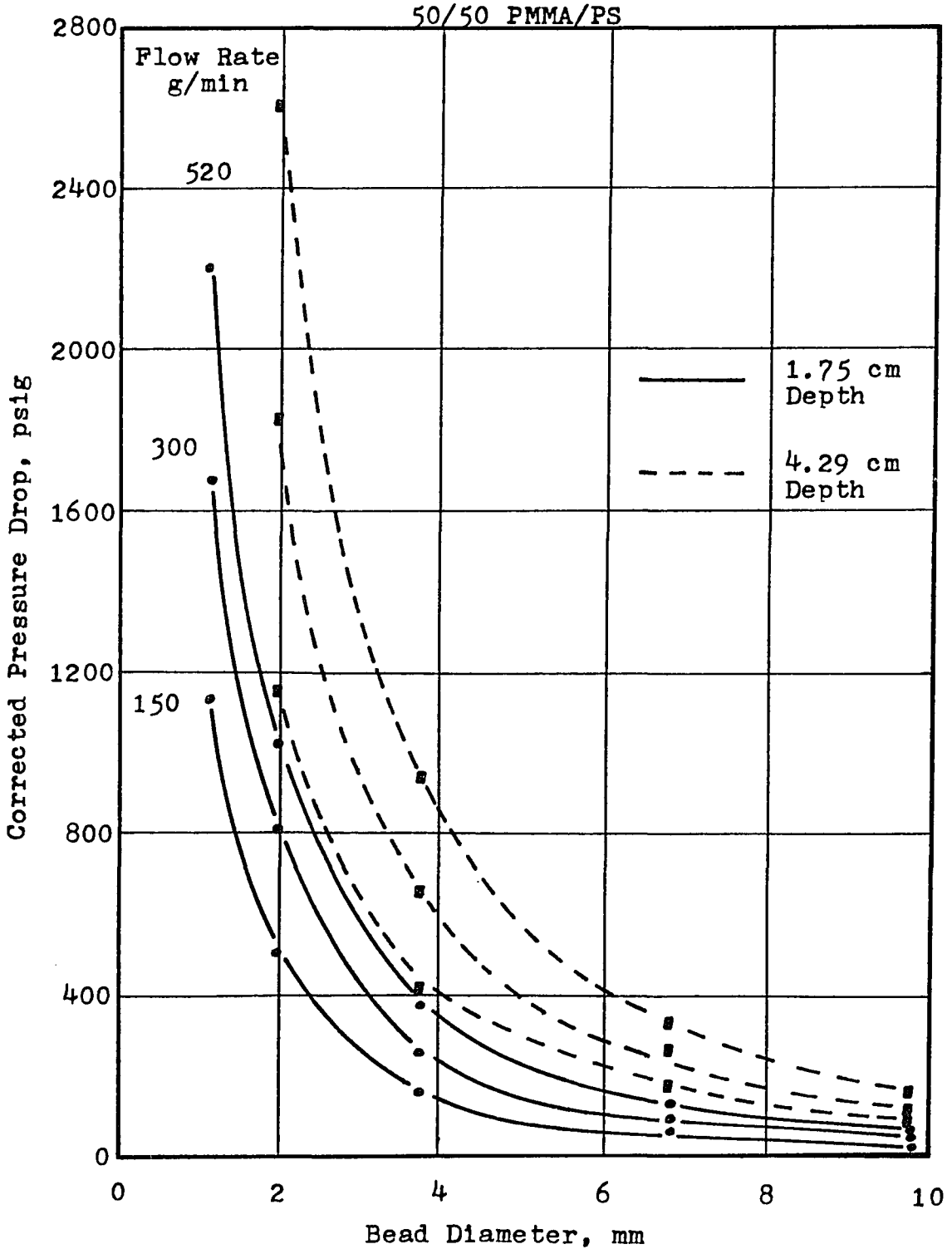

Figure 16

Composition Dependence of Pressure Drop

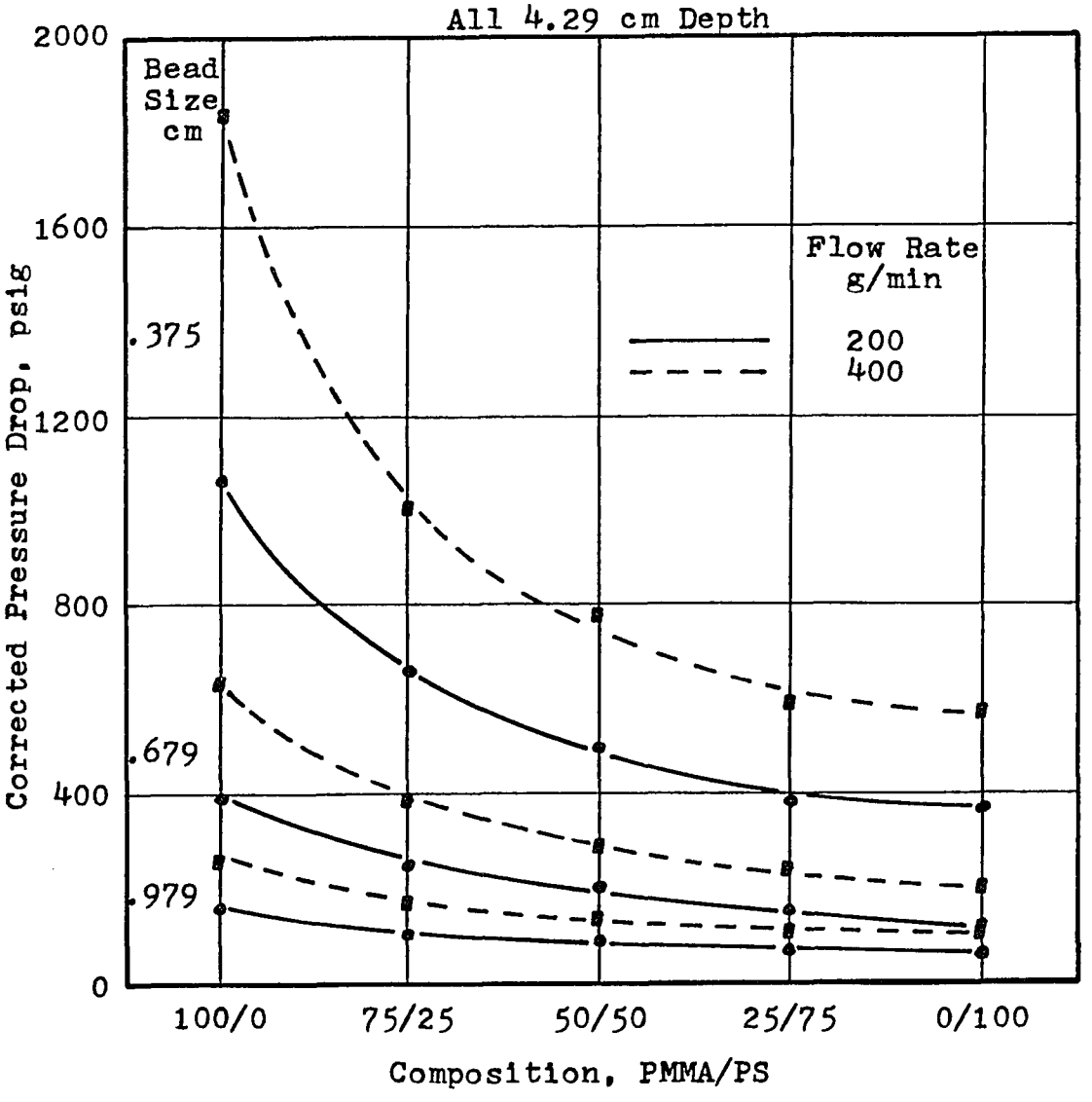

Although examination of the independent effects of each experimental variable on the responses is a useful exercise, it does not adequately represent the total system behavior. Through the friction factor - Reynolds number relationship expressed in equation (II.98), all of the packed bed data may be comprehensively represented. Both the Huang and Ellis model packed bed developments were tested. The latter is of significance primarily as a reference point of demonstrated success in other studies. To review, the friction factor represents the physical characteristics of the porous medium and of the test material, i.e.:

$$f^* = \frac{D_p}{L} \frac{\Delta P}{\rho V_0^2} \frac{\epsilon^3}{1-\epsilon} \qquad \text{(IV.1)}$$

The friction factor is independent of the rheological nature of the fluid. Its product with the Reynolds number is a constant as expressed in (II.98). The effective Reynolds number for packed bed flow is then

$$N_{re,eff} = \frac{D_p V_0 \rho}{(1-\epsilon)\eta_{eff}} \qquad \text{(IV.2)}$$

The particular equation of state selected to represent the rheology of the fluid determines the form of the effective viscosity. η_{eff} for the Huang model was given as (II.99). For the Ellis model, Sadowski gave:

$$\frac{1}{\eta_{eff}} = \frac{1}{\eta_0}\left[1 + \frac{4}{\alpha+3}\left(\frac{\tau_{Rh}}{\tau_{\frac{1}{2}}}\right)^{\alpha-1}\right] \qquad \text{(IV.3)}$$

Huang model results for each individual material are shown in Figures 17 through 21. A summary plot is given in Figure 22 for the Huang model. Only the summary results are presented for the Ellis model in Figure 23. Computer programs were developed to calculate both sets of results. These are detailed in Appendix Tables C-VII and C-VIII. The results given in the figures are tabulated in Appendix F.

The individual materials - both pure polymers and blends - are well represented by equation (II.98). The constant **c** varied among the materials from about **c**=120 for PMMA-VM to a high value of **c**=275 for 75/25 PMMA/PS. For the three blends and pure PS-678, a value of **c**=260 adequately characterizes the total 187 data points. For the Ellis model, **c** is roughly ten units higher than those given above.

Although the value of **c** was described as adjustable to give agreement with experiment, several investigators found values of **c**=150 or 180 for various systems and fluids (19, 35, 38, 92). The origin of these values was in work by Ergun (28) and Carman (15),

Figure 17

Friction Factor-Reynolds Number Correlation

for the Huang Model

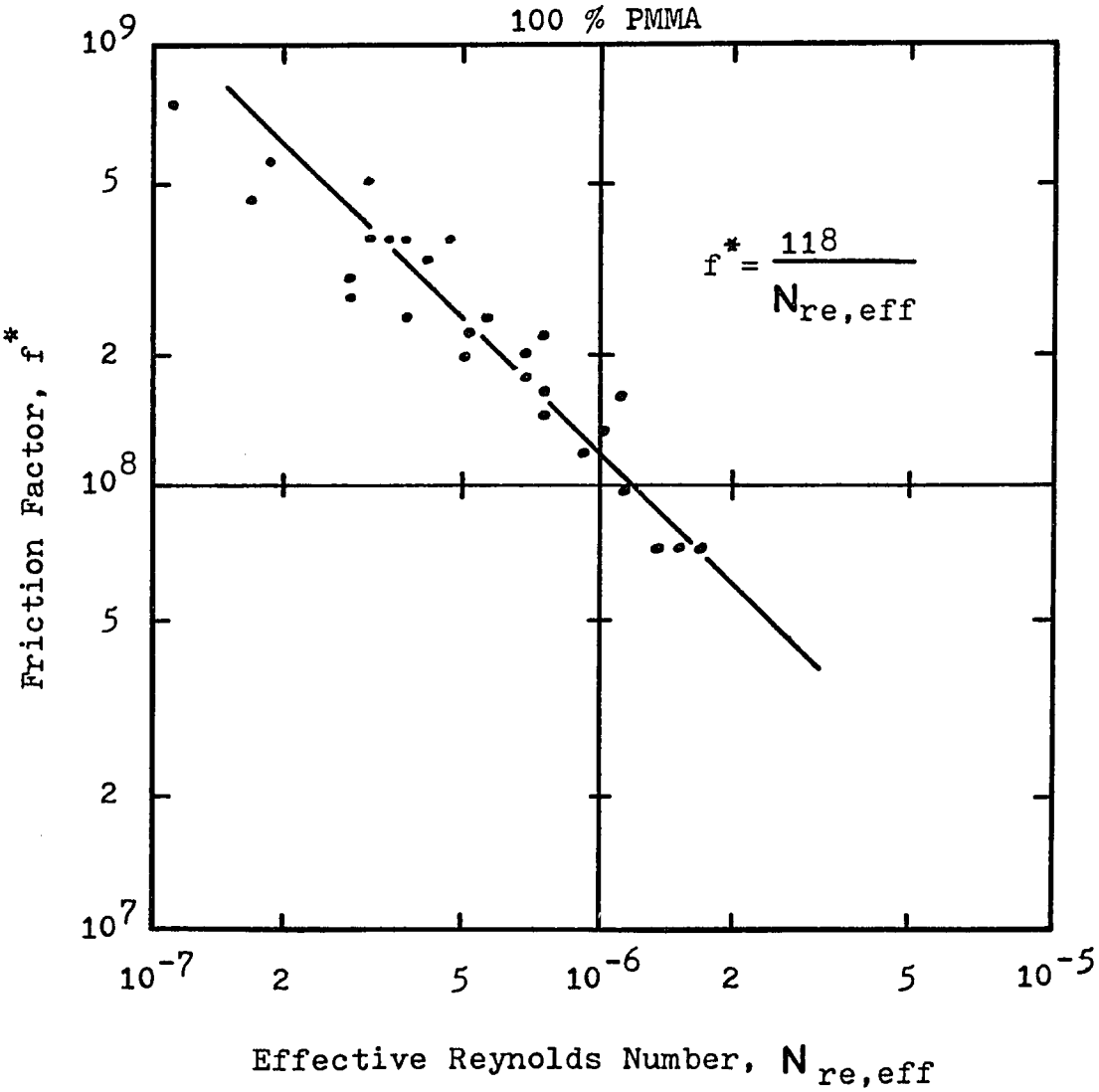

Figure 18

Friction Factor-Reynolds Number Correlation

for the Huang Model

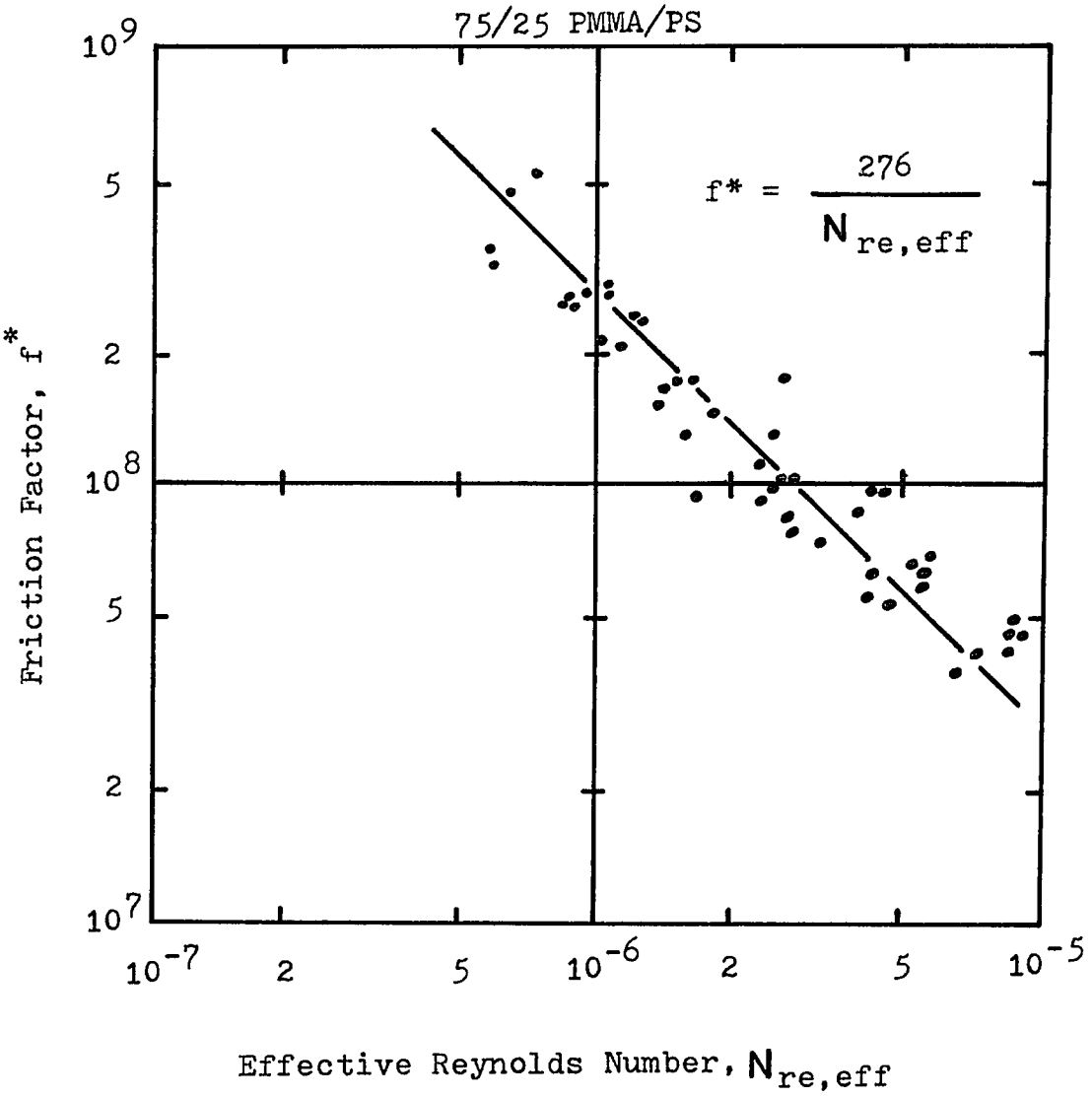

Figure 19

Friction Factor-Reynolds Number Correlation for the Huang Model

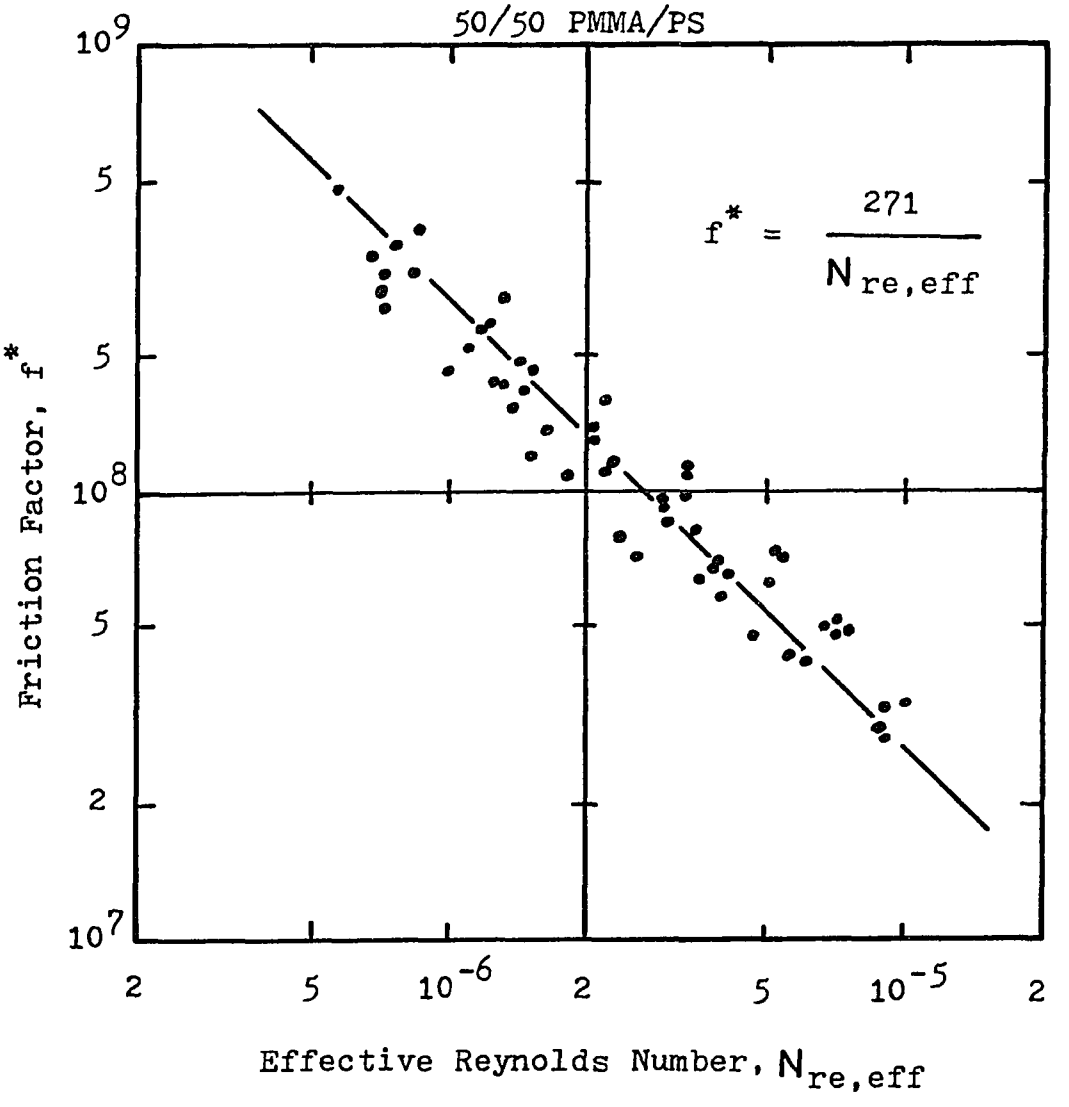

Figure 20

Friction Factor-Reynolds Number Correlation for the Huang Model

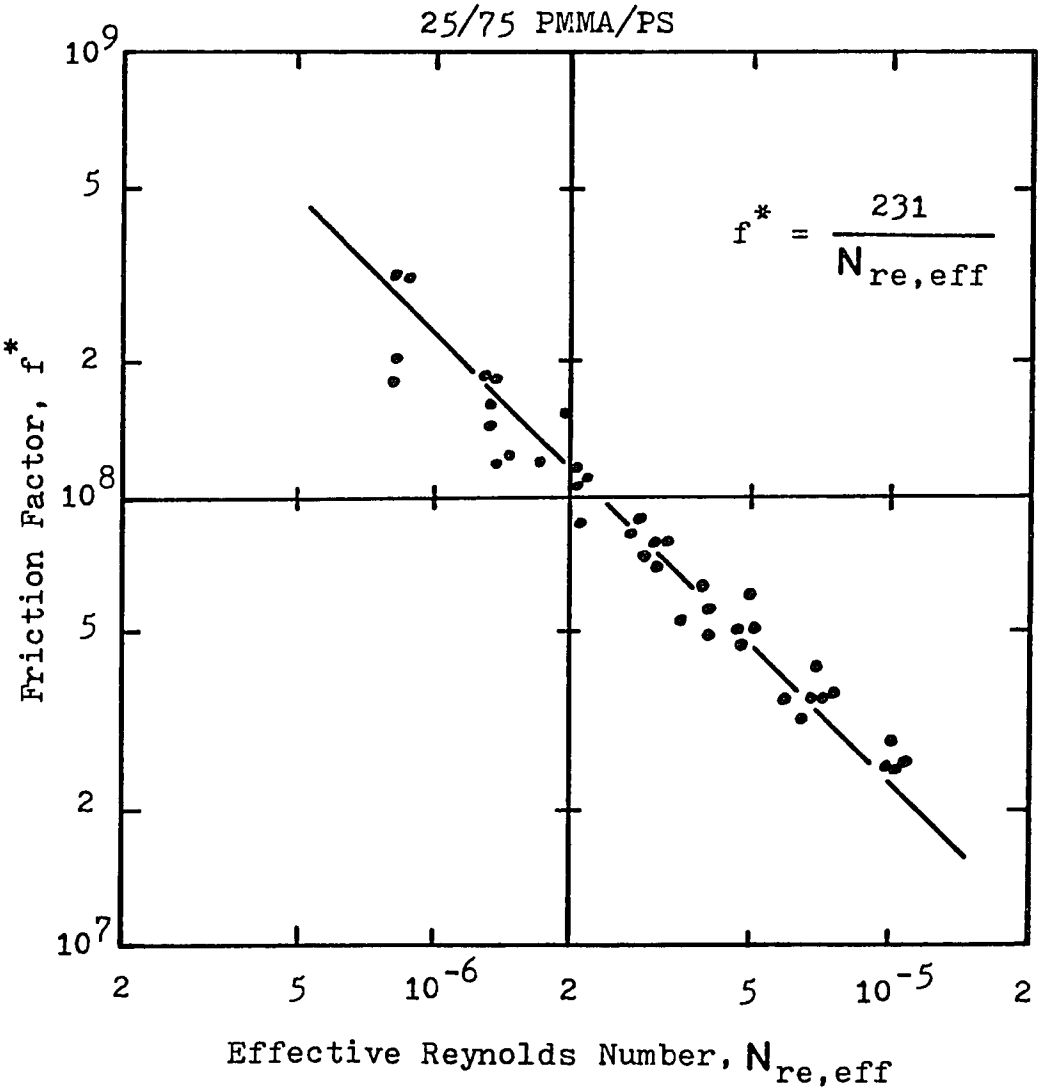

Figure 21

Friction Factor-Reynolds Number Correlation

for the Huang Model

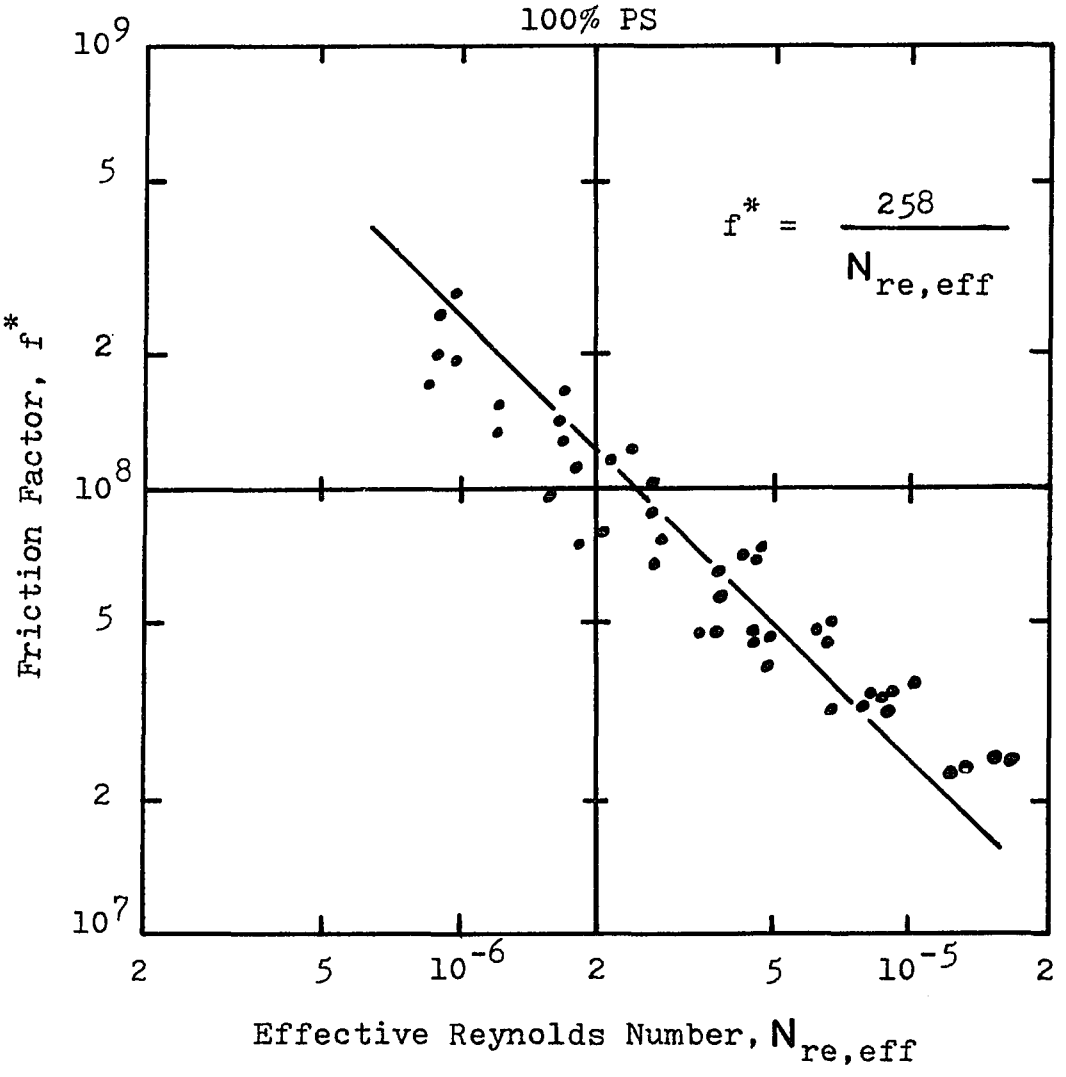

Figure 22

Friction Factor-Reynolds Number Correlation

fot the Huang Model

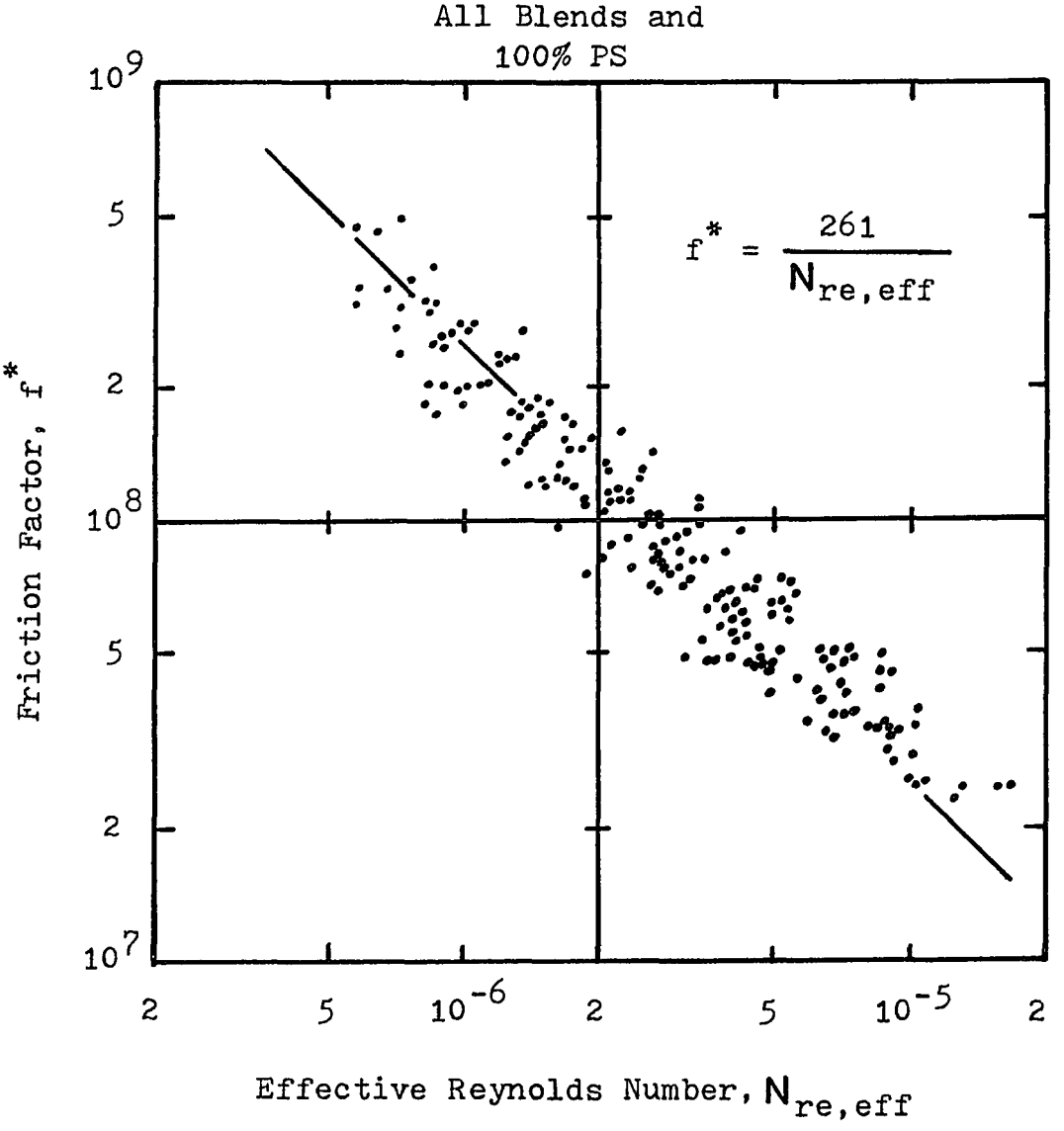

Figure 23

Friction Factor-Reynolds Number Correlation

for the Ellis Model

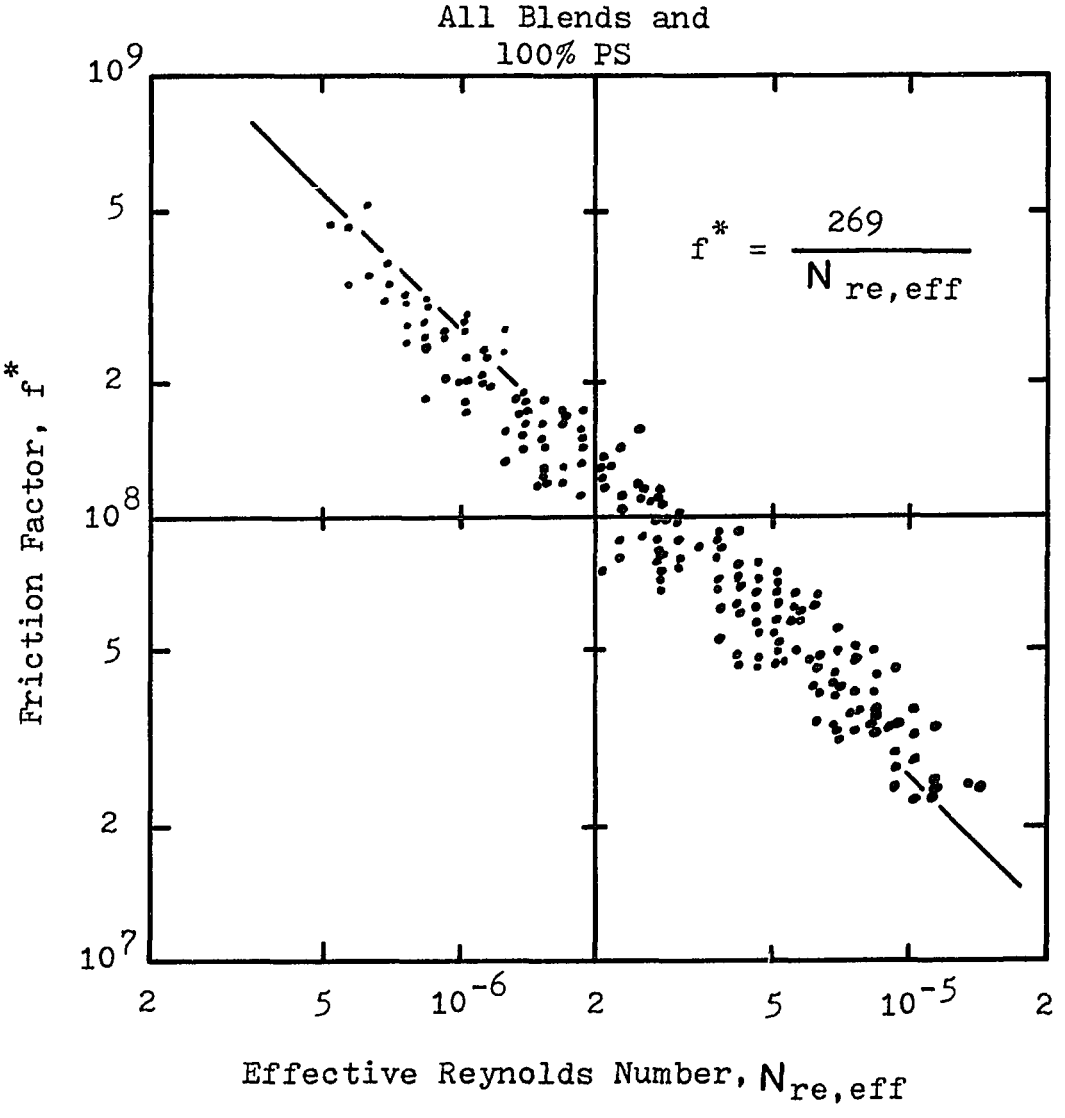

respectively. Other studies have reported values from c=118 (60a) to c=650 (50).

As originally conceived, c accounts for the tortuosity of the porous medium, reflecting the inability to accurately define path length and pore size in so complex a geometry. Deviations from the expected values of Ergun and Carman have been attributed to viscoelastic effects by Sadowski (91, 92) and to the presence of an anomalous fluid layer on the particles' surface by Kozicki, et al (59). Further, the Darcy law development leading to (II.98) ignored inertial effects as small compared to viscous effects in porous media flow.

Sadowski observed deviation of the friction factor versus Reynolds number from c=180 for a solution of high molecular weight hydroxyethylcellulose in water. The deviation occurred above $N_{re,eff} = 0.5$, but not below that value. He defined a characteristic time to account for the suspected viscoelastic effects which corrected the deviant points without significant effect on other test fluids. Christopher, however, reanalyzed Sadowski's data using the power law rather than the Ellis fluid model (19). He found that the deviation then occurred at low values of Reynolds

number, but not at the high values. Further, Kozicki was able to correlate the same data using a modified Ellis model Reynolds number which allowed for the existance of an adsorbed fluid layer on the particles' surface. Thus, no solid evidence exists in this case to support the theory of viscoelastic effects.

The assumption that inertial effects can be ignored can be tested. Scheidegger reported that the critical Reynolds number for porous media flow above which inertial forces may be significant, lies between 0.1 and 75 (97). In the present study, maximum Reynolds numbers were $<2\times10^{-5}$. The assumption seems reasonable.

From the discussion above, it seems unlikely that the variations in **c** are due to some unaccounted fluid behavior. Since different values of **c** have been calculated for the same packed beds with different fluids, it is equally unlikely that the bed geometry is alone responsible for the results. Interaction between these factors offers a plausible explanation.

The anomalous adsorbed fluid layer proposed by Kozicki is one possible interaction. Kozicki introduced two factors termed the impermeability and aspect factors to account for velocity changes resulting from polymer adsorption or gelation on the bed packing.

This idea is tested by the following reasoning.

Only the PMMA-VM results deviated significantly from a value of $c=260$. One may suppose that the adsorption phenomenon is related to the presence (or absence) of PS-678. This idea is supported by recalling that VanOene showed PS to be the continuous phase in PMMA/PS blends (116). If such a layer exists, the bed porosity ϵ should be effectively reduced. As ϵ decreases, c decreases. Thus, the four resins containing PS-678 (high values of c) are logically the ones for which adsorption occurs. Carrying the analysis further, the effect of an adsorbed layer should be greatest for small particles and low flow rates (greatest reduction in effective values of ϵ). No trend is evident that the values of c increase at the presumably inflated values of ϵ for small bead sizes. In fact, c is approximately constant for a given material, flow rate and bed depth as bead size decreases with the values of ϵ which were used. Moreover, for a given material, bed depth and bead size, c increases as flow rate increases, contrary to expectation if values of ϵ are inflated at low flow rates.

It is clear that none of the proposals reviewed

above satisfactorily explains the differences in the f^* versus $N_{re,eff}$ relationship for PMMA-VM compared to the other materials tested. One can propose various additional adjustable parameters to produce superposition of the results, but physical significance is questionable. The need for study leading to a mechanistic model which more accurately describes porous media flow, is evident. Meanwhile, correlation of data by the method of this study provides accepted working relationships.

A prime objective of this work was the assessment of blend behavior compared to that of the pure components. In all respects, the three blends responded identically to pure PS-678. No evidence of phase inversion, phase separation or other anomalous effects exists. Thus, in both the simple geometry of the rheogoniometer and the complex geometry of the packed bed, the blends behaved as though they were pure and single phase materials. This observation extends the pattern of results reported by Hill and Maxwell (52) and Han (40) for less complex flow geometries (discussion in Chapter II.).

CHAPTER V. CONCLUSIONS

The results of this investigation may be summarized by the following statements.

1. A four parameter form of the thermodynamically-based Huang rheological equation of state provided excellent representation of experimental data for pure component and blend melts of polystyrene and poly(methyl methacrylate). This study provided the first experimental test of the model with molten polymers.
2. The cone and plate rheogoniometer data from this study and the capillary rheometer data of Han (45) provided a thorough rheological characterization of the polymers and blends over a five decade shear rate range.
3. A packed bed test apparatus of commercial size was designed, fabricated and successfully tested in this study.
4. Disproportionate effects in shear stress reduction (Figure 5) and pressure drop reduction in the packed beds (Figure 16) were observed for addition of polystyrene to poly(methyl methacrylate). These effects are tentatively ascribed to the tendency of polystyrene to form the continuous phase in

blends of the two polymers as reported by VanOene (116). Melt viscosity of the PS-678 was significantly lower for a given set of conditions than was that of PMMA-VM. No other unusual effects were observed for blends of the polymers.

5. The application of the Huang equation of state to an hydraulic radius capillary model of the porous medium led to a generalized Darcy's law (II.93). Analytic solution of the resulting equations allowed the packed bed experimental data to be represented through a friction factor-Reynolds number correlation. Both this development and that given previously by Sadowski (91, 92) satisfactorily represented the total 214 data points for the five polymers and blends. Thus, a test of the Huang model for melt flow in a complex geometry was provided.

6. The values of the adjustable parameter **c** in equation (II.98) were significantly different for PMMA-VM ($c \doteq 120$) compared to PS-678 and the polymer blends ($c \doteq 260$). This result is attributed to an unidentified interaction between these fluids and the packed beds. The data from this study do not provide the basis for a phenomenological understanding

of this result. Surface tension and other surface effects may be suspected of contributing to the observed differences in behavior.

7. The analysis does provide working relationships among the experimental variables. Using the equations which were developed, the pressure drop through a packed bed can be estimated from the rheological properties of the fluid and the physical properties of the packed bed. Sensitivity of the pressure drop to the experimental variables can be tested.

8. Packed bed flow behavior of more rheologically complex fluids than those reported herein can be represented by this new model. The Huang model provides a more powerful and versatile description of fluid rheology than other models previously applied to porous media flow.

CHAPTER VI. RECOMMENDATIONS

The present investigation provided two extensive test applications of the Huang rheological equation of state. An appropriate simplification of the model for isothermal, incompressible, pseudoplastic flow gave a tractable equation which closely described experimental data. Extension of this model to other polymer systems (melt and solution) and other viscometric geometries is warranted.

The second test of the model was its adaptation to the hydraulic radius capillary representation of a packed bed producing a modified Darcy's law. The applicability of the hydraulic radius concept in correlating experimental data was demonstrated.

The variation in the adjustable parameter **c**, both among materials and from expected values, requires further study. One suggested extension of the work is limited testing of another polymer previously shown to exhibit predicted behavior. Alathon® 10 polyethylene (E.I. Du Pont, Inc.), investigated by Gregory (37, 38), could be used for this purpose. Such a study would provide a check of the apparatus.

The change in **c** from a value of about 120 for pure PMMA-VM to a value of about 260 for the other resins can be explored. In particular, tests of blends with less than 25 percent PS-678 would show whether a consistent trend between the extreme values exists.

More basic studies of the morphology of melt blends of the polymers taken from packed beds would allow direct observation of differences in those materials which gave different values of **c**. Experiments to measure surface tension and other surface effects are also recommended to understand the differences.

The apparatus used in conducting the packed bed tests is adaptable for flow studies of other melt systems. The large diameter main piping and the instrumentation would be suitable for the investigation of radial temperature and pressure distributions around a packed bed, static mixer or other test device.

Finally, the work described herein can be generalized to describe other systems of importance such as secondary oil recovery flow, filtration and related extrusion operations.

APPENDIX A. NOMENCLATURE

A = constant in the Huang equation of state, M/Lt

A_r = cross sectional area of packed bed, L^2

a = parameter of the beta function radius distribution, dimensionless

B = constant in the Huang equation of state, M/Lt

$\underline{\underline{B}}$ = tensor polynomial in the skewed capillary permeability model

b = parameter in the beta function radius distribution, dimensionless; factor related to the reciprocal resistance of a pore, L^2

C = constant in the Huang model

c = adjustable parameter associated with the hydraulic radius permeability in the friction factor-Reynolds number correlation

c_0 = the Kozeny constant, dimensionless

c_5, c_6 = constants in the Huang model

D = diameter of a tube, L

D_p = diameter of a particle, L

f = friction factor for tube flow, dimensionless

f^* = friction factor for packed bed flow, dimensionless

$f(s)$ = shape factor, dimensionless

$f(\epsilon)$ = porosity factor, dimensionless

$\underline{g}$ = gravitational acceleration, L/t^2

$\underline{\underline{g}}$ = metric tensor defining the heat flux vector in the Huang model

h = elevation, L

K = proportionality constant in Darcy's law, L^3t/M

K_{ij} = element of the permeability tensor, L^2

k = Boltzmann constant, ML^2/t^2T; permeability of a packed bed, L^2

L = depth of packing or characteristic length, L

m = parameter in the Ostwald-de-Waele model, variable dimension

N_{re} = Reynolds number, dimensionless

$N_{re,eff}$ = effective non-Newtonian Reynolds number, dimensionless

n = parameter in the Ostwald-de-Waele model, dimensionless; parameter in the Huang model, dimensionless

P = fluid pressure, M/Lt^2

Q = volumetric flow rate, L^3/t

q^i = heat flux vector in the Huang model, M/t^3

R = radius of a tube, L; largest pore radius in the Haring and Greenkorn permeability model, L

R_h = hydraulic radius, L

r = radial dimension, L

S = the entropy, ML^2/t^2; surface area per unit volume of porous medium, L^{-1}

S_0 = surface area per unit volume of solid packing, L^{-1}

T = absolute temperature, T

t = time, t

V = mass average velocity, L/t

V_0 = superficial fluid velocity, L/t

z = rectangular coordinate, L

α = parameter in the Ellis, Sisko and Sutterby models, dimensionless

β = parameter in the Sisko, Powell-Eyring and Sutterby models, variable dimensions

β_{ij} = molecular arrangement parameter in the Huang model, MT

β_e^{ij} = equilibrium value of the molecular arrangement parameter in the Huang model, MT

$\Gamma(a)$ = the gamma function of a

$\Gamma(a,z)$ = the incomplete gamma function of a and z

$\underline{\underline{\gamma}}$ = strain rate tensor, t^{-1}; same as $\underline{\underline{\Delta}}$

γ_R = wall shear rate, t^{-1}

γ_{Rh} = hydraulic radius wall shear rate, t^{-1}

$\underline{\underline{\Delta}}$ = rate of deformation tensor, t^{-1}; same as $\underline{\underline{\gamma}}$

$\underline{\underline{\delta}}$ = unit tensor, dimensionless

ϵ = packed bed porosity, (volume of voids/volume of medium), dimensionless

η = non-Newtonian viscosity, M/Lt

η_{eff} = effective non-Newtonian viscosity, M/Lt

η_0 = parameter in the Sisko and Sutterby models, M/Lt

η_N = parameter in the Powell-Eyring model, M/Lt

η_t = overall apparent viscosity in the Huang model, M/Lt

θ = angle, radians

$\underline{\lambda}$ = unit orientation vector in the skewed capillary model, dimensionless

λ = thermal conductivity, ML/t^3T

μ = Newtonian viscosity, M/Lt

ξ = coefficient in the Huang model

π = 3.14159...

ρ = fluid density, M/L^3

σ = rate of generation of entropy, ML^2/t^3

$\underline{\underline{\tau}}$ = shear stress tensor, M/Lt^2

τ_R = shear stress at the wall, M/Lt^2

τ_{Rh} = hydraulic radius shear stress at the wall, M/Lt^2

ϕ = force potential, L^2/t^2

ϕ_0, ϕ_1 = parameters in the Ellis model, Lt/M and variable dimensions, respectively

Ψ = velocity potential, L^2/t

χ = parameter in the Powell-Eyring model

Ω = the number of micromolecular states of an assembly, Huang model

Mathematical Operations

D/Dt = substantial derivative

$P(\chi^2/\nu)$ = the probability function defined as the ratio of the incomplete to the complete gamma functions

$\Gamma(a)$ = the complete gamma function = $\int_0^\infty \exp(-t)\, t^{a-1}\, dt$

$\Gamma(a,z)$ = the incomplete gamma function = $\int_0^z \exp(-t)\, t^{a-1}\, dt$

∇ = vector differential operator, del, L^{-1}

∇^2 = Laplacian operator

APPENDIX B.

MATERIALS AND APPARATUS

Figure B-1

Laboratory Polymer Press

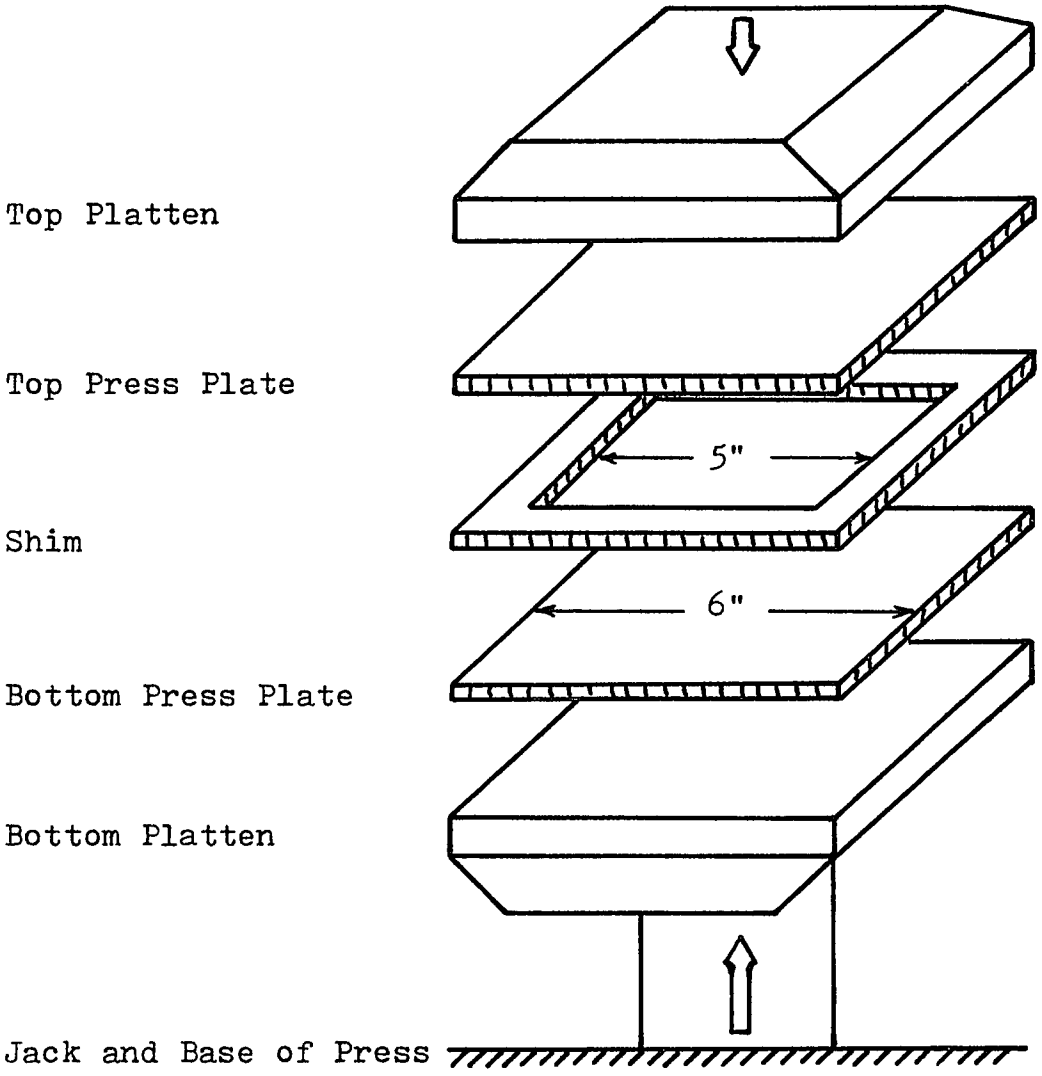

Specifications: Carver Laboratory Press
No. 15300-105
Six inch square heated plattens
25-250 °C
0-16,000 psig pressure

Manufacturer: Fred S. Carver, Inc.
Summit, New Jersey 07901

Table B-I

Rheogoniometer Specifications

Designation:	Roberts-Weissenberg Rheogoniometer
Model:	R-18
Plate Diameter:	2.50 cm
Cone Angle:	4.0042 deg
Gap Setting:	187 μ
Spring Constants:	Torsion, 1.016×10^3 dyne-cm/μ Compression, 5.90×10^3 dyne/μ
Manufacturer:	Farol Scientific Instruments Bognor Regis, England

Calculations:

Shear Rate

$$\dot{\gamma}_{\theta\phi} = \frac{\text{angular velocity}}{\text{cone angle}} = \frac{360}{4.0042t} = \frac{89.9056}{t}$$

where t= period of the plate rotation, supplied by the manufacturer as a function of gearbox settings.

Shear Stress

$$\tau_{\theta\phi} = \frac{3K_T \Delta_T}{2\pi R^3} = \frac{3(1.016 \times 10^3)\,\Delta_T}{2\pi \left(\frac{2.50}{2}\right)^3} = 248.373\,\Delta_T$$

where Δ_T= torsional deflection, μ

Normal Stress

$$\tau_{11} - \tau_{22} = \frac{2K_N \Delta_N}{\pi R^2} = \frac{2(5.90 \times 10^3)\Delta_N}{\pi (2.5/2)^2} = 2403.87\,\Delta_N$$

where Δ_N = normal deflection, μ

Table B-IIa

Temperature and Pressure Dependence of Polymer Density

Material	Temperature °F	Density, g/cm³ @ (1) Pressure, psig 0	2000	4000	6000
Polystyrene	215	1.019	1.032	1.041	1.051
	380	.977	.990	1.001	1.013
	398(est)	.972	.985	.996	1.009
Poly(methyl-methacrylate		255	5100	12,750	
	250	1.129	1.149	1.174	
	285	1.112	1.133	1.161	
	320	1.099	1.123	1.150	
	355	1.084	1.110	1.142	
	398(est)	1.064	1.092	1.133	

1. Data from Processing of Thermoplastic Materials, reference 84.

Procedure:

a) Plot data, ρ vs T with p as a parameter.
b) Extrapolate each isobar to 398°F; estimate ρ.
c) Plot ρ vs p at 398°F; estimate values of ρ over the pressure range of interest.
d) For blends, calculate weight average values of ρ from pure polymer values.
e) Values of density used in packed bed calculations are summarized in Table B-IIb.

Table B-IIb

Pressure Dependence of Resin Density at 398°F

Pressure psig	100% PS	100% PMMA	25/75 PS/PMMA	50/50 PS/PMMA	75/25 PS/PMMA
0	.972	1.062	1.039	1.017	.994
250	.974	1.064	1.041	1.019	.996
500	.976	1.065	1.043	1.020	.998
750	.977	1.067	1.045	1.022	.999
1000	.979	1.068	1.046	1.024	1.001
1250	.980	1.070	1.048	1.025	1.002
1500	.982	1.071	1.049	1.026	1.004
1750	.984	1.072	1.050	1.028	1.006
2000	.985	1.073	1.051	1.029	1.008
2250	.987	1.075	1.053	1.031	1.009
2500	.988	1.076	1.054	1.032	1.010
2750	.989	1.078	1.056	1.034	1.012
3000	.991	1.079	1.058	1.035	1.014

Figure B-2

Dependence of Polymer Density on
Temperature and Pressure

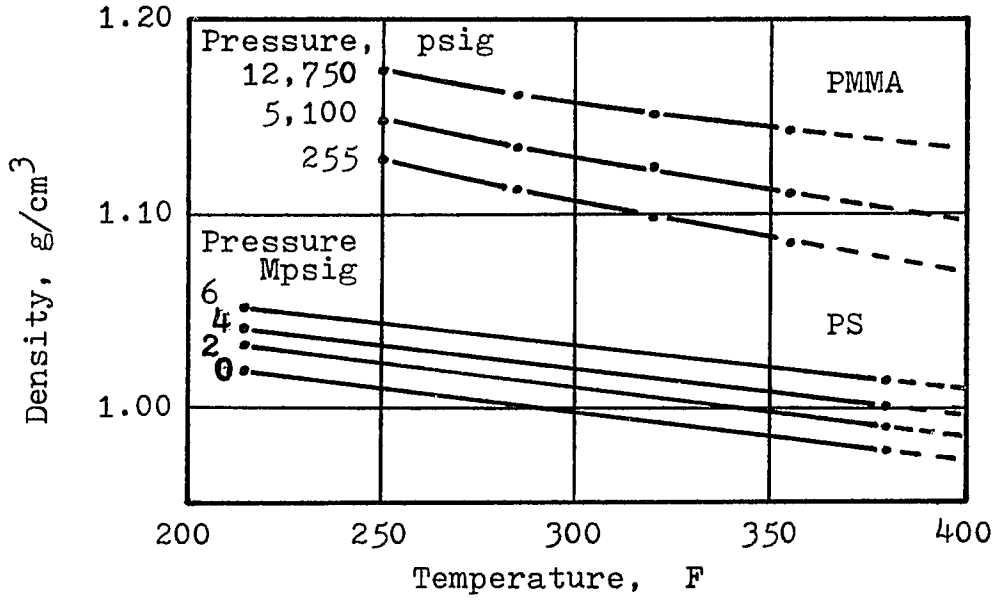

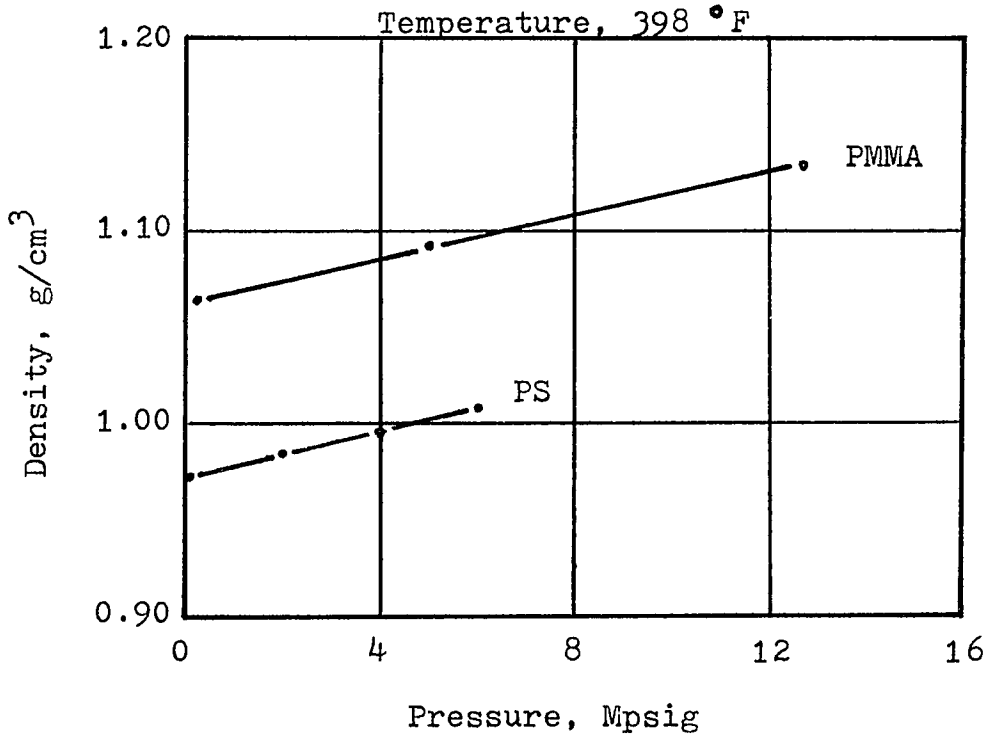

Table B-III

Manufacturer's Glass Bead Packing Specifications

Designation	Nominal Size, cm	Range US Sieves	Density g/cm^3	Mininum % in Range	Maximum Broken, %
V-390	0.96-1.05	na	2.5-3.0	90	0.3
V-280	0.66-0.75	na	2.5-3.0	90	0.3
V-1607	0.34-0.40	5-6	2.5-3.0	90	0.3
V-080	0.14-0.20	10-14	2.5-3.0	90	0.3
P-047	0.07-0.12	16-25	2.45-2.55	90	1

Glass beads manufactured by Potters Bros., Inc.,
Carlstadt, N.J.

Table B-IV

Prodex Extruder Specifications

Designation:	Compact Extruder
Size:	Two inch
Length/Bore Ratio:	24:1
Drive:	US Varidrive 15 Hp 30 to 130 rpm
Screw Type:	Metering
Manufacturer:	Prodex Corp. King George Post Road Fords, New Jersey

Table B-V

Metering Pump System Specifications

Designation:	Zenith HLB-4729
Type:	Two gear staple fiber hot pump
Nominal Delivery:	20 cm^3/rev
Manufacturer:	Zenith Products Co. 432 Cherry St. West Newton, Massachusetts
Drive:	a. Graham Transmission motor Type P, model 65643-A WF 1.5 Hp, 1750 rpm b. Transmission model 250 MR 2.8 Input 1750 rpm Output 0 to 230 rpm c. Reducer 5:1 speed reduction from transmission

Figure B-3

Detail of Leading and Trailing Pipe Sections

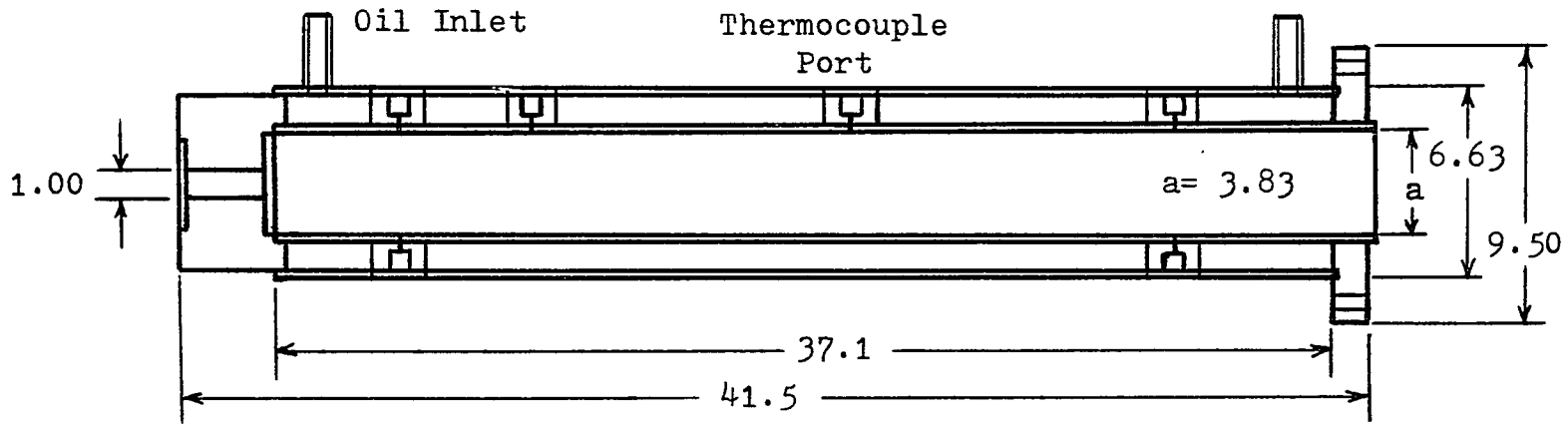

Leading Pipe Section

Dimensions: inches

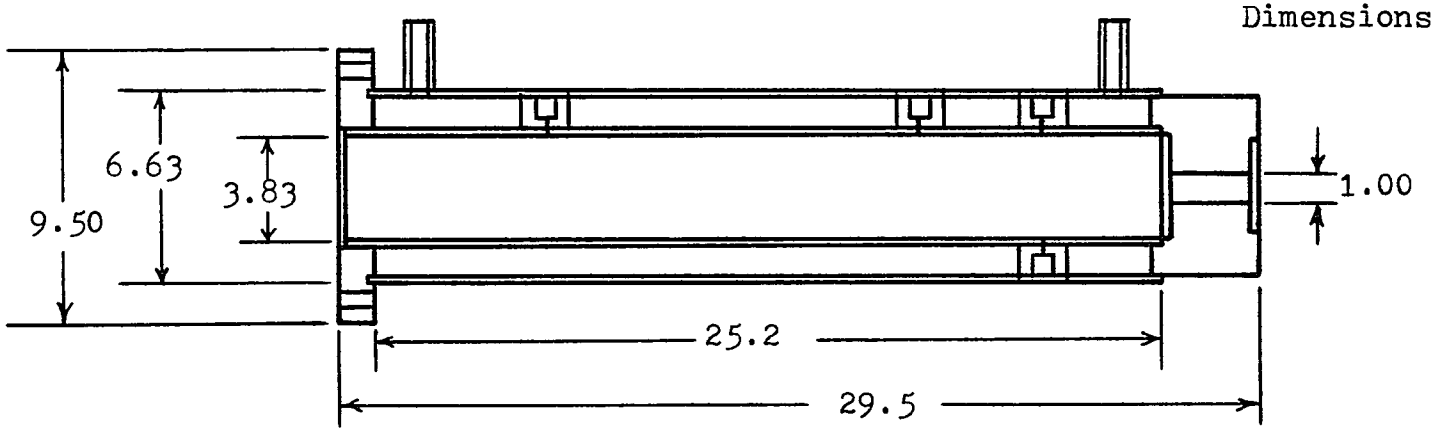

Trailing Pipe Section

Figure B-4

Detail of Pressure Transducer Flange

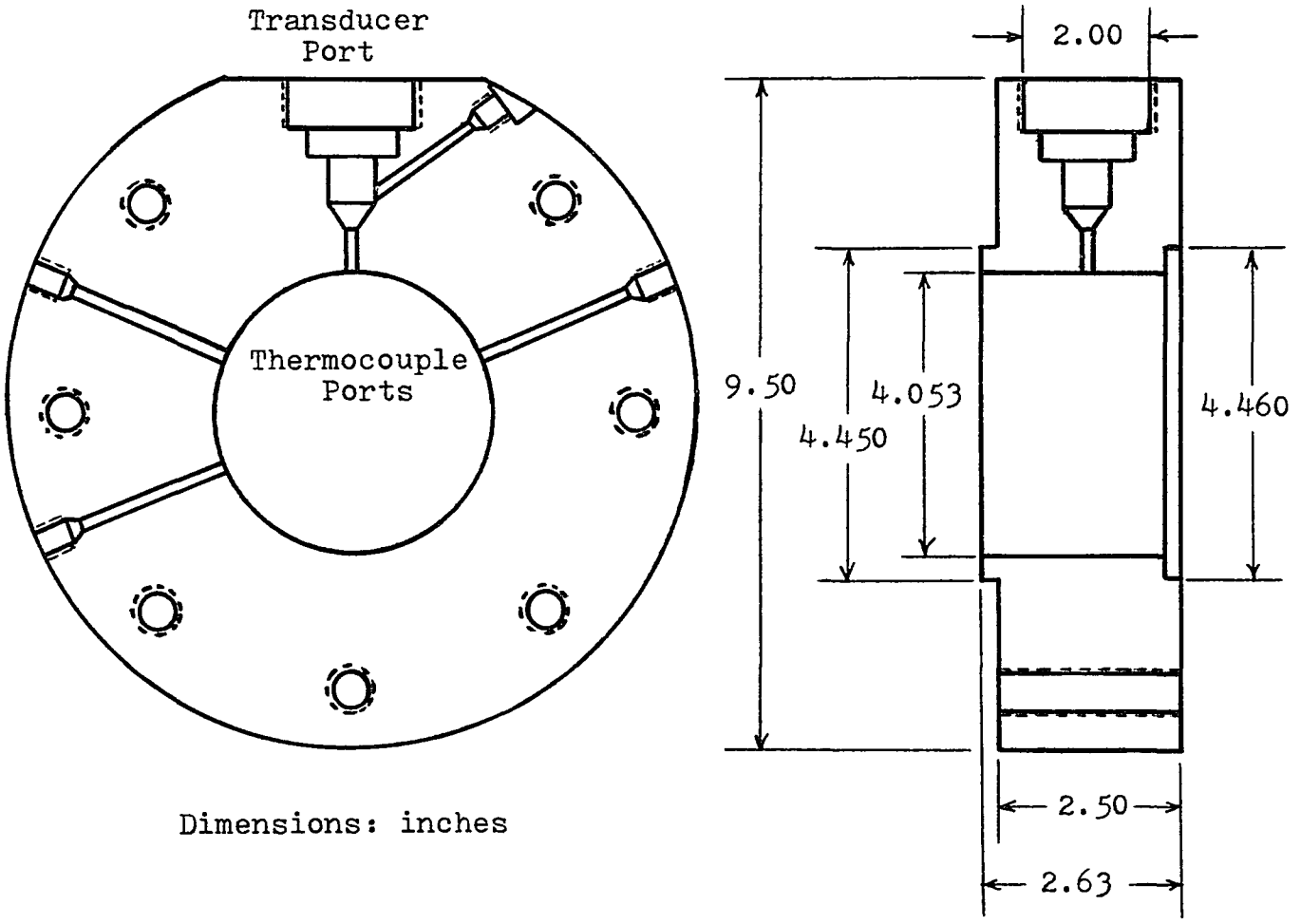

Dimensions: inches

Table B-VI

Pressure Measuring System Specifications

Designation:	Taylor Transcope Transmitters
Model:	211TN090
Input Air:	20 psig
Range:	0 to 3000 psig input 3 to 15 psig output
Sensor:	Volumetric pressure bulb no. 90
Manufacturer:	Taylor Instrument Co. 95 Ames St. Rochester, New York 14601
Readout:	Mercury manometer 90 cm, middle scale zero Fisher Scientific Co.

Figure B-5

Pressure Measuring System Instrumentation

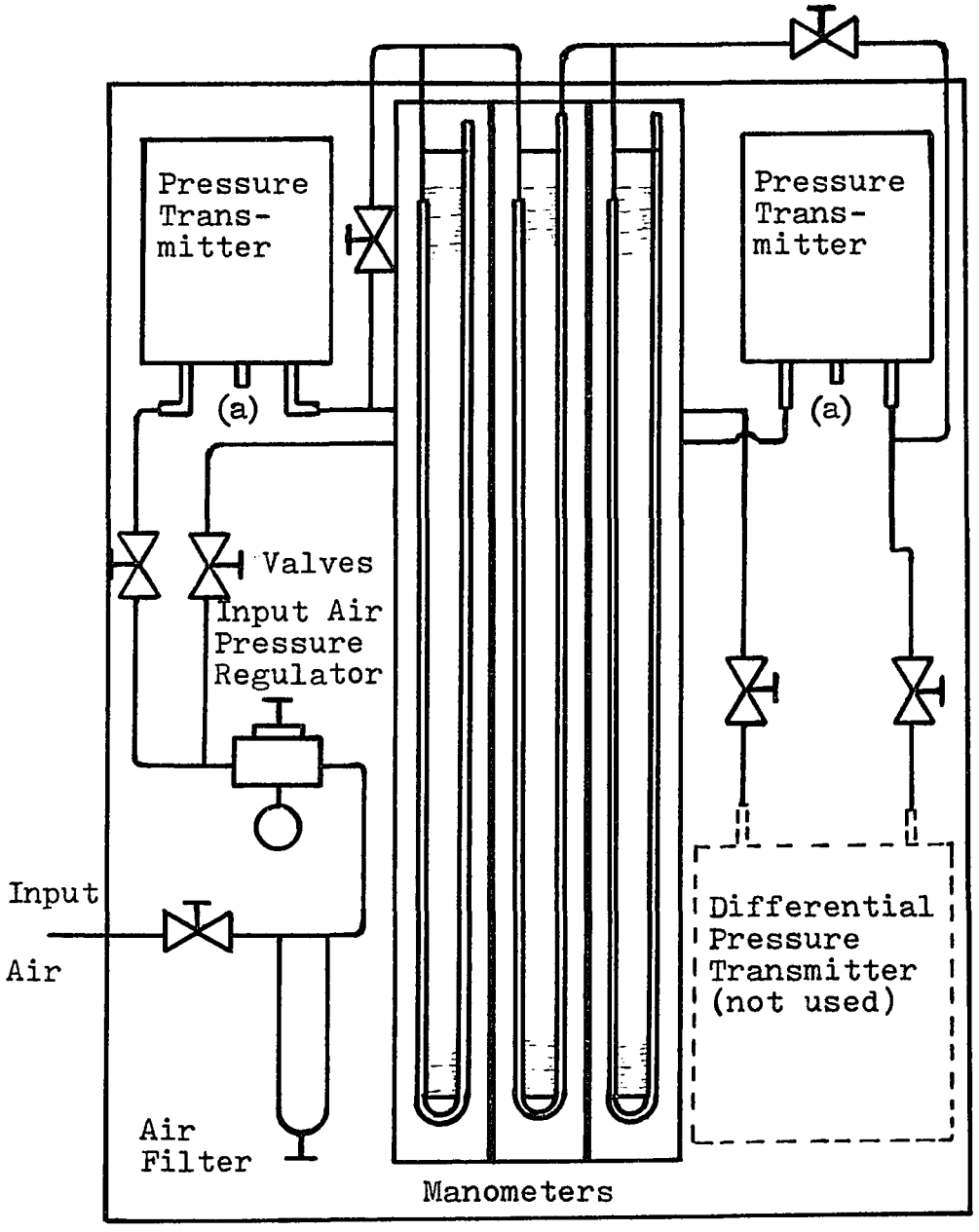

"a" is connection for pressure transducer

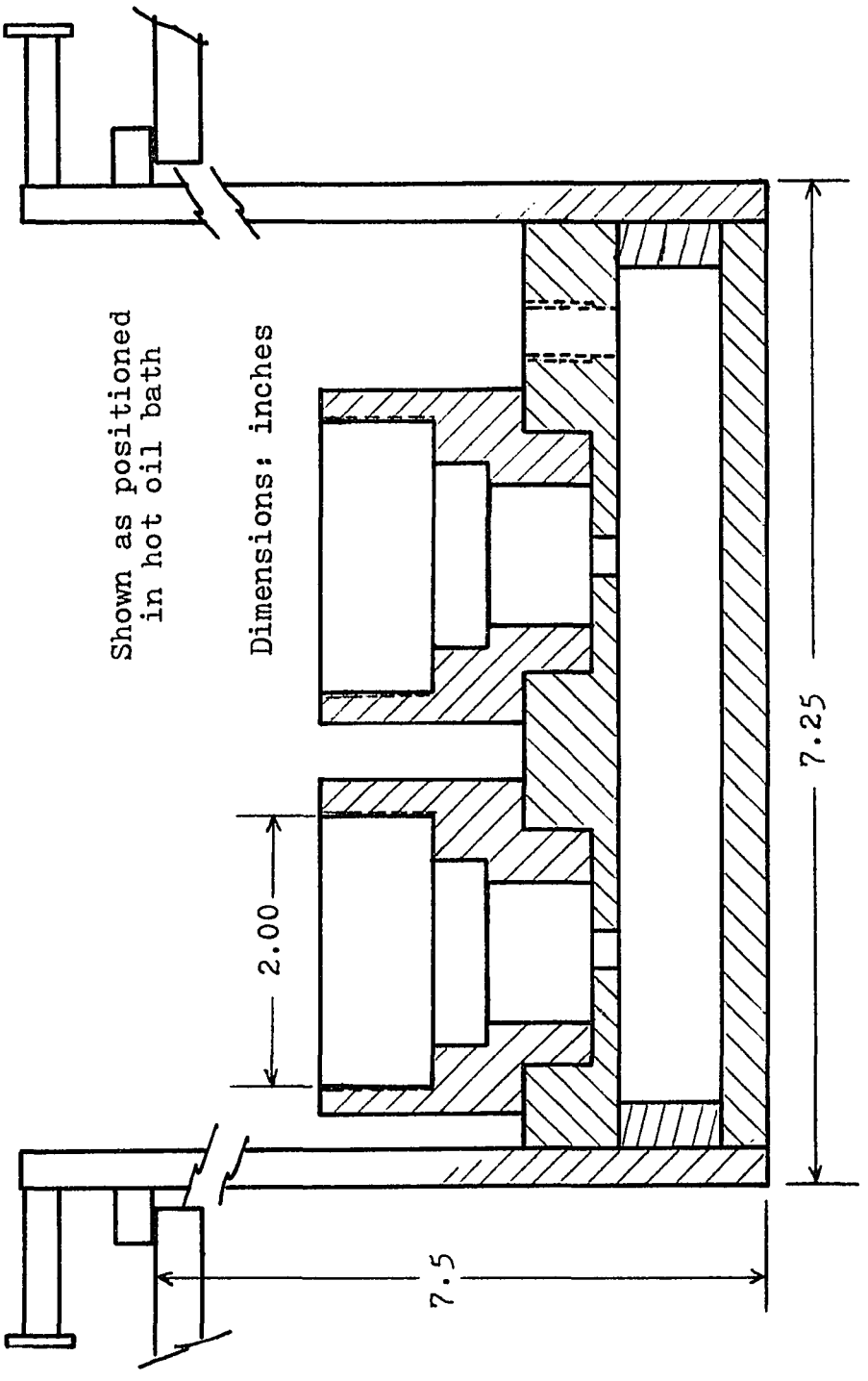

Figure B-6

Transducer Calibration Jig

Table B-VII

Hot Oil Bath Specifications

Designation:	Cannon High Temperature Bath
Model:	H-1
Range:	0 to 250 °C
Fluid:	G.E. SF-1017 silicone oil General Electric Silicone Products Division
Control Unit:	No. 666 Bronwill Scientific Co.
Manufacturer:	Cannon Instrument Co. State College Pennsylvania

Table B-VIII

Potentiometer Specifications

Designation:	Leads & Northrup Potentiometer Facility
Type:	K-3
Facility Cat. No.:	7553-A
Meter Cat. No.:	7553-6
Range:	0-1.6 volts, 3 scales
Error:	0.015% of reading
DC Null Detector Cat. No.:	9834-1
Standard Cell:	Eppley No. 779684 1.01915 volts
Power Supply:	Constant voltage no. 099034
Manufacturer:	Leads & Northrup, Inc.

APPENDIX C.

EXPERIMENTAL PROCEDURES

Procedure C-i

Rheological Testing

The general procedure followed in operating the Roberts-Weissenberg rheogoniometer is detailed below:

1. Move the heating chamber into place and preheat the apparatus to the test temperature. Purge with dry nitrogen.
2. Set the cone-to-plate gap (187μ) after reaching operating temperature.
3. Zero deflection meters as required.
4. Place a previously prepared disk of resin between the instrument cone and plate. Allow the temperature to equilibrate, air to be expelled and the polymer to melt.
5. Start the plate rotation at the minimum speed (shear rate) to be tested.
6. Observe the torsional and normal deflection readings. When steady, record.
7. Increase rotation speed stepwise through the range of shear rates. Record steady deflection readings at each step. Several instrument range changes are required.
8. Observe the sample visually as the shear rate

increases. Rough edge appearence and unsteady deflection readings indicate maximun test conditions.

9. Replicate the procedure twice more for each resin/temperature combination.

10. Average the replicate deflection readings and calculate shear and normal stress as a function of shear rate as shown in Appendix Table B-I.

Table C-I

Calculation of Ellis Rheological Model Constants

Technique

As explained in Chapter III, the Ellis model viscosity coefficient η_0 and the shear stress coefficient $\tau_{\frac{1}{2}}$ were estimated according to the graphical procedure recommended by Bird (6). The third parameter, α, was computer-estimated through a non-linear least squares estimation program. The exact program is not available (property of Celanese Corporation) but was derived from the method published by D.W. Marquardt of DuPont, "An Algorithm for Least Squares Estimation of Non-Linear Parameters" in the Journal of the Society for Industrial and Applied Mathematics, Vol. 11, No. 2 (1963).

Input to the base program required subroutines giving the form of the non-linear equation to be fitted, initial estimates of the parameters and the data. The subroutines for the Ellis model were as follows:

```
      SUBROUTINE F CODE (Y,X,B,PRNT,F,I)
      DIMENSION Y(500),X(500,10),B(50),PRNT(5)
      F=ALOG((X(I,1)/B(1))*(1.+(X(I,1)/B(2))**(B(3)-1.)))
      RETURN
      END

      SUBROUTINE SUBZ(Y,X,B,PRNT,NPRNT,N)
      DIMENSION Y(500),X(500,10),B(50),PRNT(5)
      DO 10 I = 1,N
10    Y(I)=ALOG(Y(I))
      RETURN
      END
```

Table C-II

Calculation of Huang Rheological Model Constants

Technique

All four parameters in the Huang rheological model were computer-estimated. As explained in Table C-I, the base program was derived from a published method, but is not specifically available (property of Celanese Corporation). Brief subroutines giving the form of the non-linear equation to be fitted, initial estimates of the parameters and the data were required to use the program. The subroutines are reproduced below:

```
      SUBROUTINE F CODE (Y,X,B,PRNT,F,I)
      DIMENSION Y(500),X(500,10),B(50),PRNT(5)
      F=ALOG(B(1)+B(2)*(X(I,1)**(B(3)-1.))*EXP(-B(4)*
     1(X(I,1)**B(3))))*X(I,1))
      RETURN
      END

      SUBROUTINE SUBZ(Y,X,B,PRNT,NPRNT,N)
      DIMENSION Y(500),X(500,10),B(50),PRNT(5)
      DO 10 I = 1,N
10    Y(I)=ALOG(Y(I))
      RETURN
      END
```

Procedure C-ii

Calibration of the Taylor Pressure Measuring System

The Taylor system used to measure pressure in the melt consisted of two volumetric transducer bulbs associated with appropriate transmitters which provided a proportional 3 to 15 psig pneumatic output signal. A differential transmitter to directly read pressure difference between the leading and trailing transducers was initially planned, but high cost and long delivery precluded use of this automated readout. Instead, three mercury manometers were used, one each to read gage pressure of the two transducers and one to read the difference between them as a check. Figure B-5 shows the panel constructed to house these instruments.

The transducers were calibrated by connecting the bulbs in a special housing (Figure B-6) with an hydraulic dead weight tester to provide accurate loading. The calibration jig was immersed in a constant temperature oil bath and calibrated at applied loads from 0 to 3000 psig. Readings from all three manometers were recorded. Calibration at 27, 160, 200 and 240°C was performed. Selected loads were repeated to test reproducibility.

The data are summarized in Table C-III and are plotted in Figure C-1.

The data at 200°C for the leading and trailing transducers were fitted to a least squares line of the form

$$P\ (psig) = a\ (Ht(cm\ Hg) - b)$$

The following equations resulted:

Leading $P = 49.106\ (Ht - 15.27)$

Trailing $P = 49.124\ (Ht - 15.77)$

Pressure differences were calculated using these expressions.

The residual error (95% confidence limits) in using these equations was $\pm$ 16.1 psig and $\pm$ 9.7 psig, respectively. The average error (comparing measured and predicted calibration data points) was $\pm$ 8.6 psig for the leading transducer and $\pm$ 4.9 psig for the trailing transducer.

Table C-III

Taylor Pressure Measuring System Calibration Data

Temperature, °C	27			160		
Pressure psig	Leading cm Hg	Trailing cm Hg	Diff. cm Hg	Leading cm Hg	Trailing cm Hg	Diff. cm Hg
0*	15.40	15.40	0.00	15.50	15.55	0.05
300	21.50	21.65	0.15	21.40	21.70	0.30
600	27.20	27.70	0.40	27.50	27.90	0.50
900*	33.50	33.90	0.50	33.35	34.05	0.55
1200	39.25	40.00	0.60	39.50	40.20	0.60
1500	45.40	46.10	0.50	45.70	46.30	0.60
1800*	51.70	52.30	0.55	51.70	52.45	0.65
2100	57.95	58.40	0.50	57.85	58.55	0.65
2400	64.00	64.40	0.35	64.00	64.50	0.50
2700*	70.30	70.45	0.10	70.25	70.60	0.35
3000	76.45	76.40	-0.05	76.50	76.60	0.10
Temperature, °C	200			240		
0*	15.60	15.65	0.10	15.65	15.75	0.20
300	21.45	21.80	0.35	21.45	21.85	0.35
600	27.25	27.95	0.40	27.50	28.00	0.55
900*	33.45	34.10	0.60	33.45	34.10	0.60
1200	39.50	40.30	0.75	39.45	40.15	0.75
1500	46.05	46.45	0.65	45.65	46.50	0.75
1800*	51.80	52.50	0.70	System leaked, test aborted		
2100	57.90	58.65	0.75			
2400	64.05	64.65	0.60			
2700*	70.35	70.70	0.40			
3000	76.55	76.60	0.15			

Starred (*) points are replicates taken at random during a test.

Figure C-1

Taylor Bulb Calibration Curves

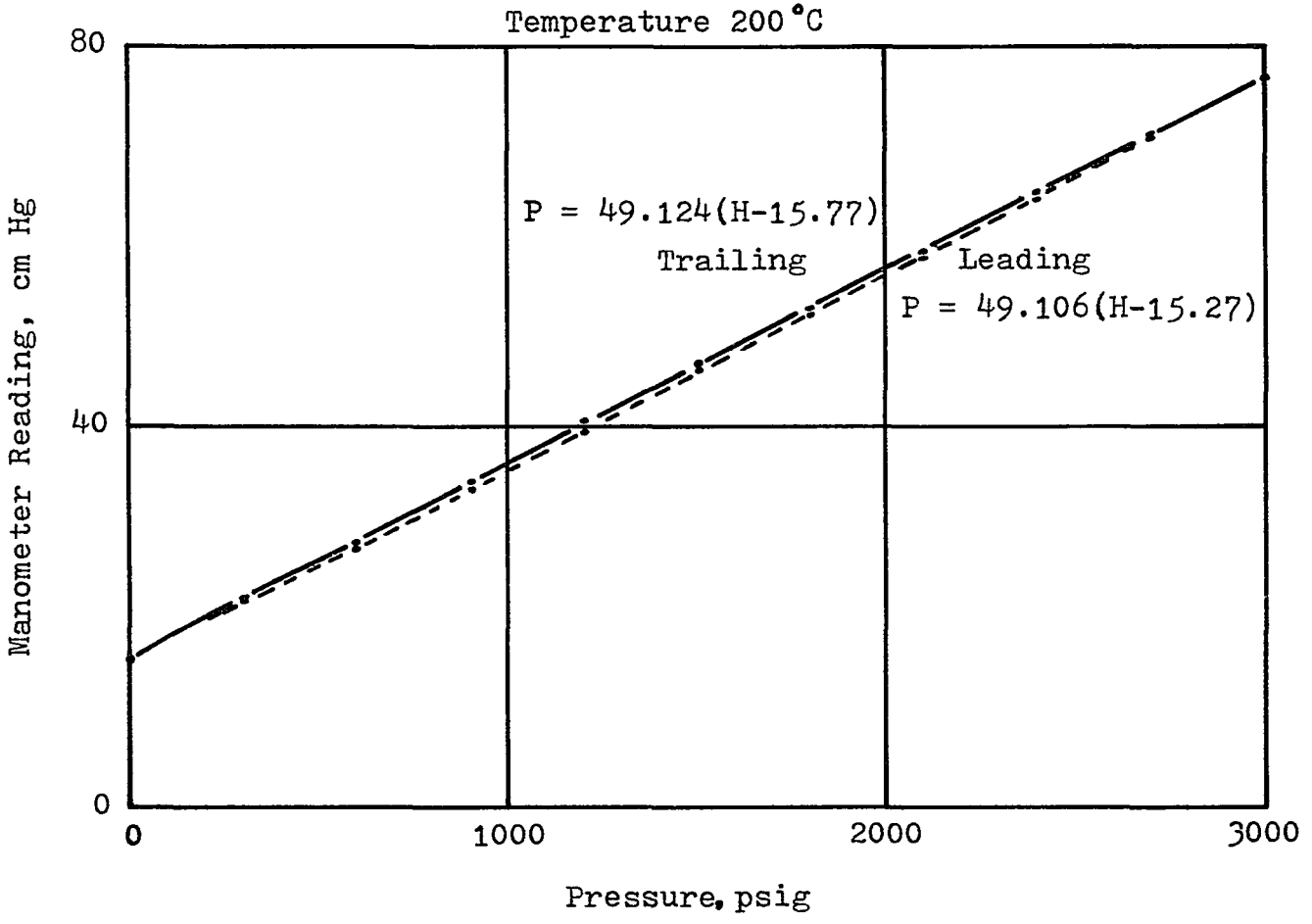

Table C-IV

Packed Bed Bead Loading Calibration

Bead Number	Bed Height cm.	Average Bead Weight g (1)	Average Deviation g (1)
V-390	1.83	176	1.4
	4.37	435	2.0
V-280	1.75	255.8	0.6
	4.29	639.8	1.3
V-1607	1.75	260.0	1.3
	4.29	654.1	1.4
V-080	1.75	271.3	1.5
	4.29	657.2	2.3
P-047	1.75	228.9	0.8
	4.29	559.1	1.4

1. For V-390 beads, values are count instead of weight.

Table C-V

Data for Determination of ϵ

Bead Number	Bead Sample Weight, g	Equiv. Vol. Water Weight, g (1)	Actual Water Volume, cm^3	Bead Density g/cm^3	Bead Wt. g/cm Bed Depth (2)
V-390	524.29	206.23	206.96	2.533	97.9 (3)
V-280	505.69	172.47	173.06	2.922	147.48
V-1607	59.39	20.08	20.15	2.947	150.35
V-080	472.30	159.99	160.55	2.942	153.94
P-o47	371.17	150.01	150.54	2.466	130.43

1. Tests conducted at 27.10 to 27.16°C; take water density = .99649 .
2. Derived from Table C-IV.
3. Number of beads/cm bed depth instead of weight.

Summary of values of ϵ is given in Table X of the text.

Procedure C-iii

Packed Bed Experiments

Each packed bed experiment required a minimum of four hours continuous, intensive work. At least two people were required to conduct an experiment, and three were scheduled when possible. The major steps in each test are listed below. A summary of all readings taken during one run is given in Table C-VI.

1. Start oil recycle and extruder preheating to approach operating temperatures.
2. Prepare the packed bed test section with the appropriate supports, sleeves and beads.
3. Install the test section, connect oil hoses, reinsulate and begin oil circulation throughout the system.
4. Check and zero manometers, calibrate the potentiometer and inspect other instrumentation for normal operation.
5. As all parts of the system (extruder, pump, piping, transducer flanges, test section and oil reservoir) approach operating temperature, start polymer flow. Monitor pressures carefully to be certain no plugs of solid material remain.

6. Record pertinent general information to identify the test, and specific operating data for the measured pressures, temperatures, etc. Record at approximately ten minute intervals.
7. When all readings equilibrate, measure the flow and record all system temperatures and pressures.
8. Continue to collect data at ten minute intervals until at least two consecutive sets show no significant differences.
9. Change the flow rate to the next higher level and adjust controls as required to maintain constant test section temperatures.
10. Repeat steps 6 through 8 for all flow rates.
11. Shut the system down after the last readings, drain the oil from the test section, remove and clean the test section while it is hot.

Table C-VI

Summary of Data for a Packed Bed Test

General

Test Number	37
Test Date	October 19, 1971
Resin	50/50 PMMA/PS
Resin Preparation	Dry 2 hr, 85°C, 45 mm Hg
Bead Designation	V-1607
Bed Depth	1.75 cm
Air Pressure to Transducers	20 psig
Ambient Temperature	79 °F

Comments: Equipment assembled and heat on at 1500.
Extruder on at 1515.
Go to 2nd flow at 1628
Go to 3rd flow at 1648
Go to 4th flow at 1708
Go to 5th flow at 1740

Extruder (Ref. Flow)	1	2	3	4	5
Rear Zone Temp., °F					
Set	375	375	375	375	375
Read	368	368	369	370	370
Zone 2 Temp., °F					
Set	380	380	380	380	380
Read	347	347	348	354	360
Zone 3 Temp., °F					
Set	375	375	375	375	375
Read	367	368	368	368	368
Die #1 Temp., °F					
Set	380	380	380	380	380
Read	370	371	371	371	371
Die # 2 Temp., °F					
Read	410	409	406	394	389
Power, volts	70	70	65	55	50
Piping to Zenith Pump, Temperature, °F					
Zone 1	337	338	338	345	351
Zone 2	352	354	358	361	362
Zone 3	369	370	372	375	374
Extruder Speed, rpm	16	24	33	43	54
Extruder Power, amps	13.0	13.2	14.0	16.0	17.5
Pressure to Zenith Pump	800	1025	850	1000	550
Zenith Pump Speed, rpm	6.2	8.8	13.1	18.1	23.1

Table C-VI (continued)

Summary of Data for a Packed Bed Test

Oil System (Ref. Flow)	1	2	3	4	5
Reservoir Temp., °F					
Set	373	373	373	373	373
Read	374	374	374	374	374
Oil Pump Press., psig	40	40	40	40	40
Potentiometer (Temp.), mv					
Trail Sec Inlet	11.12	11.14	11.13	11.16	11.20
Trail Sec Outlet	11.09	11.12	11.12	11.14	11.19
Lead Sec Inlet	11.12	11.14	11.14	11.16	11.21
Lead Sec Outlet	11.12	11.12	11.12	11.15	11.19
Gear Pump Chamber	11.08	11.08	11.10	11.13	11.16
Melt System					
Flow, g/min	149	212	303	409	530
Potentiometer (Temp.), mv					
Z Pump Irlet	10.78	10.70	10.62	10.56	10.48
Z Pump Outlet	10.80	10.84	10.88	10.95	10.96
Lead Sec Inlet	10.75	10.74	10.74	10.80	10.85
Lead Sec Midway	10.92	10.91	10.90	10.95	10.94
Lead Trans Bulb	10.68	10.68	10.69	10.71	10.72
Lead Flange	10.92	10.92	10.91	10.93	10.94
Trail Flange	10.97	11.00	11.00	11.01	11.04
Trail Trans Bulb	10.76	10.79	10.80	10.82	10.84
Trail Sec Midway	11.01	11.03	11.02	11.00	11.04
Manometers (Press.), cm Hg					
Lead Left Leg	11.20	11.90	12.80	13.60	14.70
Lead Right Leg	10.05	10.80	11.80	12.60	13.70
Lead Total	21.25	22.70	24.60	26.20	28.40
Trail Left Leg	8.25	8.35	8.45	8.60	8.70
Trail Right Leg	8.00	8.05	8.20	8.35	8.35
Trail Total	16.25	16.40	16.65	16.95	17.05
Diff Left Leg	2.10	2.75	3.55	4.20	5.20
Diff Right Leg	2.95	3.55	4.40	5.05	6.10
Diff Total	5.05	6.30	7.95	9.25	11.30

Table C-VII

Calculation of Huang Model

Friction Factor-Reynolds Number

Technique

Two separate but closely related programs were written to calculate the Reynolds number using the Huang equation of state according to equations (II.99) and (IV.2). The first program calculated the arguments "a" in $\Gamma(a)$ and "χ^2/ν" in $Q(\chi^2/\nu)$. The gamma function $\Gamma(a)$ and the probability function $P(\chi^2/\nu) = 1-Q(\chi^2/\nu)$ were not directly available and were not programmed into the computer. Thus, the required values of these functions were entered manually from tabulations into the second program to complete the calculations. Copies of both programs are attached as continuations of Table C-VII.

Table C-VII (continued)

Calculation of Huang Model

Friction Factor-Reynolds Number

Program to Calculate a and χ^2/ν

```
FORTRAN IV G LEVEL  21                 PARKER              DATE = 75050          09/05/15

0001                  REAL DATNO(214),DP(214),LENGTH(214),POROS(214),PSIG(214),A(214),B(
                     1214),C(214),N(214),DELP(214),TAURH(214),SHEAR(214),GAM1(214),GAM2(
                     2214),GAM3(214),CHI1(214),CHI2(214),CHI3(214)
0002                  READ (5,5) M,(DATNO(I),DP(I),LENGTH(I),POROS(I),PSIG(I),I=1,M)
0003            5     FORMAT (I10/(F5.0,3F10.3,20X,F10.0))
0004                  READ (5,7) (A(I),B(I),C(I),N(I),I=1,M)
0005            7     FORMAT (2F10.0,2F10.3)
0006                  DO 10 I=1,M
0007                  DELP(I)=PSIG(I)*6894.7
0008                  TAURH(I)=(DELP(I)/LENGTH(I))*(DP(I)/6.)*(POROS(I)/(1.-POROS(I)))
0009                  GAM1(I)=(N(I)+3.)/N(I)
0010                  GAM2(I)=(2.*N(I)+2.)/N(I)
0011                  GAM3(I)=(3.*N(I)+1.)/N(I)
0012                  GAMMA=1.
0013                  K=0
0014            20    SHEAR(I)=GAMMA-((A(I)*GAMMA+B(I)*GAMMA**N(I))*EXP(-C(I)*GAMMA**N(
                     1I))-TAURH(I))/(A(I)*((B(I)*N(I)*GAMMA**(N(I)-1.))*EXP(-C(I)*GAMMA
                     2**N(I)))*(1.-C(I)*GAMMA**N(I)))
0015                  TEST=(SHEAR(I)-GAMMA)/SHEAR(I)
0016                  IF (ABS(TEST).LE..001) GO TO 30
0017                  K=K+1
0018                  IF(K.LT.20) GO TO 35
0019                  WRITE (6,25)
0020            25    FORMAT (1X,'SHEAR(I) DID NOT CONVERGE IN 20 ITERATIONS')
0021                  GO TO 10
0022            35    GAMMA=SHEAR(I)
0023                  GO TO 20
0024            30    CHI1(I)=(2.*C(I)*SHEAR(I)**N(I))
0025                  CHI2(I)=(4.*C(I)*SHEAR(I)**N(I))
0026                  CHI3(I)=(6.*C(I)*SHEAR(I)**N(I))
0027            10    CONTINUE
0028                  WRITE (6,40)
0029            40    FORMAT (1X,'DATNO',5X,'DP',5X,'LENGTH',5X,'POROS',5X,'PSIG',6X,'A'
                     1,9X,'B',11X,'C',8X,'N'//)
0030                  WRITE (6,50) (DATNO(I),DP(I),LENGTH(I),POROS(I),PSIG(I),A(I),B(I),
                     1C(I),N(I),I=1,M)
0031            50    FORMAT (F5.0,3F10.3,3F10.0,2F10.4)
0032                  WRITE (6,60)
0033            60    FORMAT ('1',5X,'TAURH',9X,'SHEAR'//)
0034                  WRITE (6,70) (TAURH(I),SHEAR (I),I=1,M)
0035            70    FORMAT (F15.0,F15.4)
0036                  WRITE (6,80)
0037            80    FORMAT ('1',4X,'GAM1',8X,'GAM2',8X,'GAM3',8X,'CHI1',8X,'CHI2',8X,'
                     1CHI3'//)
0038                  WRITE (6,90) (GAM1(I),GAM2(I),GAM3(I),CHI1(I),CHI2(I),CHI3(I),I=1,
                     1M)
0039            90    FORMAT (1X,3F12.4,3F12.6)
0040                  STOP
0041                  END
```

Table C-VII (continued)

Calculation of Huang Model

Friction Factor-Reynolds Number

Program to Calculate f^* and $N_{re,eff}$ p.1

```
FORTRAN IV G LEVEL  21                PARKER              DATE = 75069          16/40/07

0001                  REAL DATNO(214),DP(214),LENGTH(214),POROS(214),RHO(214),FLOW(214),
                     &PSIG(214),A(214),B(214),C(214),N(214),DELP(214),TAURH(214),SHEAR(2
                     &14),SUPVEL(214),GAM1(214),GAM2(214),GAM3(214),GAM1F(214),GAM2F(214
                     &),GAM3F(214),CHI1F(214),CHI2F(214),CHI3F(214),EFFVIS(214),GOMEAS(2
                     &14),GOCALC(214),FF(214),LFF(214),NRE(214),LNRE(214),CONST(214),CHI
                     &1(214),CHI2(214),CHI3(214)
0002                  READ (5,3) M,(DATNO(I),DP(I),LENGTH(I),POROS(I),RHO(I),FLOW(I),PSI
                     &G(I),I=1,M)
0003                3 FORMAT (I10/(F5.0,4F10.3,2F10.0))
0004                  READ (5,7) (A(I),B(I),C(I),N(I),I=1,M)
0005              7   FORMAT (2F10.0,2F10.3)
0006                  READ (5,5) (GAM1F(I),GAM2F(I),GAM3F(I),I=1,M)
0007                5 FORMAT (3F10.3)
0008                  READ (5,9) (CHI1F(I),CHI2F(I),CHI3F(I),I=1,M)
0009                9 FORMAT (3F10.5)
0010                  DO 10 I=1,M
0011                  DELP(I)=PSIG(I)*68947.
0012                  TAURH(I)=(DELP(I)/LENGTH(I))*(DP(I)/6.)*(POROS(I)/(1.-POROS(I)))
0013                  GAM1(I)=(N(I)+3.)/N(I)
0014                  GAM2(I)=(2.*N(I)+2.)/N(I)
0015                  GAM3(I)=(3.*N(I)+1.)/N(I)
0016                  GAMMA=1.
0017                  K=0
0018              20  SHEAR(I)=GAMMA-((A(I)*GAMMA*(B(I)*GAMMA**N(I)))*EXP(-C(I)*GAMMA**N(
                     &BI)))-TAURH(I))/(A(I)*((B(I)*N(I)*GAMMA**(N(I)-1.))*EXP(-C(I)*GAMMA
                     &**N(I)))*(1.-C(I)*GAMMA**N(I)))
0019                  TEST=(SHEAR(I)-GAMMA)/SHEAR(I)
0020                  IF (ABS(TEST).LE..001) GO TO 30
0021                  K=K+1
0022                  IF(K.LT.20) GO TO 35
0023                  WRITE (6,25)
0024              25  FORMAT (1X,'SHEAR(I) DID NOT CONVERGE IN 20 ITERATIONS')
0025                  GO TO 10
0026              35  GAMMA=SHEAR(I)
0027                  GO TO 20
0028              30  CHI1(I)=(2.*C(I)*SHEAR(I)**N(I))
0029                  CHI2(I)=(4.*C(I)*SHEAR(I)**N(I))
0030                  CHI3(I)=(6.*C(I)*SHEAR(I)**N(I))
0031*                 GOMEAS(I)=FLOW(I)/4994.
0032                  SUPVEL(I)=(DP(I)/9.)*(POROS(I)**2./(1.-POROS(I)))*(SHEAR(I)-(1./TA
                     &URH(I)**3.)*(A(I)**3.*SHEAR(I)**4./4.+(3.*B(I)*A(I)**2./N(I))*((1.
                     &/C(I))**(GAM1(I)))*GAM1F(I)*(1.-CHI1F(I))+(3.*A(I)*B(I)**2./N(I))*
                     &((1./2.*C(I))**(GAM2(I)))*GAM2F(I)*(1.-CHI2F(I))+(B(I)**3./N(I))*(
                     &(1./3.*C(I))**(GAM3(I)))*GAM3F(I)*(1.-CHI3F(I))))
0033                  EFFVIS(I)=TAURH(I)/(SHEAR(I)-(1./TA
                     &URH(I)**3.)*(A(I)**3.*SHEAR(I)**4./4.+(3.*B(I)*A(I)**2./N(I))*((1.
                     &/C(I))**(GAM1(I)))*GAM1F(I)*(1.-CHI1F(I))+(3.*A(I)*B(I)**2./N(I))*
                     &((1./2.*C(I))**(GAM2(I)))*GAM2F(I)*(1.-CHI2F(I))+(B(I)**3./N(I))*(
                     &(1./3.*C(I))**(GAM3(I)))*GAM3F(I)*(1.-CHI3F(I))))
0034                  FF(I)=(RHO(I)*DELP(I)/GOMEAS(I)**2.)*(DP(I)/LENGTH(I))*(POROS(I)**
                     &3./(1.-POROS(I)))
0035                  LFF(I)=ALOG(FF(I))
0036                  NRE(I)=(DP(I)*GOMEAS(I))/((1.-POROS(I))*EFFVIS(I))
0037                  LNRE(I)=ALOG(NRE(I))
```

Table C-VII (continued)

Calculation of Huang Model

Friction Factor-Reynolds Number

Program to Calculate f^* and $N_{re,eff}$ p.2

```
FORTRAN IV G LEVEL  21                PARKER              DATE = 75069          16/40/07

0038                  CONST(I)=FF(I)*NRE(I)
0039                  GOCALC(I)=RHO(I)*SUPVEL(I)
0040            10    CONTINUE
0041                  WRITE (6,40)
0042               40 FORMAT ('1',1X,'DATNO',5X,'DP',5X,'LENGTH',5X,'POROS',5X,'RHO',5X,
                     &'FLOW',5X,'PSIG'/)
0043                  WRITE (6,50) (DATNO(I),DP(I),LENGTH(I),POROS(I),RHO(I),FLOW(I),PSI
                     &G(I),I=1,M)
0044               50 FORMAT (F5.0,3F10.3,F8.3,2F9.0)
0045                  WRITE (6,60)
0046               60 FORMAT ('1',6X,'A',9X,'B',9X,'C',9X,'N'/)
0047                  WRITE (6,70) (A(I),B(I),C(I),N(I),I=1,M)
0048               70 FORMAT (2F10.0,2F10.4)
0049                  WRITE (6,80)
0050            80    FORMAT ('1',4X,'GAM1',8X,'GAM2',8X,'GAM3',8X,'CHI1',8X,'CHI2',8X,'
                     &CHI3'//)
0051                  WRITE (6,90) (GAM1(I),GAM2(I),GAM3(I),CHI1(I),CHI2(I),CHI3(I),I=1,
                     &M)
0052            90    FORMAT (1X,3F12.4,3F12.6)
0053                  WRITE (6,93)
0054               93 FORMAT ('1',5X,'GAM1F',5X,'GAM2F',5X,'GAM3F',5X,'CHI1F',5X,'CHI2F'
                     &,5X,'CHI3F'/)
0055                  WRITE (6,96)  (GAM1F(I),GAM2F(I),GAM3F(I),CHI1F(I),CHI2F(I),CHI3F(
                     &I),I=1,M)
0056               96 FORMAT (3F10.3,3F10.5)
0057                  WRITE (6,100)
0058              100 FORMAT ('1',5X,'TAURH',8X,'SHEAR',6X,'SUPVEL',6X,'EFFVIS',6X,'GOCA
                     &LC',5X,'GOMEAS'/)
0059                  WRITE (6,110) (TAURH(I),SHEAR(I),SUPVEL(I),EFFVIS(I),GOCALC(I),GOM
                     &EAS(I),I=1,M)
0060              110 FORMAT (F12.0,2F12.4,F12.0,2F12.4)
0061                  WRITE (6,120)
0062              120 FORMAT ('1',6X,'FF',9X,'NRE',9X,'CONST',7X,'LFF',8X,'LNRE'/)
0063                  WRITE (6,130) (FF(I),NRE(I),CONST(I),LFF(I),LNRE(I),I=1,M)
0064              130 FORMAT (F11.0,F14.10,F10.1,2F11.3)
0065                  STOP
0066                  END
```

Table C-VIII

Calculation of Ellis Model

Friction Factor-Reynolds Number

Technique

A program was written for calculating the Ellis model Reynolds number as given by equations (IV.2) and (IV.3). A simplified language, specific to the time-share system used, was programmed. The calculations are readily adaptable to Fortran IV. A copy of the program is attached as a continuation of Table C-VIII.

Table C-VIII (continued)

Calculation of Ellis Model

Friction Factor-Reynolds Number

```
READY
OLD:ELLIS

READY
:F
3    GOMEAS=FLOW/4994
6    DELP=PSIG*68947
10   FF1=(RHO*DELP)/(GOMEAS*GOMEAS)
20   FF2=DP/LENGTH
30   FF3=(POROS*POROS*POROS)/(1.-POROS)
40   FF=FF1*FF2*FF3
50   NRE1=DP*GOMEAS/ETA0
60   NRE2=1./(1.-POROS)
70   RH=(DP*POROS)/(6.*(1.-POROS))
80   TAURH=DELP*RH/LENGTH
90   NRE4=LOG(TAURH/TAU)
100  NRE5=EXP((ALPHA-1.)*NRE4)
110  NRE3=(1.+(4.*NRE5/(ALPHA+3.)))
120  NRE=NRE1*NRE2*NRE3
130  GOCALC=(RHO*RH*TAURH*POROS*NRE3)/(2.*ETA0)
140  CONST=FF*NRE
150  REP FF,NRE,CONST,GOCALC,GOMEAS DIGITS 10
160  LFF=LOG(FF)
170  LNRE=LOG(NRE)
180  REP LFF,LNRE DIGITS 12
190  INP TTY

READY
BYE


OFF AT 09:44
```

APPENDIX D.

RHEOGONIOMETER EXPERIMENTAL RESULTS

Table D-I.1

Rheogoniometer Results for Experiments 20, 21 and 22

100 % PS-678

Temperature °C	t sec/rev	$\dot{\gamma}_{\theta\phi}$ sec^{-1}	Δ_T μ	$\tau_{\theta\phi}$ $dyne/cm^2$	Δ_N μ	$\tau_{11}-\tau_{22}$ $dyne/cm^2$
180	3.34×10^4	.00269	1.72	427.2		
180	1.68×10^4	.00535	4.50	1,117		
179	8.39×10^3	.01072	10.20	2,533		
179	4.22×10^3	.02130	20.00	4,965		
179	2.11×10^3	.04261	39.43	9,793		
179	1.06×10^2	.08482	72.75	18,070	2.54	6,110
179	5.30×10^2	.1696	138.0	34,280	7.77	18,670
179	2.65×10^2	.3393	238.9	59,340	20.23	48,640
180	1.33×10^2	.6760	394.3	97,930	49.30	118,500
180	66.7	1.348	611.2	151,800	100.7	242,000
180	33.4	2.692	889.0	220,800	185.9	446,900
180	16.8	5.352	1,156	287,000	322.3	774,800

From Table B-I: $\dot{\gamma}_{\theta\phi} = \frac{89.9056}{t}$

$$\tau_{\theta\phi} = 248.373\ \Delta_T$$

$$\tau_{11}-\tau_{22} = 2403.87\ \Delta_N$$

Table D-I.2

Rheogoniometer Results for Experiments 1-10 and 23

100 % PS-678

Temperature °C	t sec/rev	$\dot{\gamma}_{\theta\phi}$ sec^{-1}	Δ_T μ	$\tau_{\theta\phi}$ $dyne/cm^2$	Δ_N μ	$\tau_{11}-\tau_{22}$ $dyne/cm^2$
190	1.68×10^4	.00535	1.81	450.2		
190	8.39×10^3	.01072	3.90	969.4		
189	4.22×10^3	.02130	7.85	1,950		
190	2.11×10^3	.04261	15.22	3,781		
190	1.06×10^3	.08482	31.40	7,797		
190	5.30×10^2	.1696	60.03	14,910	1.29	3,110
190	2.65×10^2	.3393	107.4	26,670	4.80	11,540
190	1.33×10^2	.6760	188.9	46,910	13.88	33,370
190	66.7	1.348	326.5	81,090	37.69	90,590
190	33.4	2.692	501.9	124,600	78.99	189,900
190	16.8	5.352	721.9	179,300	158.4	380,700
190	8.40	10.70	960.7	238,600	282.9	680,000
189	4.22	21.30	1217.	302,200	472.3	1,135,000

From Table B-I: $\dot{\gamma}_{\theta\phi} = \frac{89.9056}{t}$

$\tau_{\theta\phi} = 248.373\ \Delta_T$

$\tau_{11}-\tau_{22} = 2403.87\ \Delta_N$

Table D-I.3

Rheogoniometer Results for Experiments 11, 12 and 13

100 % PS-678

Temperature °C	t sec/rev	$\dot{\gamma}_{\theta\phi}$ sec^{-1}	$\frac{\Delta_T}{\mu}$	$\tau_{\theta\phi}$ $dyne/cm^2$	$\frac{\Delta_N}{\mu}$	$\tau_{11}-\tau_{22}$ $dyne/cm^2$
201	1.68×10^4	.00535	0.93	231.0		
200	8.39×10^3	.01072	1.99	493.4		
200	4.22×10^3	.02130	4.06	1,008		
200	2.11×10^3	.04261	8.28	2,056		
200	1.06×10^3	.08482	17.10	4,247		
199	5.30×10^2	.1696	33.60	8,345		
199	2.65×10^2	.3393	63.90	15,870	2.35	5,650
199	1.33×10^2	.6760	119.3	29,640	6.00	14,400
199	66.7	1.348	211.3	52,490	16.17	38.860
199	33.4	2.692	347.3	86,260	42.90	103.100
199	16.8	5.352	527.8	131,100	89.3	214,700
199	8.40	10.70	767.0	190,500	173.7	417,500
199	4.22	21.30	1011.4	251,200	333.3	801,300

From Table B-I: $\dot{\gamma}_{\theta\phi} = \frac{89.9056}{t}$

$$\tau_{\theta\phi} = 248.373\, \Delta_T$$

$$\tau_{11} - \tau_{22} = 2403.87\, \Delta_N$$

Table D-I.4

Rheogoniometer Results for Experiments 14,15 and 16

100 % PS-678

Temperature °C	t sec/rev	$\dot{\gamma}_{\theta\phi}$ sec^{-1}	$\Delta\tau$ μ	$\tau_{\theta\phi}$ $dyne/cm^2$	Δ_N μ	$\tau_{11}-\tau_{22}$ $dyne/cm^2$
210	1.68×10^4	.00535	0.61	151.5		
210	8.39×10^3	.01072	1.08	269.1		
210	4.22×10^3	.02130	2.31	572.9		
209	2.11×10^3	.04261	4.91	1,219		
209	1.06×10^3	.08482	9.88	2,454		
209	5.30×10^2	.1696	19.73	4,901		
209	2.65×10^2	.3393	39.06	9,702		
209	1.33×10^2	.6760	73.92	18,360	2.83	6,811
209	66.7	1.348	135.3	33,610	8.00	19,230
209	33.4	2.692	233.4	57,960	20.67	49,680
209	16.8	5.352	372.3	92,480	49.73	119,600
209	8.40	10.70	572.1	142,100	102.1	245,400
209	4.22	21.30	799.6	198,600	195.3	469,600

From Table B-I: $\dot{\gamma}_{\theta\phi} = \frac{89.9056}{t}$

$$\tau_{\theta\phi} = 248.373\,\Delta_\tau$$

$$\tau_{11}-\tau_{22} = 2403.87\,\Delta_N$$

Table D-I.5

Rheogoniometer Results for Experiments 17, 18 and 19

100 % PS-678

Temperature °C	t sec/rev	$\dot{\gamma}_{\theta\phi}$ sec^{-1}	Δ_T μ	$\tau_{\theta\phi}$ $dyne/cm^2$	Δ_N μ	$\tau_{11}-\tau_{22}$ $dyne/cm^2$
221	1.68×10^4	.00535	0.29	72.6		
222	8.39×10^3	.01072	0.71	176.3		
222	4.22×10^3	.02130	1.33	331.2		
222	2.11×10^3	.04261	2.78	689.6		
221	1.06×10^3	.08482	5.97	1,482		
221	5.30×10^2	.1696	12.17	3,022		
221	2.65×10^2	.3393	24.73	6,143		
220	1.33×10^2	.6760	48.56	12,060	1.20	2,885
220	66.7	1.348	92.32	22,930	3.43	8,253
220	33.4	2.692	167.0	41,480	10.50	25,240
220	16.8	5.352	285.0	70,790	27.10	65,140
220	8.40	10.70	401.4	99,690	62.23	149,600
220	4.22	21.30	633.3	157,300	124.0	298,100

From Table B-I: $\dot{\gamma}_{\theta\phi} = \frac{89.9056}{t}$

$$\tau_{\theta\phi} = 248.373\,\Delta_T$$

$$\tau_{11}-\tau_{22} = 2403.87\,\Delta_N$$

Table D-II.1

Rheogoniometer Results for Experiments 81, 82 and 83

75/25 PS-678 /PMMA-VM

Temperature °C	t sec/rev	$\dot{\gamma}_{\theta\phi}$ sec^{-1}	Δ_T μ	$\tau_{\theta\phi}$ $dyne/cm^2$	Δ_N μ	$\tau_{11}-\tau_{22}$ $dyne/cm^2$
180	3.34×10^4	.00269	2.31	573.7		
180	1.68×10^4	.00535	4.67	1,160		
180	8.39×10^3	.01072	10.01	2,485		
180	4.22×10^3	.02130	19.60	4,868		
180	2.11×10^3	.04261	41.15	10,220		
180	1.06×10^3	.08482	77.79	19,320	2.45	5,881
180	5.30×10^2	.1696	143.3	35,600	6.66	16,020
180	2.65×10^2	.3393	244.7	60,770	20.20	48,560
180	1.33×10^2	.6760	383.3	95,210	46.67	112,180
180	66.7	1.348	594.7	147,700	94.57	227,300
180	33.4	2.692	889.0	220,800	167.8	403,400
180	16.8	5.352	1,183.0	293,800	280.7	674,700

From Table B-I: $\dot{\gamma}_{\theta\phi} = \frac{89.9056}{t}$

$$\tau_{\theta\phi} = 248.373\,\Delta_T$$

$$\tau_{11}-\tau_{22} = 2403.87\,\Delta_N$$

Table D-II.2

Rheogoniometer Results for Experiments 78, 79 and 80

75/25 PS-678 /PMMA-VM

Temperature °C	t sec/rev	$\dot{\gamma}_{\theta\phi}$ sec^{-1}	Δ_T μ	$\tau_{\theta\phi}$ $dyne/cm^2$	Δ_N μ	$\tau_{11}-\tau_{22}$ $dyne/cm^2$
190	3.34×10^4	.00269	1.01	251.7		
190	1.68×10^4	.00535	2.28	566.3		
190	8.39×10^3	.01072	4.67	1,159		
190	4.22×10^3	.02130	9.43	2,343		
190	2.11×10^3	.04261	18.47	4,587		
190	1.06×10^3	.08482	36.40	9,041		
190	5.30×10^2	.1696	67.24	16,700	2.22	5,345
190	2.65×10^2	.3393	123.6	30,710	6.78	16,290
190	1.33×10^2	.6760	205.3	50,990	16.23	39,020
190	66.7	1.348	339.0	84,200	39.60	95,190
190	33.4	2.692	511.3	127,000	79.43	190,900
190	16.8	5.352	733.2	182,100	150.3	361,400
190	8.40	10.70	1,001.0	248,500	242.0	581,700

From Table B-I: $\dot{\gamma}_{\theta\phi} = \frac{89.9056}{t}$

$\tau_{\theta\phi} = 248.373\,\Delta_T$

$\tau_{11}-\tau_{22} = 2403.87\,\Delta_N$

Table D-II.3

Rheogoniometer Results for Experiments 75, 76 and 77

75/25 PS-678 /PMMA-VM

Temperature °C	t sec/rev	$\dot{\gamma}_{\theta\phi}$ sec^{-1}	Δ_T μ	$\tau_{\theta\phi}$ $dyne/cm^2$	Δ_N μ	$\tau_{11}-\tau_{22}$ $dyne/cm^2$
201	3.34×10^4	.00269	0.62	154.8		
200	1.68×10^4	.00535	1.30	323.7		
200	8.39×10^3	.01072	2.32	575.4		
200	4.22×10^3	.02130	4.92	1,222		
200	2.11×10^3	.04261	9.82	2,439		
200	1.06×10^3	.08482	19.60	4,868		
200	5.30×10^2	.1696	37.77	9,380	0.94	2,268
200	2.65×10^2	.3393	70.02	17,390	2.61	6,282
200	1.33×10^2	.6760	128.0	31,790	7.39	17,760
200	66.7	1.348	221.0	54,890	18.90	45,430
200	33.4	2.692	361.3	89,740	43.10	103,600
200	16.8	5.352	566.5	140,700	89.43	215,000
200	8.40	10.70	844.7	209,800	165.2	397,000
200	4.22	21.30	1095.0	271,900	283.3	681,100

From Table B-I: $\dot{\gamma}_{\theta\phi} = \frac{89.9056}{t}$

$$\tau_{\theta\phi} = 248.373\,\Delta_T$$

$$\tau_{11}-\tau_{22} = 2403.87\,\Delta_N$$

Table D-II.4

Rheogoniometer Results for Experiments 72, 73 and 74

75/25 PS-678 /PMMA-VM

Temperature °C	t sec/rev	$\dot{\gamma}_{\theta\phi}$ sec^{-1}	Δ_T μ	$\tau_{\theta\phi}$ $dyne/cm^2$	Δ_N μ	$\tau_{11}-\tau_{22}$ $dyne/cm^2$
210	3.34×10^4	.00269	0.39	96.9		
210	1.68×10^4	.00535	0.70	173.0		
210	8.39×10^3	.01072	1.56	386.7		
210	4.22×10^3	.02130	3.06	759.2		
210	2.11×10^3	.04261	6.05	1,503		
210	1.06×10^3	.08482	11.39	2,829		
210	5.30×10^2	.1696	21.27	5,282	0.67	1,611
210	2.65×10^2	.3393	40.87	10,150	1.17	2,813
210	1.33×10^2	.6760	75.57	18,770	2.72	6,547
210	66.7	1.348	138.3	34,360	8.00	19,230
210	33.4	2.692	239.0	59,360	20.40	99,040
210	16.8	5.352	388.7	96,540	46.7	112,260
210	8.40	10.70	616.4	153,100	95.6	229,700
210	4.22	21.30	888.6	220,700	175.0	420,700

From Table B-I: $\dot{\gamma}_{\theta\phi} = \frac{89.9056}{t}$

$$\tau_{\theta\phi} = 248.373 \Delta_T$$

$$\tau_{11} - \tau_{22} = 2403.87 \Delta_N$$

Table D-II.5

Rheogoniometer Results for Experiments 69, 70 and 71

75/25 PS-678 /PMMA-VM

Temperature °C	t sec/rev	$\dot{\gamma}_{\theta\phi}$ sec^{-1}	Δ_T μ	$\tau_{\theta\phi}$ $dyne/cm^2$	Δ_N μ	$\tau_{11}-\tau_{22}$ $dyne/cm^2$
220	3.34×10^4	.00269	0.21	52.2		
220	1.68×10^4	.00535	0.50	124.2		
220	8.39×10^3	.01072	0.93	231.0		
220	4.22×10^3	.02130	1.84	456.2		
220	2.11×10^3	.04261	3.67	910.7		
220	1.06×10^3	.08482	7.22	1,794		
220	5.30×10^2	.1696	13.77	3,419		
220	2.65×10^2	.3393	26.40	6,557	0.50	1,202
220	1.33×10^2	.6760	49.44	12,280	1.56	3,742
220	66.7	1.348	93.33	23,180	4.17	10,020
220	33.4	2.692	167.0	41,480	11.37	27,320
220	16.8	5.352	286.3	71,120	27.90	67,070
220	8.40	10.70	444.5	110,400	60.00	144,230
220	4.22	21.30	683.6	169,800	116.7	280,450

From Table B-I: $\dot{\gamma}_{\theta\phi} = \frac{89.9056}{t}$

$\tau_{\theta\phi} = 248.373 \Delta_T$

$\tau_{11} - \tau_{22} = 2403.87 \Delta_N$

Table D-III.1

Rheogoniometer Results for Experiments 51 and 53

50/50 PS-678 /PMMA-VM

Temperature °C	t sec/rev	$\dot{\gamma}_{\theta\phi}$ sec^{-1}	Δ_T μ	$\tau_{\theta\phi}$ $dyne/cm^2$	Δ_N μ	$\tau_{11}-\tau_{22}$ $dyne/cm^2$
180	3.34×10^4	.00269	4.42	1,098		
180	1.68×10^4	.00535	9.92	2,463		
180	8.39×10^3	.01072	19.80	4,918		
179	4.22×10^3	.02130	38.80	9,637		
179	2.11×10^3	.04261	73.32	18,210	1.33	3,197
180	1.06×10^3	.08482	130.0	32,280	3.83	9,208
180	5.30×10^2	.1696	220.7	54,810	12.05	28,970
180	2.65×10^2	.3393	356.4	88.520	28.10	67,540
180	1.33×10^2	.6760	558.0	188,600	60.82	146,200
180	66.7	1.348	858.0	213,100	106.5	256,000
180	33.4	2.692	1,166	289,600	191.5	460,400

From Table B-I: $\dot{\gamma}_{\theta\phi} = \frac{89.9056}{t}$

$$\tau_{\theta\phi} = 248.373 \Delta_T$$

$$\tau_{11} - \tau_{22} = 2403.87 \Delta_N$$

Table D-III.2

Rheogoniometer Results for Experiments 39, 40 and 41

50/50 PS-678 /PMMA-VM

Temperature °C	t sec/rev	$\dot{\gamma}_{\theta\phi}$ sec^{-1}	$\frac{\Delta_T}{\mu}$	$\tau_{\theta\phi}$ $dyne/cm^2$	$\frac{\Delta_N}{\mu}$	$\tau_{11}-\tau_{22}$ $dyne/cm^2$
190	3.34×10^4	.00269	1.82	452.0		
190	1.68×10^4	.00535	3.75	931.4		
190	8.39×10^3	.01072	7.72	1,918		
190	4.22×10^3	.02130	14.83	3,684		
190	2.11×10^3	.04261	28.36	7,044		
190	1.06×10^3	.08482	53.87	13,380	0.92	2,200
190	5.30×10^2	.1696	98.96	24,580	2.89	6,947
190	2.65×10^2	.3393	168.1	41,740	8.43	20,270
190	1.33×10^2	.6760	300.0	74,500	22.09	53,090
190	66.7	1.348	483.1	120,000	48.92	117,600
190	33.4	2.692	733.2	182,100	100.7	242,000
190	16.8	5.352	1,044	259,400	182.0	437,500
190	8.40	10.70	1,405	349,000	312.5	751,200
190	4.22	21.30	1,776	441,100	500.0	1,202,000

From Table B-I: $\dot{\gamma}_{\theta\phi} = \frac{89.9056}{t}$

$\tau_{\theta\phi} = 248.373 \Delta_T$

$\tau_{11}-\tau_{22} = 2403.87 \Delta_N$

Table D-III.3

Rheogoniometer Results for Experiments 42, 43 and 44

50/50 PS-678 /PMMA-VM

Temperature °C	t sec/rev	$\dot{\gamma}_{\theta\phi}$ sec^{-1}	Δ_T μ	$\tau_{\theta\phi}$ $dyne/cm^2$	Δ_N μ	$\tau_{11}-\tau_{22}$ $dyne/cm^2$
200	3.34×10^4	.00269	1.07	265.7		
200	1.68×10^4	.00535	2.17	538.1		
200	8.39×10^3	.01072	4.11	1,020		
200	4.22×10^3	.02130	7.77	1,931		
200	2.11×10^3	.04261	15.02	3,731		
200	1.06×10^3	.08482	28.47	7,070		
200	5.30×10^2	.1696	52.78	13,110	0.78	1,875
200	2.65×10^2	.3393	98.36	24,430	2.37	5,703
200	1.33×10^2	.6760	181.6	45,100	9.73	23,380
200	66.7	1.348	306.0	75,990	23.90	57,450
200	33.4	2.692	494.4	122,800	52.46	126,100
200	16.8	5.352	744.4	184,900	109.6	263,400
200	8.40	10.70	1,072	266,300	204.7	492,000
200	4.22	21.30	1,439	357,400	347.0	834,200

From Table B-I: $\dot{\gamma}_{\theta\phi} = \frac{89.9056}{t}$

$$\tau_{\theta\phi} = 248.373 \Delta_T$$

$$\tau_{11} - \tau_{22} = 2403.87 \Delta_N$$

Table D-III.4

Rheogoniometer Results for Experiments 45, 46 and 47

50/50 PS-678 /PMMA-VM

Temperature °C	t sec/rev	$\dot{\gamma}_{\theta\phi}$ sec^{-1}	Δ_T μ	$\tau_{\theta\phi}$ $dyne/cm^2$	Δ_N μ	$\tau_{11}-\tau_{22}$ $dyne/cm^2$
210	3.34×10^4	.00269	0.60	148.2		
210	1.68×10^4	.00535	1.05	261.6		
210	8.39×10^3	.01072	2.08	517.4		
210	4.22×10^3	.02130	4.11	1,020		
210	2.11×10^3	.04261	7.39	1,835		
210	1.06×10^3	.08482	14.43	3,585		
210	5.30×10^2	.1696	27.27	6,772	0.50	1,202
210	2.65×10^2	.3393	50.57	12,560	1.50	3,606
210	1.33×10^2	.6760	95.58	23,740	4.11	9,881
210	66.7	1.348	171.5	42,600	10.83	26,040
210	33.4	2.692	294.5	73,150	26.23	63,060
210	16.8	5.352	466.6	115,900	57.45	138,100
210	8.40	10.70	722.3	179,400	113.3	272,400
210	4.22	21.30	1022	253,800	203.9	490,100

From Table B-I: $\dot{\gamma}_{\theta\phi} = \frac{89.9056}{t}$

$\tau_{\theta\phi} = 248.373 \Delta_T$

$\tau_{11}-\tau_{22} = 2403.87 \Delta_N$

Table D-III.5

Rheogoniometer Results for Experiments 48, 49 and 50

50/50 PS-678 /PMMA-VM

Temperature °C	t sec/rev	$\dot{\gamma}_{\theta\phi}$ sec^{-1}	Δ_T μ	$\tau_{\theta\phi}$ $dyne/cm^2$	Δ_N μ	$\tau_{11}-\tau_{22}$ $dyne/cm^2$
221	3.34×10^4	.00269	0.29	72.9		
221	1.68×10^4	.00535	0.57	141.6		
220	8.39×10^3	.01072	1.24	307.2		
220	4.22×10^3	.02130	2.44	606.9		
220	2.11×10^3	.04261	4.67	1,159		
220	1.06×10^3	.08482	9.28	2,304		
220	5.30×10^2	.1696	17.63	4,380		
220	2.65×10^2	.3393	34.13	8,478	0.89	2,132
220	1.33×10^2	.6760	63.86	15,860	2.16	5,200
220	66.7	1.348	119.9	29,770	5.67	13,620
220	33.4	2.692	212.4	52,760	13.53	32,530
220	16.8	5.352	355.4	88,270	34.63	83,250
220	8.40	10.70	560.9	139,300	76.58	184,100
220	4.22	21.30	844.3	209,700	147.6	354,700

From Table B-I: $\dot{\gamma}_{\theta\phi} = \frac{89.9056}{t}$

$\tau_{\theta\phi} = 248.373 \Delta_T$

$\tau_{11}-\tau_{22} = 2403.87 \Delta_N$

Table D-IV.1

Rheogoniometer Results for Experiments 54, 55 and 56

25/75 PS-678 /PMMA-VM

Temperature °C	t sec/rev	$\dot{\gamma}_{\theta\phi}$ sec^{-1}	Δ_T μ	$\tau_{\theta\phi}$ $dyne/cm^2$	Δ_N μ	$\tau_{11}-\tau_{22}$ $dyne/cm^2$
180	3.34×10^4	.00269	6.50	1,614		
180	1.68×10^4	.00535	14.00	3,478		
180	8.39×10^3	.01072	25.47	6,326		
180	4.22×10^3	.02130	49.48	12,290		
180	2.11×10^3	.04261	90.55	22,499		
180	1.06×10^3	.08482	162.0	40,240	3.67	8,820
180	5.30×10^2	.1696	276.6	68,710	9.46	22,730
180	2.65×10^2	.3393	461.0	114,500	29.33	70,510
180	1.33×10^2	.6760	705.4	175,200	67.77	162,900
180	66.7	1.348	1,060	263,300	124.8	300,000
180	33.4	2.692	1,375	341,500	218.8	526,000

From Table B-I: $\dot{\gamma}_{\theta\phi} = \frac{89.9056}{t}$

$$\tau_{\theta\phi} = 248.373\,\Delta_T$$

$$\tau_{11}-\tau_{22} = 2403.87\,\Delta_N$$

Table D-IV.2

Rheogoniometer Results for Experiments 57, 58 and 59

25/75 PS-678 /PMMA-VM

Temperature °C	t sec/rev	$\dot{\gamma}_{\theta\phi}$ sec^{-1}	Δ_T μ	$\tau_{\theta\phi}$ dyne/cm^2	Δ_N μ	$\tau_{11}-\tau_{22}$ dyne/cm^2
190	3.34×10^4	.00269	3.36	834.5		
190	1.68×10^4	.00535	6.67	1,656		
190	8.39×10^3	.01072	13.63	3,386		
190	4.22×10^3	.02130	26.67	6,623		
190	2.11×10^3	.04261	51.09	12,690		
190	1.06×10^3	.08482	94.54	23,480	2.15	5,170
190	5.30×10^2	.1696	164.0	40,740	5.28	12,680
190	2.65×10^2	.3393	311.6	77,930	13.43	32,290
190	1.33×10^2	.6760	466.6	115,900	37.23	89,500
190	66.7	1.348	744.4	184,900	75.53	181,600
190	33.4	2.692	1,083	269,000	144.9	348,200
190	16.8	5.352	1,522	378,100	261.3	628,200

From Table B-I: $\dot{\gamma}_{\theta\phi} = \frac{89.9056}{t}$

$$\tau_{\theta\phi} = 248.373\,\Delta_T$$

$$\tau_{11}-\tau_{22} = 2403.87\,\Delta_N$$

Table D-IV.3

Rheogoniometer Results for Experiments 60, 61 and 62

25/75 PS-678 /PMMA-VM

Temperature °C	t sec/rev	$\dot{\gamma}_{\theta\phi}$ sec^{-1}	Δ_T μ	$\tau_{\theta\phi}$ $dyne/cm^2$	Δ_N μ	$\tau_{11}-\tau_{22}$ $dyne/cm^2$
199	3.34×10^4	.00269	1.42	352.7		
200	1.68×10^4	.00535	2.86	711.2		
200	8.39×10^3	.01072	5.94	1,476		
200	4.22×10^3	.02130	11.65	2,894		
200	2.11×10^3	.04261	21.53	5,347		
200	1.06×10^3	.08482	40.83	10,140		
200	5.30×10^2	.1696	72.19	17,930	2.18	5,230
200	2.65×10^2	.3393	132.7	32,970	6.05	14,550
200	1.33×10^2	.6760	235.98	58,610	14.87	35,740
200	66.7	1.348	411.1	102,100	35.27	84,780
200	33.4	2.692	672.4	167,000	76.13	183,000
200	16.8	5.352	1,000	248,400	139.0	334,100
200	8.40	10.70	1,389	345,000	243.0	584,100

From Table B-I: $\dot{\gamma}_{\theta\phi} = \frac{89.9056}{t}$

$\tau_{\theta\phi} = 248.373 \Delta_T$

$\tau_{11}-\tau_{22} = 2403.87 \Delta_N$

Table D-IV.4

Rheogoniometer Results for Experiments 63, 64 and 65

25/75 PS-678 /PMMA-VM

Temperature °C	t sec/rev	$\dot{\gamma}_{\theta\phi}$ sec^{-1}	Δ_T μ	$\tau_{\theta\phi}$ $dyne/cm^2$	Δ_N μ	$\tau_{11}-\tau_{22}$ $dyne/cm^2$
210	3.34×10^4	.00269	0.74	183.0		
210	1.68×10^4	.00535	1.52	376.7		
210	8.39×10^3	.01072	2.75	683.0		
210	4.22×10^3	.02130	5.89	1,463		
210	2.11×10^3	.04261	11.60	2,881		
210	1.06×10^2	.08482	21.37	5,307		
210	5.30×10^2	.1696	39.47	9,803	1.05	2,532
210	2.65×10^2	.3393	75.53	18,760	2.67	6,410
210	1.33×10^2	.6760	140.7	34,940	7.15	17,200
210	66.7	1.348	258.7	64,250	17.17	41,270
210	33.4	2.692	433.2	107,600	40.30	96,880
210	16.8	5.352	672.0	166,900	83.87	201,600
210	8.40	10.70	988.8	245,600	154.3	371,000
210	4.22	21.30	1,333	331,200	276.3	664,300

From Table B-I: $\dot{\gamma}_{\theta\phi} = \frac{89.9056}{t}$

$\tau_{\theta\phi} = 248.373\,\Delta_T$

$\tau_{11}-\tau_{22} = 2403.87\,\Delta_N$

Table D-IV.5

Rheogoniometer Results for Experiments 66, 67 and 68

25/75 PS-678 /PMMA-VM

Temperature °C	t sec/rev	$\dot{\gamma}_{\theta\phi}$ sec^{-1}	$\frac{\Delta_T}{\mu}$	$\tau_{\theta\phi}$ $dyne/cm^2$	$\frac{\Delta_N}{\mu}$	$\tau_{11}-\tau_{22}$ $dyne/cm^2$
221	3.34×10^4	.00269	0.47	117.6		
220	1.68×10^4	.00535	0.85	211.1		
220	8.39×10^3	.01072	1.70	421.4		
220	4.22×10^3	.02130	3.47	861.9		
220	2.11×10^3	.04261	7.05	1,752		
220	1.06×10^3	.08482	12.83	3,187		
220	5.30×10^2	.1696	23.33	5,795		
220	2.65×10^2	.3393	42.80	10,630	1.18	2,837
220	1.33×10^2	.6760	82.78	20,560	2.94	7,075
220	66.7	1.348	147.4	36,600	8.33	20,020
220	33.4	2.692	262.7	65,240	23.07	55,450
220	16.8	5.352	439.3	109,100	51.10	122,800
220	8.40	10.70	694.9	172,600	104.7	251,600
220	4.22	21.30	1,000	248,400	189.0	454,300

From Table B-I: $\dot{\gamma}_{\theta\phi} = \frac{89.9056}{t}$

$\tau_{\theta\phi} = 248.373 \Delta_T$

$\tau_{11}-\tau_{22} = 2403.87 \Delta_N$

Table D-V.1

Rheogoniometer Results for Experiments 36, 37 and 38

100% PMMA-VM

Temperature °C	t sec/rev	$\dot{\gamma}_{\theta\phi}$ sec^{-1}	Δ_T μ	$\tau_{\theta\phi}$ $dyne/cm^2$	Δ_N μ	$\tau_{11}-\tau_{22}$ $dyne/cm^2$
180	3.34×10^4	.00269	13.77	3,419		
180	1.68×10^4	.00535	29.86	7,416		
180	8.39×10^3	.01072	61.12	15,180		
180	4.22×10^3	.02130	112.2	27,870		
180	2.11×10^3	.04261	217.8	54,100	8.33	20,020
180	1.06×10^3	.08482	415.9	103,300	21.39	51,420
180	5.30×10^2	.1696	755.3	187,600	49.77	119,600
180	2.65×10^2	.3393	1,311	325,600	122.3	294,100
180	1.33×10^2	.6760	2,050	509,200	261.3	628,200

From Table B-I: $\dot{\gamma}_{\theta\phi} = \frac{89.9056}{t}$

$$\tau_{\theta\phi} = 248.373\,\Delta_T$$

$$\tau_{11}-\tau_{22} = 2403.87\,\Delta_N$$

Table D-V.2

Rheogoniometer Results for Experiments 24, 25 and 26

100% PMMA-VM

Temperature °C	t sec/rev	$\dot{\gamma}_{\theta\phi}$ sec^{-1}	Δ_T μ	$\tau_{\theta\phi}$ $dyne/cm^2$	Δ_N μ	$\tau_{11}-\tau_{22}$ $dyne/cm^2$
190	3.34×10^4	.00269	4.53	1,126		
190	1.68×10^4	.00535	11.37	2,823		
190	8.39×10^3	.01072	21.00	5,216		
190	4.22×10^3	.02130	43.36	10,770		
190	2.11×10^3	.04261	84.75	21,050		
190	1.06×10^3	.08482	172.7	42,890	4.89	11,750
190	5.30×10^2	.1696	323.7	80,390	12.40	29,810
190	2.65×10^2	.3393	577.8	143,500	38.47	92,470
190	1.33×10^2	.6760	1,022	253,900	99.0	238,000
190	66.7	1.348	1,644	408,400	22.3	534,500

From Table B-I: $\dot{\gamma}_{\theta\phi} = \frac{89.9056}{t}$

$$\tau_{\theta\phi} = 248.373\,\Delta_T$$

$$\tau_{11}-\tau_{22} = 2403.87\,\Delta_N$$

Table D-V.3

Rheogoniometer Results for Experiments 27, 28 and 29

100% PMMA-VM

Temperature °C	t sec/rev	$\dot{\gamma}_{\theta\phi}$ sec^{-1}	Δ_T μ	$\tau_{\theta\phi}$ $dyne/cm^2$	Δ_N μ	$\tau_{11}-\tau_{22}$ $dyne/cm^2$
200	3.34×10^4	.00269	2.25	558.0		
200	1.68×10^4	.00535	4.44	1,103		
200	8.39×10^3	.01072	9.12	2,264		
200	4.22×10^3	.02130	17.9	4,446		
200	2.11×10^3	.04261	36.37	9,033		
200	1.06×10^3	.08482	71.67	17,800		
200	5.30×10^2	.1696	141.7	35,190	2.75	6,611
200	2.65×10^2	.3393	272.0	67,560	9.40	22,600
200	1.33×10^2	.6760	494.4	122,800	28.73	69,100
200	66.7	1.348	877.7	218,000	77.73	186,900
200	33.4	2.692	1,422	353,300	179.3	431,100
200	16.8	5.352	2,100	521,600	366.6	881,300

From Table B-I: $\dot{\gamma}_{\theta\phi} = \frac{89.9056}{t}$

$$\tau_{\theta\phi} = 248.373 \Delta_T$$

$$\tau_{11} - \tau_{22} = 2403.87 \Delta_N$$

Table D-V.4

Rheogoniometer Results for Experiments 30, 31 and 32

100% PMMA-VM

Temperature °C	t sec/rev	$\dot{\gamma}_{\theta\phi}$ sec^{-1}	Δ_T μ	$\tau_{\theta\phi}$ $dyne/cm^2$	Δ_N μ	$\tau_{11}-\tau_{22}$ $dyne/cm^2$
211	3.34×10^4	.00269	1.12	279.4		
210	1.68×10^4	.00535	2.13	528.2		
210	8.39×10^3	.01072	4.22	1,049		
210	4.22×10^3	.02130	8.56	2,125		
210	2.11×10^3	.04261	17.07	4,239		
210	1.06×10^2	.08482	34.43	8,552		
210	5.30×10^2	.1696	67.24	16,700	0.87	2,091
210	2.65×10^2	.3393	135.0	33,530	2.46	5,906
210	1.33×10^2	.6760	255.3	63,420	8.95	21,510
210	66.7	1.348	466.6	115,900	28.89	69,450
210	33.4	2.692	816.5	202,800	76.67	184,300
210	16.8	5.352	1,327	329,700	172.2	414,000
210	8.40	10.70	1,922	477,400	361.3	868,600

From Table B-I: $\dot{\gamma}_{\theta\phi} = \frac{89.9056}{t}$

$$\tau_{\theta\phi} = 248.373\,\Delta_T$$

$$\tau_{11}-\tau_{22} = 2403.87\,\Delta_N$$

Table D-V.5

Rheogoniometer Results for Experiments 33, 34 and 35

100% PMMA-VM

Temperature °C	t sec/rev	$\dot{\gamma}_{\theta\phi}$ sec^{-1}	Δ_T μ	$\tau_{\theta\phi}$ $dyne/cm^2$	Δ_N μ	$\tau_{11}-\tau_{22}$ $dyne/cm^2$
220	3.34×10^4	.00269	0.54	135.0		
220	1.68×10^4	.00535	1.02	253.4		
220	8.39×10^3	.01072	2.22	552.2		
219	4.22×10^3	.02130	4.33	1,076		
220	2.11×10^3	.04261	8.50	2,111		
220	1.06×10^3	.08482	16.93	4,206		
220	5.30×10^2	.1696	34.43	8,552		
220	2.65×10^2	.3393	67.76	16,830	0.84	2,007
220	1.33×10^2	.6760	133.9	33,250	2.39	5,745
220	66.7	1.348	256.9	63,800	9.56	22,970
220	33.4	2.692	466.6	115,900	28.73	69,070
220	16.8	5.352	827.8	205,600	74.90	180,000
220	8.40	10.70	1,289	320,100	172.1	413,700

From Table B-I: $\dot{\gamma}_{\theta\phi} = \frac{89.9056}{t}$

$$\tau_{\theta\phi} = 248.373\,\Delta_T$$

$$\tau_{11}-\tau_{22} = 2403.87\,\Delta_N$$

APPENDIX E.

PACKED BED EXPERIMENTAL RESULTS

Table E-I.1

Packed Bed Results 100% PMMA-VM Blank

Run No. & Bed Depth cm	Flow Rate g/min	Temperature Inlet °F	Temperature Outlet °F	Pressure Inlet psig	Pressure Outlet psig	Pressure Drop "Blank" psig
#12	151	395	396	173	46	127
0	238	393	394	236	61	175
	310	395	395	290	90	200
	410	397	396	335	117	218
	505	399	398	370	139	231

Table E-I.2

Packed Bed Results 100% PMMA-VM V-390 (0.979 cm) Beads

Run No. & Bed Depth cm	Flow Rate g/min	Temperature Inlet °F	Temperature Outlet °F	Pressure Inlet psig	Pressure Outlet psig	Pressure Drop Total psig	Pressure Drop Blank psig	Pressure Drop Net psig
#7	147	399	399	202	36	166	126	40
	228	395	397	310	61	249	170	79
1.83	306	397	398	374	85	289	198	91
#6	144	396	397	295	41	254	125	129
	235	396	400	423	63	360	174	186
4.37	309	395	399	521	80	441	200	241
	418	399	402	576	105	471	220	251
	457	400	402	616	111	505	225	280

Table E-I.3

Packed Bed Results 100% PMMA-VM V-280 (0.679 cm) Beads

Run No. & Bed Depth cm	Flow Rate g/min	Temperature Inlet °F	Temperature Outlet °F	Pressure Inlet psig	Pressure Outlet psig	Pressure Drop Total psig	Pressure Drop Blank psig	Pressure Drop Net psig
#11	156	398	398	272	49	223	131	92
1.75	236	396	397	401	70	331	174	157
	314	396	397	489	89	400	202	198
	425	400	399	593	127	466	222	244
	516	401	400	625	133	492	233	259
	148	401	400	260	48	212	126	86
#10	154	398	398	467	44	423	130	293
4.29	238	397	399	717	71	646	175	471
	308	397	399	832	91	741	199	542

Table E-I.4

Packed Bed Results 100% PMMA-VM V-1607 (0.375cm) Beads

Run No. & Bed Depth cm	Flow Rate g/min	Temperature Inlet °F	Temperature Outlet °F	Pressure Inlet psig	Pressure Outlet psig	Pressure Drop Total psig	Pressure Drop Blank psig	Pressure Drop Net psig
#8	149	400	400	439	44	395	126	269
1.75	223	395	398	694	63	631	167	464
	302	398	399	793	87	706	196	510
#9	151	398	401	988	42	946	127	819
4.29	229	398	401	1448	62	1386	170	1216
	407	407	408	2152	103	2049	216	1833

Table E-I.5

Packed Bed Results 100% PMMA-VM V-080 (0.198cm) Beads

Run No. & Bed Depth cm	Flow Rate g/min	Temperature Inlet °F	Temperature Outlet °F	Pressure Inlet psig	Pressure Outlet psig	Pressure Drop Total psig	Pressure Drop Blank psig	Pressure Drop Net psig
#5	148	399	401	1106	32	1074	126	948
1.75	225	395	400	1700	52	1648	168	1480
	294	397	402	2011	66	1945	195	1750
	415	397	403	2479	90	2389	219	2170

Table E-II.1

Packed Bed Results 75/25 PMMA/PS Blank

Run No. & Bed Depth cm	Flow Rate g/min	Temperature Inlet °F	Temperature Outlet °F	Pressure Inlet psig	Pressure Outlet psig	Pressure Drop "Blank" psig
#48	152	398	399	141	26	115
0	207	398	400	170	33	137
	310	397	399	224	51	173
	421	397	399	269	65	204
	532	398	400	306	83	223

Table E-II.2

Packed Bed Results 75/25 PMMA/PS V-390 (0.979 cm) Beads

Run No. & Bed Depth cm	Flow Rate g/min	Temperature Inlet °F	Temperature Outlet °F	Pressure Inlet psig	Pressure Outlet psig	Pressure Drop Total psig	Pressure Drop Blank psig	Pressure Drop Net psig
#53	154	398	398	188	25	163	117	46
1.83	213	398	399	227	34	193	139	54
	301	398	400	280	53	227	168	59
	411	398	400	347	72	275	201	74
	534	399	400	405	86	319	223	96
#50	153	398	400	232	23	209	117	92
4.37	208	399	401	284	41	243	136	107
	297	397	400	364	56	308	167	141
	403	397	400	445	75	370	200	170
	516	398	401	513	94	419	220	199

Table E-II.3

Packed Bed Results 75/25 PMMA/PS V-280 (0.679 cm) Beads

Run No. & Bed Depth cm	Flow Rate g/min	Temperature Inlet °F	Temperature Outlet °F	Pressure Inlet psig	Pressure Outlet psig	Pressure Drop Total psig	Pressure Drop Blank psig	Pressure Drop Net psig
#51	151	398	400	216	19	197	114	83
1.75	214	398	400	266	28	238	139	99
	305	398	400	336	44	292	170	122
	419	398	400	413	65	348	203	145
	531	397	400	466	81	385	223	162
#54	154	397	399	357	28	329	117	212
4.29	216	398	400	448	35	413	140	273
	303	399	400	538	55	483	169	314
	408	398	400	632	75	557	201	356
	524	401	402	792	93	699	222	477
#57	152	399	400	344	20	324	115	209
4.29	214	398	400	433	34	399	139	260
	306	397	399	551	51	500	170	330
	412	397	399	674	73	601	201	400
	546	398	401	785	90	695	227	468
#58	155	398	399	464	28	436	117	319
6.10	231	398	400	588	37	551	144	407
	306	398	400	693	57	636	170	466
	414	398	401	824	74	750	202	548
	538	398	402	953	91	862	225	637

Table E-II.4

Packed Bed Results 75/25 PMMA/PS V-1607 (0.375 cm) Beads

Run No. & Bed Depth cm	Flow Rate g/min	Temperature Inlet °F	Temperature Outlet °F	Pressure Inlet psig	Pressure Outlet psig	Pressure Drop Total psig	Pressure Drop Blank psig	Pressure Drop Net psig
#55	154	397	401	348	24	324	117	207
1.75	212	397	400	424	35	389	138	251
	301	397	400	542	51	491	168	323
	406	397	400	653	67	586	201	385
	525	397	400	753	90	663	222	441
#49	151	400	402	662	22	640	114	526
4.29	207	399	401	856	40	816	136	680
	296	398	402	1066	45	1021	167	854
	400	399	402	1276	66	1210	199	1011
	513	400	404	1416	86	1330	220	1110

Table E-II.5

Packed Bed Results 75/25 PMMA/PS V-080 (0.198 cm) Beads

Run No. & Bed Depth cm	Flow Rate g/min	Temperature Inlet °F	Temperature Outlet °F	Pressure Inlet psig	Pressure Outlet psig	Pressure Drop Total psig	Pressure Drop Blank psig	Pressure Drop Net psig
#52	152	398	399	788	26	762	115	647
	214	399	401	959	35	924	139	785
1.75	300	398	401	1170	50	1120	168	952
	403	398	401	1354	64	1290	200	1090
	531	400	403	1537	80	1457	223	1234
#56	153	399	402	1910	26	1884	116	1768
	215	400	404	2068	34	2034	139	1895
4.29								

Table E-III.1

Packed Bed Results 50/50 PMMA/PS Blank

Run No. & Bed Depth cm	Flow Rate g/min	Temperature Inlet °F	Temperature Outlet °F	Pressure Inlet psig	Pressure Outlet psig	Pressure Drop "Blank" psig
#36	147	396	397	124	14	110
	210	397	397	161	24	137
0	301	395	396	198	40	158
	410	395	396	245	54	191
	539	396	396	273	73	200

Table E-III.2

Packed Bed Results 50/50 PMMA/PS V-390 (0.979 cm) Beads

Run No. & Bed Depth cm	Flow Rate g/min	Temperature Inlet °F	Temperature Outlet °F	Pressure Inlet psig	Pressure Outlet psig	Pressure Drop Total psig	Pressure Drop Blank psig	Pressure Drop Net psig
#42	151	395	396	168	25	143	110	33
1.83	210	395	397	207	28	179	137	42
	307	393	396	262	46	216	163	53
	419	395	396	306	60	246	186	60
	537	395	397	340	71	269	203	66
#40	152	396	397	222	76	196	111	85
4.37	208	398	401	264	34	230	135	95
	299	399	401	317	45	272	161	111
	400	396	400	379	58	321	184	137
	522	396	399	430	69	361	202	159

Table E-III.3

Packed Bed Results 50/50 PMMA/PS V-280 (0.679 cm) Beads

Run No. & Bed Depth cm	Flow Rate g/min	Temperature Inlet °F	Temperature Outlet °F	Pressure Inlet psig	Pressure Outlet psig	Pressure Drop Total psig	Pressure Drop Blank psig	Pressure Drop Net psig
#44	145	395	396	189	26	163	107	56
1.75	197	397	399	233	33	200	132	68
	290	397	399	283	38	245	158	87
	393	397	398	339	52	287	182	105
	509	396	398	391	66	325	201	124
#38	149	396	398	301	26	275	110	165
4.29	199	397	399	356	33	323	132	191
	296	396	399	463	46	417	160	257
	406	396	399	542	62	480	185	295
	519	397	400	598	73	525	202	323

Table E-III.4

Packed Bed Results 50/50 PMMA/PS V-1607 (0.375 cm) Beads

Run No. & Bed Depth cm	Flow Rate g/min	Temperature Inlet °F	Temperature Outlet °F	Pressure Inlet psig	Pressure Outlet psig	Pressure Drop Total psig	Pressure Drop Blank psig	Pressure Drop Net psig
#37	149	397	398	293	24	269	110	159
1.75	212	397	399	365	31	334	138	196
	303	396	399	459	43	416	162	254
	409	397	399	538	58	480	185	295
	530	397	400	646	64	582	202	380
#41	144	397	400	520	16	504	109	395
4.29	199	397	400	628	20	608	132	476
	294	396	400	837	34	803	159	644
	406	395	399	1049	45	1004	185	819
	522	396	400	1161	63	1098	202	896
#47	139	398	400	706	16	690	104	586
6.10	197	398	401	883	26	857	132	725
	293	397	401	1145	36	1109	159	950
	400	398	402	1385	56	1329	184	1145
	515	398	403	1578	65	1513	201	1312

Table E-III.5

Packed Bed Results 50/50 PMMA/PS V-080 (0.198 cm) Beads

Run No. & Bed Depth cm	Flow Rate g/min	Temperature Inlet °F	Temperature Outlet °F	Pressure Inlet psig	Pressure Outlet psig	Pressure Drop Total psig	Pressure Drop Blank psig	Pressure Drop Net psig
#39	148	398	401	647	21	626	109	517
1.75	200	397	401	825	27	798	132	666
	295	395	400	1067	43	1024	159	865
	405	396	401	1193	58	1135	185	950
	519	396	401	1347	68	1279	202	1077
#46	147	398	399	581	21	560	108	452
1.75	204	397	400	761	26	735	134	601
	298	397	401	907	36	871	160	711
	405	397	401	1092	48	1044	185	859
	517	397	402	1227	63	1164	201	963
#45	147	398	402	1288	11	1277	108	1169
4.29	199	398	402	1534	20	1514	132	1382
	293	398	404	1970	31	1939	159	1780
	396	398	404	2421	46	2375	183	2192
	497	400	406	2777	56	2721	199	2522

Table E-III.6

Packed Bed Results 50/50 PMMA/PS P-047 (0.117 cm) Beads

Run No. & Bed Depth cm	Flow Rate g/min	Temperature Inlet °F	Temperature Outlet °F	Pressure Inlet psig	Pressure Outlet psig	Pressure Drop Total psig	Pressure Drop Blank psig	Pressure Drop Net psig
#43	146	399	401	1251	26	1225	107	1118
1.75	198	399	402	1483	31	1452	132	1320
	292	398	403	1839	42	1797	159	1638
	399	398	404	2132	53	2074	184	1895
	507	399	405	2474	63	2411	200	2211

Table E-IV.1

Packed Bed Results 25/75 PMMA/PS Blank

Run No. & Bed Depth cm	Flow Rate g/min	Temperature Inlet °F	Temperature Outlet °F	Pressure Inlet psig	Pressure Outlet psig	Pressure Drop "Blank" psig
#25	144	396	399	100	14	86
0	205	395	398	119	23	96
	299	393	396	152	32	120
	413	394	396	181	44	137
	519	394	396	210	53	157

Table E-IV.2

Packed Bed Results 25/75 PMMA/PS V-390 (0.979 cm) Beads

Run No. & Bed Depth cm	Flow Rate g/min	Temperature Inlet °F	Temperature Outlet °F	Pressure Inlet psig	Pressure Outlet psig	Pressure Drop Total psig	Pressure Drop Blank psig	Pressure Drop Net psig
#34	147	401	401	117	13	104	82	22
1.83	205	398	399	152	20	132	100	32
	298	396	398	191	26	165	120	45
	402	396	398	227	40	187	138	49
	509	396	398	256	48	208	154	54
#26	148	397	398	169	18	151	82	69
4.37	204	397	399	194	24	170	100	70
	300	396	398	242	30	212	120	92
	406	396	398	302	43	259	139	120
	512	396	398	337	51	286	154	132

Table E-IV.3

Packed Bed Results 25/75 PMMA/PS V-280 (0.679 cm) Beads

Run No. & Bed Depth cm	Flow Rate g/min	Temperature Inlet °F	Temperature Outlet °F	Pressure Inlet psig	Pressure Outlet psig	Pressure Drop Total psig	Pressure Drop Blank psig	Pressure Drop Net psig
#31	148	396	398	145	16	129	82	47
1.75	209	396	398	181	22	159	101	58
	302	396	398	222	30	192	120	72
	414	396	398	272	43	229	140	89
	532	397	399	310	49	261	156	105
#27	144	397	398	219	16	203	81	122
4.29	200	397	399	276	21	255	99	156
	296	396	399	349	28	321	119	202
	400	396	398	420	38	382	138	244
	509	397	399	471	46	425	154	271

Table E-IV.4

Packed Bed Results 25/75 PMMA/PS V-1607 (0.375 cm) Beads

Run No. & Bed Depth cm	Flow Rate g/min	Temperature Inlet °F	Temperature Outlet °F	Pressure Inlet psig	Pressure Outlet psig	Pressure Drop Total psig	Pressure Drop Blank psig	Pressure Drop Net psig
#28	143	398	400	207	16	191	81	110
1.75	204	397	400	265	21	244	100	144
	295	396	399	337	30	307	119	188
	404	396	398	400	40	360	138	222
	519	397	400	457	50	407	155	252
#29	144	396	398	397	16	381	81	300
4.29	206	397	400	495	24	471	100	371
	299	396	400	654	31	623	120	503
	407	397	401	774	41	733	139	594
	518	399	402	880	50	830	155	675

Table E-IV.5

Packed Bed Results 25/75 PMMA/PS V-080 (0.198 cm) Beads

Run No. & Bed Depth cm	Flow Rate g/min	Temperature Inlet °F	Temperature Outlet °F	Pressure Inlet psig	Pressure Outlet psig	Pressure Drop Total psig	Pressure Drop Blank psig	Pressure Drop Net psig
#32	148	396	399	532	16	516	82	434
1.75	209	398	401	643	26	617	101	516
	302	399	402	791	31	760	120	640
	409	398	402	926	42	884	140	744
	518	398	403	1030	52	978	155	823
#33	144	399	401	1117	16	1101	81	1020
4.29	210	400	403	1387	21	1366	101	1265
	295	398	403	1718	31	1687	119	1568
	399	398	404	2105	39	2066	138	1928
	506	400	407	2399	46	2353	153	2200

Table E-V.1

Packed Bed Results 100% PS-678 Blank

Run No. & Bed Depth cm	Flow Rate g/min	Temperature Inlet °F	Temperature Outlet °F	Pressure Inlet psig	Pressure Outlet psig	Pressure Drop "Blank" psig
#13	151	396	397	101	12	89
0	220	396	397	125	22	103
	304	395	396	150	31	119
	397	396	397	176	39	137
	512	396	398	199	51	148

Table E-V.2

Packed Bed Results 100% PS-678 V-390 (0.979 cm) Beads

Run No. & Bed Depth cm	Flow Rate g/min	Temperature Inlet °F	Temperature Outlet °F	Pressure Inlet psig	Pressure Outlet psig	Pressure Drop Total psig	Pressure Drop Blank psig	Pressure Drop Net psig
#22	142	397	398	106	9	97	80	17
1.83	209	396	398	142	16	126	100	26
	301	395	397	181	24	157	120	37
	406	395	397	223	36	187	139	48
	512	396	398	253	46	207	151	56
#16	139	398	398	138	7	131	79	52
4.37	208	396	398	185	16	169	100	69
	301	396	398	234	26	208	120	88
	406	396	397	300	36	264	139	125
	509	396	398	329	46	283	151	132

Table E-V.3

Packed Bed Results 100% PS-678 V-280 (0.679 cm) Beads

Run No. & Bed Depth cm	Flow Rate g/min	Temperature Inlet °F	Temperature Outlet °F	Pressure Inlet psig	Pressure Outlet psig	Pressure Drop Total psig	Pressure Drop Blank psig	Pressure Drop Net psig
#21	142	397	398	132	11	121	80	41
1.75	206	396	398	168	16	152	100	52
	303	395	398	211	25	186	120	66
	406	396	398	255	36	219	139	80
	513	397	399	287	43	244	152	92
#23	137	398	400	197	9	188	78	110
4.29	204	398	400	230	16	214	99	115
	304	397	399	307	23	284	121	163
	407	396	398	376	31	345	139	206
	515	396	398	434	42	392	152	240

Table E-V.4

Packed Bed Results 100% PS-678 V-1607 (0.375 cm) Beads

Run No. & Bed Depth cm	Flow Rate g/min	Temperature Inlet °F	Temperature Outlet °F	Pressure Inlet psig	Pressure Outlet psig	Pressure Drop Total psig	Pressure Drop Blank psig	Pressure Drop Net psig
#15	148	397	398	202	7	195	82	113
1.75	211	396	398	265	16	249	101	148
	305	396	397	338	26	312	121	191
	396	396	397	394	36	358	137	221
	504	396	398	447	46	401	151	250
#18	147	399	400	404	11	393	82	311
4.29	209	396	398	514	21	493	100	393
	307	396	398	630	31	599	121	478
	410	396	400	724	36	688	139	549
	525	397	400	844	46	798	153	645
#24	143	397	398	394	13	381	80	301
4.29	212	397	399	499	19	480	101	379
	307	396	399	640	26	614	121	493
	406	396	399	766	36	730	139	591
	519	398	400	860	41	819	152	667

Table E-V.5

Packed Bed Results 100% PS-678 V-080 (0.198 cm) Beads

Run No. & Bed Depth cm	Flow Rate g/min	Temperature Inlet °F	Temperature Outlet °F	Pressure Inlet psig	Pressure Outlet psig	Pressure Drop Total psig	Pressure Drop Blank psig	Pressure Drop Net psig
#19	143	398	401	418	9	409	80	329
1.75	212	397	400	538	16	522	101	421
	303	396	400	671	26	645	120	525
	407	396	399	786	34	752	139	613
	513	396	400	879	41	838	152	686
#20	140	397	401	959	11	948	79	869
4.29	207	397	402	1250	16	1234	100	1134
	300	397	402	1582	26	1556	120	1436
	399	397	403	1817	34	1783	138	1645
	506	398	403	2062	41	2021	151	1870

APPENDIX F.

FRICTION FACTOR-REYNOLDS NUMBER

Table F-I

Packed Bed Friction Factor-Reynolds Number 100% PMMA-VM

D_p cm	L cm	ρ g/cm^3	Flow g/min	ΔP psig	f^*	Huang NRE	Huang c	Ellis NRE	Ellis c
.979	1.83	1.062	147	40	233.1	38.1	89	36.5	85
.979	1.83	1.062	228	79	191.3	68.5	131	71.3	136
.979	1.83	1.062	306	91	122.4	96.5	118	102.6	125
.979	4.37	1.063	144	129	328.3	39.4	129	38.8	127
.979	4.37	1.063	235	186	177.7	70.3	125	73.0	130
.979	4.37	1.064	309	241	133.3	101.5	135	109.6	146
.979	4.37	1.064	418	251	75.9	139.7	106	151.8	115
.979	4.37	1.064	457	280	70.8	161.2	114	177.4	126
.679	1.75	1.062	156	92	270.3	28.9	78	28.8	78
.679	1.75	1.062	148	86	280.8	27.0	76	26.7	75
.679	1.75	1.063	236	157	201.8	51.6	104	55.7	112
.679	1.75	1.063	314	198	143.7	77.4	111	85.7	123
.679	1.75	1.064	425	244	96.8	113.8	110	135.0	131
.679	1.75	1.064	516	259	69.7	149.0	104	171.8	120
.679	4.29	1.064	154	293	361.1	30.5	110	31.6	114
.679	4.29	1.065	238	471	243.3	57.6	140	63.7	155
.679	4.29	1.065	308	542	167.1	76.8	128	90.9	152
.375	1.75	1.064	149	269	449.2	17.2	77	18.3	82
.375	1.75	1.065	223	464	346.2	33.5	116	39.3	136
.375	1.75	1.065	302	510	207.5	50.4	105	57.4	119
.375	4.29	1.067	151	819	544.7	19.2	105	21.1	115
.375	4.29	1.070	229	1216	352.6	36.6	129	42.5	150
.375	4.29	1.072	407	1833	168.6	112.7	190	109.2	184
.198	1.75	1.068	148	948	730.1	11.6	85	13.5	99
.198	1.75	1.071	225	1480	494.5	31.5	156	30.4	150
.198	1.75	1.072	294	1750	342.8	46.0	158	46.9	161
.198	1.75	1.075	415	2170	213.9	72.0	154	83.1	178

Table F-II

Packed Bed Friction Factor-Reynolds Number 75/25 PMMA/PS

D_p cm	L cm	ρ g/cm^3	Flow g/min	ΔP psig	f*	Huang NRE	Huang c	Ellis NRE	Ellis c
.979	1.83	1.040	154	46	239.1	118.1	283	116.1	278
.979	1.83	1.040	213	54	146.8	179.3	263	185.5	272
.979	1.83	1.039	301	59	80.2	269.3	216	285.6	229
.979	1.83	1.039	411	74	54.0	428.1	231	494.1	267
.979	1.83	1.039	534	96	41.5	864.8	359	866.4	359
.979	4.37	1.039	153	92	202.7	108.0	219	99.9	203
.979	4.37	1.039	208	107	127.6	157.4	201	153.3	196
.979	4.37	1.040	297	141	82.5	265.9	219	282.0	233
.979	4.37	1.040	403	170	54.0	406.4	220	464.5	251
.979	4.37	1.041	516	199	38.6	632.8	244	708.9	274
.679	1.75	1.039	151	83	254.7	84.0	214	86.9	221
.679	1.75	1.039	214	99	151.2	135.7	205	146.6	222
.679	1.75	1.039	305	122	91.8	230.4	211	261.8	240
.679	1.75	1.040	419	145	57.8	425.2	246	439.5	254
.679	1.75	1.040	531	162	40.2	714.5	288	637.2	256
.679	4.29	1.041	154	212	255.6	88.0	225	92.1	236
.679	4.29	1.041	216	273	167.3	147.1	246	167.6	280
.679	4.29	1.041	303	314	97.8	247.2	242	274.8	269
.679	4.29	1.042	408	356	61.2	416.2	255	428.7	262
.679	4.29	1.042	524	477	49.7	875.2	435	792.2	394
.679	4.29	1.041	152	209	258.7	86.1	223	89.7	232
.679	4.29	1.041	214	260	162.3	140.7	228	157.5	256
.679	4.29	1.042	306	330	100.9	268.3	271	294.0	297

Table F-II (continued)

Packed Bed Friction Factor-Reynolds Number 75/25 PMMA/PS

D_p cm	L cm	ρ g/cm^3	Flow g/min	ΔP psig	f*	Huang NRE	Huang c	Ellis NRE	Ellis c
.679	4.29	1.043	412	400	67.5	563.2	380	490.8	337
.679	4.29	1.043	546	468	45.0	900.4	405	805.5	362
.679	6.10	1.043	155	319	267.5	92.3	247	98.0	262
.679	6.10	1.043	231	407	153.7	165.1	254	188.8	290
.679	6.10	1.043	306	466	100.3	263.8	265	291.6	292
.679	6.10	1.043	414	548	64.4	517.7	334	478.8	308
.679	6.10	1.044	538	637	44.4	855.2	380	750.7	333
.375	1.75	1.041	154	207	316.6	57.0	181	65.0	206
.375	1.75	1.042	212	251	202.7	101.5	206	111.2	225
.375	1.75	1.042	301	323	129.4	247.2	320	214.3	277
.375	1.75	1.042	406	385	84.8	385.8	327	361.9	307
.375	1.75	1.043	525	441	58.1	539.6	314	559.9	326
.375	4.29	1.043	151	526	342.0	57.6	197	66.3	227
.375	4.29	1.044	207	680	235.4	122.5	288	122.2	288
.375	4.29	1.045	296	854	144.8	262.0	379	231.9	336
.375	4.29	1.046	400	1011	93.9	416.0	391	390.2	367
.375	4.29	1.045	513	1110	62.6	534.3	335	566.8	355
.198	1.75	1.045	152	647	462.2	63.2	292	54.9	254
.198	1.75	1.045	214	785	282.9	105.0	297	98.9	280
.198	1.75	1.046	300	952	174.8	163.5	286	179.1	313
.198	1.75	1.046	403	1090	110.9	231.6	257	289.4	321
.198	1.75	1.047	531	1234	72.4	315.9	229	452.7	328
.198	4.29	1.050	153	1768	511.0	70.8	362	63.4	324
.198	4.29	1.050	215	1895	277.3	104.4	290	97.4	270

Table F-III

Packed Bed Friction Factor-Reynolds Number 50/50 PMMA/PS

D_p cm	L cm	ρ g/cm^3	Flow g/min	ΔP psig	f*	Huang		Ellis	
						NRE	c	NRE	c
.979	1.83	1.019	151	33	174.8	145.9	255	141.7	248
.979	1.83	1.019	210	42	115.1	231.4	266	239.7	276
.979	1.83	1.020	307	53	68.0	388.9	264	434.7	296
.979	1.83	1.019	419	60	41.3	612.6	253	672.2	278
.979	1.83	1.019	537	66	27.6	897.8	248	952.3	263
.979	4.37	1.019	152	85	186.1	152.4	284	151.2	281
.979	4.37	1.017	208	95	110.9	221.7	246	226.6	251
.979	4.37	1.018	299	111	62.7	353.8	222	373.7	234
.979	4.37	1.019	400	137	43.3	553.0	240	612.9	265
.979	4.37	1.019	522	159	29.5	885.4	261	934.5	276
.679	1.75	1.019	145	56	182.8	97.4	178	97.1	177
.679	1.75	1.018	197	68	120.1	148.7	179	155.6	187
.679	1.75	1.018	290	87	70.9	259.3	184	289.5	285
.679	1.75	1.018	393	105	46.6	462.5	216	477.6	223
.679	1.75	1.018	509	124	32.8	900.9	296	744.4	244
.679	4.29	1.019	149	165	208.0	111.6	232	116.6	243
.679	4.29	1.019	199	191	135.0	162.4	219	178.3	241
.679	4.29	1.019	296	257	82.1	346.9	285	359.1	295
.679	4.29	1.019	406	295	50.1	668.4	335	573.9	287
.679	4.29	1.019	519	323	33.6	1008.5	339	813.9	273
.375	1.75	1.019	149	159	254.2	70.7	180	79.6	202
.375	1.75	1.019	212	196	154.8	136.6	212	140.8	218
.375	1.75	1.019	303	254	98.2	332.9	327	269.7	265
.375	1.75	1.019	409	295	62.6	502.8	315	435.2	272
.375	1.75	1.019	530	380	48.0	741.0	356	772.7	371
.375	4.29	1.020	144	395	276.1	69.6	192	78.0	215
.375	4.29	1.020	199	476	174.2	125.8	219	130.9	228

Table F-III (continued)

Packed Bed Friction Factor-Reynolds Number 50/50 PMMA/PS

D_p cm	L cm	ρ g/cm^3	Flow g/min	ΔP psig	f*	Huang NRE	Huang c	Ellis NRE	Ellis c
.375	4.29	1.021	294	644	108.1	332.9	360	272.3	294
.375	4.29	1.023	406	819	72.2	536.1	387	503.4	364
.375	4.29	1.024	522	896	47.9	718.4	344	724.4	341
.375	6.10	1.020	139	586	309.2	70.5	218	78.6	243
.375	6.10	1.022	197	725	190.8	144.4	276	139.7	266
.375	6.10	1.024	293	950	113.3	334.7	379	283.4	321
.375	6.10	1.024	400	1145	73.2	523.4	383	485.6	356
.375	6.10	1.025	515	1312	50.7	717.3	364	741.8	376
.198	1.75	1.020	148	517	380.3	84.0	320	68.1	259
.198	1.75	1.021	200	666	268.5	134.7	362	125.0	336
.198	1.75	1.023	295	865	160.6	220.5	354	256.8	412
.198	1.75	1.024	405	950	93.7	309.8	290	398.3	373
.198	1.75	1.025	519	1077	64.7	406.0	263	602.3	390
.198	1.75	1.021	147	452	337.3	67.0	226	58.0	195
.198	1.75	1.021	204	601	232.9	129.5	302	112.4	262
.198	1.75	1.022	298	711	129.2	207.3	268	202.0	261
.198	1.75	1.023	405	859	84.6	302.1	256	349.4	296
.198	1.75	1.024	517	963	58.2	396.6	231	517.6	302
.198	4.29	1.025	147	1169	357.3	75.4	270	61.6	220
.198	4.29	1.026	199	1382	230.7	118.9	274	101.5	234
.198	4.29	1.028	293	1780	137.3	205.8	283	204.0	280
.198	4.29	1.029	396	2192	92.7	298.6	277	359.9	333
.198	4.29	1.031	497	2522	67.8	386.0	262	542.8	368
.117	1.75	1.024	146	1118	472.8	56.5	267	51.2	242
.117	1.75	1.025	198	1320	303.8	82.8	252	85.5	260
.117	1.75	1.027	292	1638	173.7	130.5	227	166.5	289
.117	1.75	1.028	399	1895	107.7	183.0	197	275.8	297
.117	1.75	1.030	507	2211	78.0	236.5	185	430.8	336

Table F-IV

Packed Bed Friction Factor-Reynolds Number 25/75 PMMA/PS

D_p cm	L cm	ρ g/cm^3	Flow g/min	ΔP psig	f*	Huang NRE	Huang c	Ellis NRE	Ellis c
.979	1.83	.994	147	22	120.0	172.5	207	164.6	198
.979	1.83	.995	205	32	89.8	282.1	253	288.2	259
.979	1.83	.995	298	45	59.8	488.9	292	546.7	327
.979	1.83	.995	402	49	35.8	717.7	257	795.0	284
.979	1.83	.995	509	54	24.6	1026.3	252	1100.9	271
.979	4.37	.995	148	69	155.6	193.5	301	194.3	302
.979	4.37	.995	204	70	83.1	268.6	223	270.3	225
.979	4.37	.995	300	92	50.5	463.7	234	484.2	244
.979	4.37	.995	406	120	36.0	748.6	269	821.4	295
.979	4.37	.995	512	132	24.9	1066.5	265	1132.2	282
.679	1.75	.995	148	47	143.8	131.6	189	133.4	192
.679	1.75	.995	209	58	89.0	210.4	187	219.4	195
.679	1.75	.995	302	72	52.9	340.3	180	379.1	201
.679	1.75	.995	414	89	34.8	587.0	204	632.4	220
.679	1.75	.995	532	105	24.9	1001.5	249	959.6	239
.679	4.29	.995	144	122	160.8	131.9	212	135.0	217
.679	4.29	.995	200	156	106.6	204.5	218	226.1	241
.679	4.29	.996	296	202	63.1	389.6	246	420.1	265
.679	4.29	.996	400	244	41.7	700.7	292	682.9	285
.679	4.29	.996	509	271	28.6	1010.7	289	968.9	277

Table F-IV (continued)

Packed Bed Friction Factor-Reynolds Number 25/75 PMMA/PS

D_p cm	L cm	ρ g/cm^3	Flow g/min	ΔP psig	f^*	Huang NRE	Huang c	Ellis NRE	Ellis c
.375	1.75	.995	143	110	186.5	79.6	148	83.0	155
.375	1.75	.995	204	144	119.9	135.3	162	148.9	179
.375	1.75	.996	295	188	75.0	287.5	216	278.6	209
.375	1.75	.997	404	222	47.2	464.7	220	454.5	215
.375	1.75	.997	519	252	32.5	647.5	210	671.6	218
.375	4.29	.997	144	300	205.0	81.1	166	91.2	187
.375	4.29	.998	206	371	124.0	145.8	181	157.4	195
.375	4.29	.999	299	503	79.9	322.9	258	309.2	247
.375	4.29	.998	407	594	50.9	496.3	252	504.1	256
.375	4.29	.999	518	675	35.7	677.8	242	741.3	265
.198	1.75	.998	148	434	312.3	85.2	266	82.4	257
.198	1.75	.998	209	516	186.2	135.0	251	140.7	262
.198	1.75	.998	302	640	110.6	216.0	239	261.0	289
.198	1.75	.999	409	744	70.2	306.9	215	423.8	297
.198	1.75	.999	518	823	48.4	397.8	193	607.8	294
.198	4.29	1.001	144	1020	317.2	80.1	254	76.7	243
.198	4.29	1.001	210	1265	185.0	135.6	251	141.4	262
.198	4.29	1.004	295	1568	116.6	210.9	246	254.8	297
.198	4.29	1.008	399	1928	78.7	303.5	239	442.6	348
.198	4.29	1.008	506	2200	55.8	395.5	220	661.7	369

Table F-V

Packed Bed Friction Factor-Reynolds Number 100% PS

D_p cm	L cm	ρ g/cm^3	Flow g/min	ΔP psig	f*	Huang NRE	Huang c	Ellis NRE	Ellis c
.979	1.83	.973	142	17	97.3	159.4	155	152.4	148
.979	1.83	.973	209	26	68.7	268.0	184	275.5	189
.979	1.83	.974	301	37	47.2	450.3	212	521.4	246
.979	1.83	.974	406	48	33.6	863.4	290	920.3	309
.979	1.83	.973	512	56	24.6	1668.1	411	1397.0	344
.979	4.37	.973	139	52	130.0	167.1	217	165.7	215
.979	4.37	.973	208	69	77.0	279.7	216	294.3	227
.979	4.37	.973	301	88	46.9	448.4	210	519.5	244
.979	4.37	.973	406	125	36.6	1034.1	379	1019.1	373
.979	4.37	.973	509	132	24.6	1592.9	392	1366.3	336
.679	1.75	.973	142	41	133.2	121.8	162	125.8	168
.679	1.75	.973	206	52	80.3	200.5	161	217.9	175
.679	1.75	.974	303	66	47.1	348.9	165	401.5	189
.679	1.75	.973	406	80	31.8	665.3	212	668.1	212
.679	1.75	.973	513	92	22.9	1232.9	282	1006.2	230
.679	4.29	.973	137	110	156.7	122.5	192	129.1	202
.679	4.29	.973	204	115	73.9	186.7	138	198.7	147
.679	4.29	.973	304	163	47.1	354.1	167	406.0	191
.679	4.29	.975	407	206	33.3	800.6	267	711.2	237
.679	4.29	.975	515	240	24.2	1312.4	318	1097.1	266

Table F-V (continued)

Packed Bed Friction Factor-Reynolds Number 100% PS

D_p cm	L cm	ρ g/cm^3	Flow g/min	ΔP psig	f*	Huang NRE	Huang c	Ellis NRE	Ellis c
.375	1.75	.974	148	113	175.0	84.6	148	98.2	172
.375	1.75	.974	211	148	112.8	184.5	208	187.8	212
.375	1.75	.974	305	191	69.7	439.7	306	377.3	263
.375	1.75	.975	396	221	47.9	628.6	301	603.2	289
.375	1.75	.975	504	250	33.4	849.7	284	923.8	309
.375	4.29	.974	147	311	199.2	95.6	191	109.8	219
.375	4.29	.975	209	393	124.7	243.2	303	205.2	256
.375	4.29	.976	307	478	70.3	449.4	316	390.9	275
.375	4.29	.977	410	549	45.3	655.7	297	636.8	289
.375	4.29	.977	525	645	32.5	902.6	293	1041.4	338
.375	4.29	.975	143	301	204.0	89.6	183	103.2	210
.375	4.29	.975	212	379	116.9	215.8	252	198.9	232
.375	4.29	.976	307	493	72.6	459.4	333	408.2	296
.375	4.29	.977	406	591	49.8	673.7	335	704.1	351
.375	4.29	.977	519	667	34.4	902.6	310	1084.9	373
.198	1.75	.974	143	329	247.5	88.4	219	73.4	182
.198	1.75	.975	212	421	144.3	166.7	241	151.8	219
.198	1.75	.977	303	525	88.2	266.5	235	301.8	266
.198	1.75	.977	407	613	57.1	375.1	214	518.1	296
.198	1.75	.977	513	686	40.2	483.4	194	784.9	316
.198	4.29	.978	140	869	279.4	96.4	269	79.1	221
.198	4.29	.980	207	1134	167.1	172.1	288	170.1	284
.198	4.29	.982	300	1436	101.0	273.3	276	355.0	358
.198	4.29	.982	399	1645	65.4	374.6	245	588.7	385
.198	4.29	.984	506	1870	46.3	483.8	224	924.4	428

REFERENCES

1. Aranow, R.H., "A Statistical Approach to Flow Through Porous Media," The Physics of Fluids, vol. 9, September, 1966, pp. 1721-1727.

2. Ashare, E. and R.B. Bird, "Falling Cylinder Viscometer for Non-Newtonian Fluids," A.I.Ch.E. Journal, vol. 11, September, 1965, pp. 910-916.

3. Bear, Jacob, Dynamics of Fluids in Porous Media, New York: American Elsevier Publishing Company, Inc., 1972, p. 125.

4. Ibid., p. 165,587.

5. Ibid., p. 171.

6. Bird, R.B., "Experimental Tests of Generalized Newtonian Models Containing a Zero-Shear Viscosity and a Characteristic Time," Canadian Journal of Chemical Engineering, August, 1965, pp. 161-168.

7. Bird, R.B., E.N. Lightfoot and W.E. Stewart, Transport Phenomena, New York: John Wiley and Sons, Inc., 1965, p. 101.

8. Ibid., pp. 45, 46.

9. Ibid., pp. 180-182.

10. Ibid., p. 198.

11. Blake, F.C., "The Resistance of Packing to Fluid Flow," Transactions A.I.Ch.E., vol. 14, 1922, p. 415.

12. Bogue, D.C. and J.O. Doughty, "Comparison of Constitutive Equations for Viscoelastic Fluids," I&EC Fundamentals, vol. 5, no. 2, May, 1966, p. 243.

13. Brenner, H., "The Stokes Resistance of an Arbitrary Particle," Chemical Engineering Science, vol. 18. Great Britain: Pergamon Press, Ltd., 1963, pp. 1-25.

14. Brinkman, H.C., "A Calculation of the Viscous Force Exerted by a Flowing Fluid on a Dense Swarm of Particles," Applied Science Research, vol. A1, 1947, p. 27.

15. Carman, P.C., "Fluid Flow Through a Granular Bed," Transactions Institute of Chemical Engineers, vol. 15. London: 1937, pp. 150-156.

16. Carman, P.C., Flow of Gases Through Porous Media, London: Butterworth, 1956.

17. Chase, C.A., "Theory of Fluid Motion in Porous Media," I&EC, vol. 62, no. 12, December, 1970, p. 83.

18. Christopher, R.H., Power Law Flow Through a Packed Tube, MS Thesis, University of Rochester, Rochester, N.Y., 1965.

19. Christopher, R.H. and Stanley Middleman, "Power Law Flow Through a Packed Tube," I&EC Fundamentals, vol.4, no. 4, November, 1965, p.422.

20. Coleman, B.D. and W. Noll, "Recent Results in the Continuum Theory of Viscoelastic Fluids," Annual New York Academy of Science, vol. 89, 1961, p. 672.

21. Collins, R.E., Flow of Fluids Through Porous Media, New York: Reinhold Publishing Company, Inc., 1961.

22. Dallavalle, J.M., Micromeritics - The Technology of Fine Particles, New York: Pitman Publishing Corporation, 2nd ed., 1948, ch. 13.

23. Darcy, H.P.G., Les Fontaines Publiques de la Ville de Dijon, Paris: Victor Dalmont, 1856.

24. De Jong, J., "The Tensor Character in the Dispersion Coefficient in Anisotropic Porous Media," 1st I.A.H.R. Symposium Fundamentals of Transport Phenomena in Porous Media, Haifa, Israel, 1969.

25. Dullien, F.A.L. and V.K. Batra, "Determination of the Structure of Porous Media," I&EC, vol. 62, no. 10, October, 1970, p. 25.

26. Dullien, F.A.L., "New Network Permeability Model of Porous Media," A.I.Ch.E. Journal, vol. 21, 1975, p. 299.

27. Dullien, F.A.L., "Prediction of Tortuosity Factors from Pore Structure Data," A.I.Ch.E. Journal, vol. 21, July, 1975, pp. 820-822.

28. Ergun, Sabri, "Fluid Flow Through Packed Columns," Chem. Eng. Prog., vol. 48, Feb., 1952, p. 89.

29. Fair, G.M. and L.P. Hatch, "Fundamental Factors Governing the Streamline Flow of Water Through Sand," Journal American Water Works Assoc,, vol. 25, 1933, pp. 1551-1565.

30. Ferry, J.D., Viscoelastic Properties of Polymers, New York: John Wiley and Sons, Inc., 1970.

31. Fredrickson, A.G. and R.B. Bird, "Non-Newtonian Flow in Annuli," I&EC, vol. 50, 1958, pp. 347-352.

32. Fredrickson, A.G. and R.B. Bird, "Friction Factors for Axial Non-Newtonian Annular Flow," I&EC, vol. 50, 1958, p. 1599.

33. Fredrickson, A.G. and R.B. Bird, "Non-Newtonian Flow in Annuli," I&EC Fund., vol. 3, 1964, p. 383.

34. Fredrickson, A.G., Principles and Applications of Rhelogy, Englewood Cliffs, N.J.: Prentice-Hall, Inc., 1964, pp. 207-214.

35. Gaitonde, N.Y. and S. Middleman, "Flow of Viscoelastic Fluids Through Porous Media," I&EC Fund., vol. 6, Feb., 1967, p. 145.

36. Glasstone, S., K.J. Laidler and H. Eyring, Theory of Rate Processes, New York: McGraw Hill, Inc., 1941, ch 9.

37. Gregory, D.R., Non-Newtonian Flow Through Porous Media, PhD Thesis, Virginia Polytechnic Institute, Blacksburg, Va., 1965.

38. Gregory, D.R. and R.G. Griskey, "Flow of Molten Polymers Through Porous Media," A.I.Ch.E. Journal, vol. 13, January, 1967, p. 122.

39. Hall, W.A., "An Analytical Derivation of the Darcy Equation," Transactions American Geophysical Union, vol. 37, 1956, p. 185.

40. Han, C.D., T.C. Yu and K.U. Kim, "Rheological Properties of Molten Polymers: I. Homopolymer Systems," Journal of Applied Polymer Science, vol. 15, 1971, pp. 1149-1162.

41. Han, C.D. and T.C. Yu, "Rheological Properties of Molten Polymers: II. Two Phase Systems," Journal of Applied Polymer Science, vol. 15, 1971, pp. 1163-1180.

42. Han, C.D. and R.R. Lamonte, "Melt Flow Instabilities in Capillary Flow of Two Phase Polymer Systems," Polymer Engineering and Science, vol. 12, March, 1972, pp. 77-80.

43. Han, C.D. and T.C. Yu, "Rheological Behavior of Two Phase Polymer Melts," Polymer Engineering and Science, vol. 12, March, 1972, pp. 81-90.

44. Han, C.D. and T.C. Yu, "Die Swell Behavior of Two Phase Polymer Melts," A.I.Ch.E. Journal, vol. 17, November, 1971, pp. 1512-1514.

45. Han, C.D., K.U. Kim, et al, "Measurements of the Viscoelastic Properties of Poly(methylmethacrylate) and Polystyrene Blends," New York: John Wiley and Sons, Inc., Applied Polymer Symposium, vol. 20, 1973, pp. 191-198.

46. Handbook of Mathematical Functions, M. Abramowitz and I.A. Stegun (eds.), National Bureau of Standards Applied Mathematics Series 55, June, 1964, p. 260, eqn. 6.5.3.

47. Ibid., p. 941, eqn. 26.4.19.

48. Haring, R.E. and R.A. Greenkorn, "A Statistical Model of a Porous Medium with Nonuniform Pores," A.I.Ch.E. Journal, vol. 16, May, 1970, p. 477.

49. Harvey, A.H., An Investigation of the Flow of Polymer Solutions Through Porous Media, PhD Thesis, Oklahoma University, Norman, Oklahoma, 1968.

50. Hassell, H.L. and A. Bondi, "Mixing of Viscous Non-Newtonian Fluids in Packed Beds," A.I.Ch.E. Journal, vol. 11, March, 1965, p. 217.

51. Herzig, J.P., D.M. Leclerc and P. Legoff, "Flow of Suspensions Through Porous Media - Application to Deep Filtration," I&EC, vol. 62, May, 1970, pp. 8-35.

52. Hill, A.S. and B. Maxwell, "Dynamic Melt Properties of Polymer Blends," Polymer Engineering and Science, vol. 10, September, 1970, p. 289.

53. Huang, C.R., "A Thermodynamic Approach to Generalized Rheological Equations of State for Time-Dependent and Time-Independent Non-Newtonian Fluids," Chemical Engineering Journal, vol. 3, 1972, 100-104.

54. Hubbert, M.K., "Darcy's Law and the Field Equations of the Flow of Underground Fluids," Transactions A.I.M.E., vol. 207, 1956, p. 222.

55. Iberall, A.S., "Permeability of Glass Wool and Other Highly Porous Media," Journal Res. Nat. Bur. Stand., vol. 45, 1950, p. 398.

56. Irmay, S., "On the Derivation of Darcy and Forscheimer Formulas," Transactions American Geophysical Union, vol. 39, 1958, p. 702.

57. Jobling, A., "Flow Testing of Viscoelastic Materials. Design and Calibration of the Roberts-Weissenberg Model R8 Rheogoniometer," Journal Polymer Science, vol. 36, 1959, p. 421.

58. Kozeny, J., Uber Kapillare Leitung des Wassers im Boden, Sitzungsber Akad. Wiss. Wien, vol. 136, 1927, pp. 271-306.

59. Kozicki, W., C.J. Hsu and C. Tiu, "Non-Newtonian Flow Through Packed Beds and Porous Media," Chemical Engineering Science, vol. 22, 1967, pp. 487-502.

60. Kwei, T.K., T. Nishi and R.F. Roberts, "Study of Compatible Polymer Mixtures," Rubber Chemistry and Technology, vol. 48, May, 1975, pp. 218-235.

61. LeClair, B.P. and A.E. Hamielec, "Viscous Flow Through Particle Assemblages at Intermediate Reynolds Numbers," I&EC Fundamentals, vol. 7, November, 1968, pp. 542-549.

62. LeClair, B.P. and A.E. Hamielec, "Viscous Flow Through Particle Assemblages at Intermediate Reynolds Numbers," I&EC Fundamentals, vol. 9, November, 1970, pp. 608-613.

63. Leva, M., "Flow Through Packings and Beds," Chemical Engineering, vol. 64, 1957, series inc. January, p.204 and December, p. 267.

64. Marshall, R.J. and A.B. Metzner, "Flow of Viscoelastic Fluids Through Porous Media," I&EC Fundamentals, vol. 6, August, 1967, p. 393.

65. Matsuhisa, S. and R.B. Bird, "Analytical and Numerical Solutions for Laminar Flow of the Non-Newtonian Ellis Fluid," A.I.Ch.E. Journal, vol. 11, July, 1965, pp. 588-595.

66. McKelvey, J.M., Polymer Processing, New York: John Wiley and Sons, Inc., 1962.

67. McKennel, R., "Cone-Plate Viscometer," Analytical Chemistry, vol. 28, 1956, p. 1710.

68. McKinley, R.M., H.O. Jahns, W.W. Harris and R.A. Greenkorn, "Non-Newtonian Flow in Porous Media," A.I.Ch.E. Journal, vol. 12, January, 1966, p. 17.

69. Metzner, A.B., J.L. White and M.M. Denn, "Behavior of Viscoelastic Materials in Short-time Processes," Chemical Engineering Progress, vol. 62, December, 1966, p. 81.

70. Metzner, A.B., J.L. White and M.M. Denn, "Constitutive Equations for Viscoelastic Fluids for Short Deformation Periods and for Rapidly Changing Flows," A.I.Ch.E. Journal, vol. 12, September, 1966, pp. 863-866.

71. Middleman, S. The Flow of High Polymers, New York: Interscience Publishers, Division of John Wiley, 1968.

72. Mokadam, R.G., "Thermodynamic Analysis of the Darcy Law," Journal Applied Mechanics (Transactions A.S.M.E.), vol. 28, 1961, p. 208.

73. Mott, R.A., Some Aspects of Fluid Flow, London: Edward Arnold and Company, 1951, p. 242.

74. Multicomponent Polymer Systems, (Advances in Chemistry Series), R.F. Gould (ed.), Washington, DC: ACS Publications, 1971. Papers presented at Symposium, February 23-26, 1970.

75. Muscat, Morris, "The Flow of Fluids Through Porous Media," Journal Applied Physics, vol. 8, 1937, pp. 274-282.

76. Muscat, Morris, The Flow of Homogenous Fluids Through Porous Media, New York: McGraw-Hill, first edition, 1937.

77. Noel, O.F., III and J.F. Carley, "Properties of Polypropylene - Polyethylene Blends," SPE 31st ANTEC, 1972, p. 97.

78. Pakula, R.J. and R.A. Greenkorn, "An Experimental Investigation of a Porous Medium Model with Nonuniform Pores," A.I.Ch.E. Journal, vol. 17, September, 1971, pp. 1265-1268.

79. Park, H.C., M.C. Hawley and R.F. Blanks, "Flow of Aqueous Solutions of Polymethylcellulose (A Non-Newtonian Fluid) Through Porous Media," draft article for A.I.Ch.E. Journal, April, 1972.

80. Payatakes, A.C., Chi Tien and R.M. Turian, "A New Model for Granular Porous Media. I. Model Formation. II. Numerical Solution of Steady State Incompressible Newtonian Flow Through Periodically Constricted Tubes," A.I.Ch.E. Journal, vol. 19, January, 1973, pp. 58-67, 67-76.

81. Payne, L.W. and H.W. Parker, "Axial Dispersion of Non-Newtonian Fluids in Porous Media," A.I.Ch.E. Journal, vol. 19, January, 1973, pp. 202-204.

82. Platzer, N.A.J., "Copolymers, Polyblends and Composites," Chemical Technology, vol. 4, February, 1974, pp. 90-95.

83. Powell, R.E. and H. Eyring, "Mechanisms of the Relaxation Theory of Viscosity," Nature, vol. 154, 1944, p. 427.

84. Processing of Thermoplastic Materials, E.C. Bernhardt (ed.), New York: Reinhold Publishing Company, 1959.

85. Reiner, M., Deformation, Strain and Flow, New York: Interscience Publishers, Inc., 1960.

86. Rheology - Theory and Applications - Volume 2, F.R. Eirich (ed.), New York: Academic Press, 1958, p. 145.

87. Rheology - Theory and Applications - Volume 3, F.R. Eirich (ed.), New York: Academic Press, 1960, ch. 2.

88. Rheology - Theory and Applications - Volume 5, F.R. Eirich (ed.), New York: Academic Press, 1969.

89. Rice, P.A., D.J. Fontugne, R.G. Latini and A.J. Barduhn, "Anisotropic Permeability in Porous Media," I.&EC, vol. 62, June, 1970, p. 23.

90. Rivlin, R.S. and J.L. Ericksen, "Stress Deformation Relations for Isotropic Materials," Journal Rational Mechanics and Analysis, vol. 4, 1955, p. 323.

91. Sadowski, T.J., Non-Newtonian Flow Through Porous Media, PhD Thesis, The University of Wisconsin, Madison, Wisconsin, 1963.

92. Sadowski, T.J. and R.B. Bird, "Non-Newtonian Flow Through Porous Media. I. Theoretical. II. Experimental," Transactions Society Rheology, vol. 9, 1965, pp. 243-250, 251-271.

93. Savins, J.G., "Non-Newtonian Flow Through Porous Media," I&EC, vol. 61, October, 1969, p. 18.

94. Scheidegger, A.E., The Physics of Flow Through Porous Media, New York: The Mac Millan Company, 1957, p. 92.

95. Ibid., p. 98.

96. Ibid., p. 108.

97. Scheidegger, A.E., The Physics of Flow Through Porous Media, New York: The MacMillan Company, 1960 rev. ed.

98. Scheidegger, A.E., "Hydrodynamics in Porous Media," Encyclopedia of Physics, vol. 9, Springer, Berlin, 1960.

99. Scheidegger, A.E., "Statistical Theory of Flow Through Porous Media," Transactions Society Rheology, vol. 9, 1965, pp. 313-319.

100. Scheidegger, A.E., "Statistical Hydrodynamics in Porous Media," Journal Applied Physics, vol. 25, 1954, pp. 994-1001.

101. Seymour, R.B., "Composition vs. Properties of Polyolefin Blends," Modern Plastics, vol. 50, January, 1973, pp. 98-100.

102. Sieglaff, C.L., "Rheological Behavior of Poly-(Vinyl Chloride) Mixtures. I. Viscous Behavior," Polymer Engineering and Science, vol. 9, March, 1969, p. 81.

103. Sieglaff, C.L. and C.G. Vinson, "Rheological Behavior of Poly(Vinyl Chloride) Mixtures. II. Elastic Behavior," Polymer Engineering and Science, vol. 9, January, 1969, p. 73.

104. Sisko, A.W., "The Flow of Lubricating Greases," I&EC, vol. 50, December, 1958, pp. 1789-1792.

105. Siskovic, N., R.G. Griskey and D.R. Gregory, "Viscoelastic Behavior of Molten Polymers in Porous Media," A.I.Ch.E. Journal, vol. 17, March, 1971, pp. 281-285.

106. Slattery, J.C., "Approximations to the Drag Force on a Sphere Moving Slowly Through Either an Ostwald-de-Waele or a Sisko Fluid," A.I.Ch.E. Journal, vol. 8, 1962, p. 663.

107. Slattery, J.C., "Flow of Viscoelastic Fluids Through Porous Media," A.I.Ch.E. Journal, vol. 13, November, 1967, pp. 1066-1071.

108. Slattery, J.C., "Multiphase Viscoelastic Flow Through Porous Media," A.I.Ch.E. Journal, vol. 14, January, 1968, p. 50.

109. Slattery, J.C.,"Single Phase Flow Through Porous Media," A.I.Ch.E. Journal, vol. 15, December, 1969, p. 866.

110. Slattery, J.C., "Two-Phase Flow Through Porous Media," A.I.Ch.E. Journal, vol. 16, May, 1970, pp. 345-352.

111. Spriggs, T.W. and R.B. Bird, "Some Nonlinear Viscoelastic Models with Inclusion of Results from Molecular Theory," I&EC Fundamentals, vol. 4, 1964, pp. 182-186.

112. Spriggs, T.W., J.D. Huppler and R.B. Bird, "An Experimental Appraisal of Viscoelastic Models," Transactions Society Rheology, vol. 10, 1966, pp. 191-213.

113. Sutterby, J.L., "Laminar Converging Flow of Dilute Polymer Solutions in Conical Sections. II," Transactions Society Rheology, vol 9, 1965, pp. 227-241.

114. Tobolsky, A.V., Properties and Structure of Polymers, New York: John Wiley and Sons, Inc., 1967, pp. 78-83.

115. Tobolsky, A.V. and H.F. Mark, Polymer Science and Materials, New York: Interscience Publishers, Division of John Wiley, 1971, p. 217.

116. VanOene, H., "Modes of Dispersion of Viscoelastic Fluids in Flow," Journal Colloid & Interface Science, vol. 40, September, 1972, pp. 448-467.

117. Van Wazer, J.R., J.W. Lyons, K.Y. Kim and R.E. Colwell, Viscosity and Flow Measurement, New York: Interscience Publishers, Division of John Wiley, 1963, p. 113.

118. Volssoughi, S. and F.A. Seyer, "Pressure Drop for Flow of Polymer Solution in a Model Porous Medium," Canadian Journal Chemical Engineering, vol. 52, October, 1974, pp. 666-669.

119. Wampler, F.C., and D.R. Gregory, "Flow of Molten Poly(ethyleneterephthalate) Through Packed Beds of Glass Beads," 70th National A.I.Ch.E. Meeting, August 29 - September 1, 1971, Atlantic City, New Jersey.

120. Weissenberg, K., "Rheology of Hydrocarbon Gels," Proceedings Royal Society, London, A200, 1950, pp. 183-188.

121. Whitaker, S., "Advances in Theory of Fluid Motion in Porous Media," I&EC, vol. 61, December, 1961, pp. 14-28.

122. White, D.A., "Non-Newtonian Flow in Stratified Porous Media and in Axisymmetric Geometries," Chemical Engineering Science, vol. 23, 1968, pp. 243-251.

123. Williams, A.G., Personal communication ref. moisture sensitivity of PET.

124. Williams, M.C. and R.B. Bird, "Oscillatory Behavior of Normal Stresses in Viscoelastic Fluids," I&EC Fundamentals, vol. 3, 1964, pp. 42-49.

125. Wissler, E.H., "Viscoelastic Effects in the Flow of Non-Newtonian Fluids Through a Porous Medium," I&EC Fundamentals, vol. 10, August, 1971, pp. 411-417.

126. Wyllie, M.R.J. and A.R. Gregory, "Fluid Flow Through Unconsolidated Porous Aggregates. Effect of Porosity and Particle Shape on Kozeny - Carman Constants," I&EC, vol. 47, 1955, p. 1379.

53a. Huang, C.R., N. Siskovic, R.W.J. Robertson, W. Fabisiak, E.H. Smithberg and A.L. Copley, "Quantitative Characterization of Thixotropy of Whole Human Blood," Biorheology, vol. 12, 1975, p. 279.

53b. Huang, C.R. and W. Fabisiak, "Thixotropic Parameters of Whole Human Blood," Thrombosis Research, vol. 8, sppl. II, 1976, p. 1.

53c. Huang, C.R., W. Fabisiak and N.L. Polston, "Correlation of Thixotropic and Application Properties of Latex Paints," VI International Congress on Rheology, Gothenburg, Sweden, August 23-27, 1976.

53d. Huang, C.R., Personal communication.

60a. Larkins, R.P., R.R. White and D.W. Jeffrey, "Two-phase Concurrent Flow in Packed Beds," A.I.Ch.E. Journal, vol. 7, June, 1961, p. 231.

VITA

The author was born James Atwood Parker, Jr., in on He was educated in Norfolk public schools and received an academic high school diploma from Granby High School in 1961.

In the fall of 1961, he entered the cooperative engineering program of Virginia Polytechnic Institute and graduated with a B.S.Ch.E. degree in 1966. Work experience during this undergraduate program was with Celanese Fibers Company in Narrows, Virginia. He continued study at V.P.I. and received the M.S.Ch.E. degree in 1968.

In 1967, while completing the M.S.Ch.E degree requirements, he joined Celanese Research Company, Summit, New Jersey. Graduate work at the New Jersey Institute of Technology was conducted simultaneously during his employment with Celanese Research Company. Full time research was conducted during the 1971-72 academic year.

The candidate is currently employed by Celanese Fibers Marketing Company in Charlotte, North Carolina, where he and his family reside.